PHOTO-DYNAMIC XPS FOR INVESTIGATING PHOTOINDUCED VOLTAGE CHANGES IN SEMICONDUCTING MATERIALS

A DISSERTATION SUBMITTED TO
THE DEPARTMENT OF CHEMISTRY
AND THE GRADUATE SCHOOL OF ENGINEERING AND SCIENCE
OF BILKENT UNIVERSITY
IN PARTIAL FULFILLMENT OF THE REQUIREMENTS
FOR THE DEGREE OF
DOCTOR OF PHILOSOPHY

By

HİKMET SEZEN

December, 2011

I certify that I have read this thesis and that in my opinion is it is fully adequate, in scope and in quality, as a dissertation for the degree of the doctor of philosophy,

……..

Prof. Dr. Şefik Süzer (Principal Advisor)

I certify that I have read this thesis and that in my opinion is it is fully adequate, in scope and in quality, as a dissertation for the degree of the doctor of philosophy,

……..

Prof. Dr. O. Yavuz Ataman

I certify that I have read this thesis and that in my opinion is it is fully adequate, in scope and in quality, as a dissertation for the degree of the doctor of philosophy,

……..

Prof. Dr. Ekmel Özbay

I certify that I have read this thesis and that in my opinion is it is fully adequate, in scope and in quality, as a dissertation for the degree of the doctor of philosophy,

……..

Assoc. Prof. Dr. Oğuz Gülseren

I certify that I have read this thesis and that in my opinion is it is fully adequate, in scope and in quality, as a dissertation for the degree of the doctor of philosophy,

……..

Assist. Prof. Dr. Emrah Özensoy

Approved for the Graduate School of Engineering and Science:

……..

Prof. Dr. Levent Onural (Director of the Institute)

ABSTRACT

PHOTO-DYNAMIC XPS FOR INVESTIGATING PHOTOINDUCED VOLTAGE CHANGES IN SEMICONDUCTING MATERIALS

HİKMET SEZEN

Ph.D. in Chemistry

Supervisor: Prof. Dr. Şefik Süzer

December, 2011

The main motivation of this Ph.D. study is investigation of the photoinduced voltage changes in semiconductive materials with X-ray Photoelectron Spectroscopy (XPS). For this purpose, we have developed a technique for recording the shifts in the positions of the XPS peaks in response to different waveforms of electrical and/or optical stimuli for tracing dynamics of the developed potentials originating from intrinsic or extrinsic factors of the semiconductive materials such as charging/discharging, photoconductivity, surface photovoltage, band-bending/flattening/inversion, etc.

Within this purpose, the surface photovoltage behaviors of n- and p-type doped Si and GaN samples are examined with the photo-dynamic XPS, to follow the behavior of the band-bending under photoillumination in both static and dynamic fashions. The band inversion effects are clearly observed on the n- and p-Si samples in the presence of a dielectric silica overlayer and on the p-GaN sample due to variation of the illuminating laser energies.

Moreover, the extent of the dopant dependent XPS peak shifts of the n- and p-Si samples are assessed after correction of their surface photovoltage values.

A laser patterned silicon wafer with a high-power near infrared fiber laser is also investigated. While the patterned silica domains have identical chemical composition with the non-patterned regions, an investigation with dynamic XPS clearly reveals distinct dielectric characteristics of the patterned domains.

Electrical parameters of CdS thin film are extracted by dynamic XPS with and without photoillumination. The photo-dynamic XPS technique has also provided useful information by disentanglement of processes; charging/discharging, photoconductivity, and surface photovoltage. Furthermore, location (space) dependent resistance and chemical profile of a CdS based Light Dependent Resistor (LDR) is also probed during realistic operational conditions, by utilizing spatially resolved XPS analysis (in the area mapping mode). In addition, with the XPS mapping analysis defects and malfunctioning sites/domains have been located under various experimental and preparation conditions.

Keywords: XPS, Dynamic XPS, Photo-Dynamic XPS, Charging, Discharging, Charge Contrast, Photoconductivity, Surface Photovoltage, Band-Bending, Band-Flattening, and Band-Inversion, Laser Patterning, Light Dependent Photoresistor.

ÖZET

IŞIK ALTINDA YARIİLETKEN MALZEMELERİN ÜZERİNDE OLUŞAN VOLTAJ YÜKLENMELERİNİN FOTO-DİNAMİK XPS İLE İNCELENMESİ

HİKMET SEZEN

Kimya Doktora Tezi

Danışman: Prof. Dr. Şefik Süzer

Aralık, 2011

Bu doktora tezinin temel amacı, ışık uyarılmaları altında, yarıiletken malzemeler üzerinde meydana gelen voltaj yüklenmelerinin X-ışını fotoelektron spektroskopisi (XPS) ile incelenmesidir. Öncelikle malzemeleri değişik şekil ve hızlarda hem elektriksel hem de ışıksal olarak uyarabileceğimiz, aynı zamanda yarıiletken malzemelerin içsel ve dışsal özelliklerine bağlı olarak meydana gelebilecek potansiyel değişimlerini takip edebileceğimiz yeni bir teknik olan foto-dinamik XPS tekniğini geliştirdik.

Bu amaç doğrultusunda, hem n- ve p-Si hem de n- ve p-GaN numunelerinin yüzey fotovoltaj davranışları, yüzey bant düzlenmeleri statik ve dinamik ışık uyarımları yardımı ile XPS kullanılarak takip edildi. Ayrıca, yarıiletkenler üzerinde bant ters-eğrilme etkileri n- ve p-Si için ince bir silika tabakası oluşturulduğu zaman, ayrıca p-GaN için farklı dalga boylarında bulunan ışıklar ile uyarıldığı süreçlerde gözlemlendi. Ek olarak, bu teknik ile silikon numunelerindeki eser miktarda eklenmiş bulunan elementler vasıtasıyla ortaya çıkan enerji

kaymalarının yüzey fotovoltaj değerleri ile düzeltildikten sonra foto-dinamik XPS tekniğini kullanarak takip edilebileceğini gösterdik.

Yüksek yoğunluktaki kızılötesi lif lazer ile silikon üzerindeki desenlendirilmiş bölgeler XPS yardımı ile incelendi. Kimyasal içerik olarak, lazere maruz tutulan ve tutulmayan bölgeler arasında herhangi bir fark yok iken, dinamik XPS ile yaptığımız deneyler sayesinde lazer ile desenlendirilmiş bölgelerin kendine özgü dieletriksel özelliği olduğu gösterildi.

CdS filminin elektriksel özellikleri, ışık varlığında ve yokluğunda dinamik XPS kullanılarak ölçüldü. Ayrıca, foto-dinamik XPS tekniğinden, yüklenme, yük boşalması, fotoiletkenlik ve yüzey fotovoltaj gibi etkileri birbirlerinden ayırmada etkin bir şekilde yararlanılabileceği gösterildi. Ek olarak, CdS içeren bir fotoselin konuma bağımlı direnç ve kimyasal analizleri alan haritalamalı XPS ile ölçülmüştür. İlaveten, alan haritalamalı XPS kusurlu veya hatalı bölgelerin farklı koşullar altında ortaya çıkması ve bu farklı bölgeler arasında karşılaştırmalar yapabilmemizi sağladı.

Anahtar Kelimeler: XPS, Dinamik XPS, Foto-Dinamik XPS, Yüklenme, Yük Boşalması, Yük Ayrışımı, Fotoiletkenlik, Yüzey Fotovoltaj, Bant Eğrilmesi, Bant Düzelmesi, Bant Ters-Eğrilmesi, Lazer, Laser Desenlendirme, Işığa Bağımlı Direnç (Fotosel).

LIST OF ABBREVATIONS

XPS: X-Ray Photoelectron Spectroscopy

UHV: Ultra High Vacuum

BE: Binding Energy

KE: Kinetic Energy

eV: Electron-Volt

hυ: Kinetic Energy of Photon

Φ: Work Function

FWHM: Full With Half Maximum

AL: Attenuation Length

IMFP: Inelastic Mean Free Path

I: Electric Current or Intensity of Light

$I_{x\text{-}ray}$: X-rays Induced Current

I_{fil}: Flood Gun Induced Current

DC: Direct Current

SQW: Squarewave

ZPC: Zero Point Charge

B.E. Diff.: Binding Energy Difference

V: Electric Potential

R: Resistance or Resistor

R_{ph}: Photoresistance or Photoresistor

C: Capacitance or Capacitor

RC: Parallel Connected Resistor and Capacitor unit

FG: Flood Gun or Function Generator

VCCS: Voltage Controlled Current Source

σ: Conductivity

SPV: Surface Photovoltage

a.u.: Arbitrary Unit

KP: Kelvin Probe

NIR: Near Infrared

CW: Continuous Wave

Ei: Intrinsic Fermi level

Ef: Fermi level

VB: Valance Band

CB: Conduction Band

NDF: Neutral Density Filter

OD: Optical Density

LDR: Light Dependent Resistor

Rsb: Electron Excitation from Surface to Bulk

Rbs: Electron Excitation from Bulk to Surface

TC: Time Constant

ACKNOWLEDGEMENTS

This short, but comprehensively scientific survey is more than achieving my Ph.D. degree, but is an enjoyable period of my life, and an impressive preface of my academic carrier. The most probable reason is the great interaction with my supervisor, Prof. Dr. Şefik Süzer, for the whole duration. I am aware of the privilege of working with my supervisor, and so I express my deepest thankfulness to him.

I would also like to convey my deepest thanks to Dr. Gülay Ertaş, who also supervised me during each step of my work. I thank to Prof. Dr. Mehmet Erbudak, Prof. Dr. Ekmel Özbay, Prof. Dr. Atilla Aydınlı, Assist. Prof. Dr. Ömer İlday, Assist. Prof. Dr. Özgür Aktaş, Assist. Prof. Dr. Özgür Birer, and Assoc. Prof. Dr. Oğuz Gülseren, who have significant roles in completion of my thesis. In addition, I also thank to Dr. Tim Nunney, Dr. Kevin S Robinson, and members of Surface Analysis Department of the ThermoFisher Co., UK, for their patience and kindness to our endless requests about the K-Alpha instrument.

Thanks also to current and previous Süzer-lab members; Merve Taner, Eda Yılmaz (Özkaraoğlu), Pınar Cönger, İlknur Kaya Tunç, Hacı Osman Güvenç, Sinem Yılmaz, Sevnur Kömürlü, Korcan Demirok, Bora İnci, Ferdi Karadaş, and Engin Karabudak.

I would like to express my appreciations to my dear friends for moral support without any remuneration; Cemal Albayrak, Mustafa Fatih Genişel, Yurdanur Türker, Emre Emmez and Emrah Parmak. Also special thanks to Ethem Anber, Emine Yiğit, Hüsnü İçer, and Bülent Öktem.

I always feel myself indebted to Bilkent University and Chemistry Department for providing a high level education and research opportunity.

Finally, I want to express my deepest gratitude to my family and my love Feriza Sezen if I could.

Table of Contents

LIST OF FIGURES

LIST OF TABLE

1. Introduction

1.1. X-Ray Photoelectron Spectroscopy

X-Ray Photoelectron Spectroscopy (XPS) is one of the most frequently used methods for surface chemical analysis. The XPS technique was developed by Kai Siegbahn, who was awarded with the Nobel Prize for his crucial contributions to the field of electron spectroscopy in 1981, and it has been in use intensively since the 1970s.[1-5] The reason that XPS is an admired surface analysis technique is due to its relative simplicity, and ability in deriving straightforward chemical information with a high precision and sensitivity.[6]

As illustrated in Figure 1, XPS analysis is based on the photoelectric effect, where the photon source is x-rays. Therefore, the XPS technique requires an x-ray source as a probe source and an electron energy analyzer to resolve kinetic energy of photoemitted electrons to yield a chemically resolved output. The electron energy analyzer usually comprises a series of electrostatic lenses, a hemispherical kinetic energy separator and a detector for efficiently determining the kinetic energy of photoelectrons emitted from x-rays irritated region of a sample. In addition, an ultra high vacuum (UHV) condition is obligatory for this technique to increase the mean free path of photoelectron, so the chance of photoelectron reaching the detector is enhanced before getting lost. The electrostatic lenses and the hemispherical electron energy analyzer discriminate photoelectrons according to their kinetic energies and allow only energetically selected photoelectrons to reach the detector. The detector counts the number of the energetically

selected photoelectrons which pass through the exit slit of the hemispherical electron energy analyzer for a certain time period. The next step is determination of binding energy value from the kinetic energy information, which is the required energy to bring an electron to Fermi level from its own orbital energy level. The b**i**nding energy of the photoemitted electrons is obtained by using the Einstein's relation which is actually based on the energy conservation of the photoelectric effect;[3-5]

$$BE = h\upsilon - KE - \Phi_{spec} \quad (1)$$

where BE refers to the binding energy, KE to the measured kinetic energy of photoelectron, and hυ is the energy of x-ray photons. Φ_{spec} is the work-function of the electron energy analyzer of the instrument, which is the minimum required energy to remove one electron from the Fermi level of a solid to the vacuum level as demonstrated in Figure 1.

The work-function, Φ, is usually eliminated from Equation 1 because the binding energies of photoelectrons are tabulated by referencing to their Fermi levels rather than the vacuum level.[1, 3-5] This is actually a necessity to eliminate instrumental errors because each energy analyzer has its own characteristic work function and electronic behavior. The elimination of work-function values or with an appropriate energy calibration, the XPS spectrometers can provide at least a universal binding energy measurement for conductive samples in the absence of any charging effect. But for nonconducting samples charging effects are very important and will be discussed in the next section.

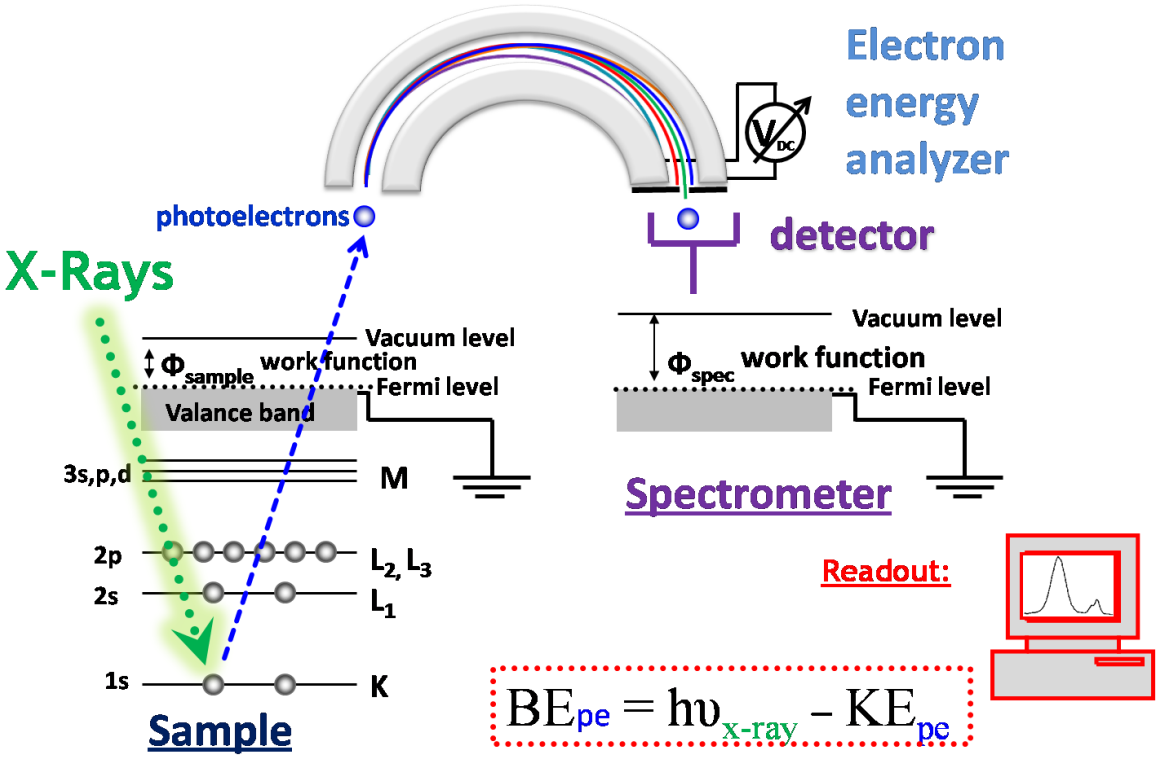

Figure 1. Basic principles and components of XPS experimental setup.

The analytical value of binding energy of the emitted photoelectron includes distinctive information about specific signals of the corresponding atoms. The photoelectrons are preferentially extracted from core (inner) levels instead of valance or outer levels as a consequence of better energy matching between the wavelength (or energy) of the x-rays and the wavelength of the core electrons as represented in Figure 2. Therefore, classifying XPS signals provides distinct chemical and physical information about the sample. However, the XPS technique is able to gather information from only a few outermost atomic layers of the sample due to inelastic collisions of photoelectrons with lattice atom. Although x-rays can reach a 1-20 μm depth into the sample, the probe length of XPS is only approximately 10-20 nm, which essentially depends on the type

(actually the kinetic energy of the emitted photoelectron) of x-ray source and chemical composition of the sample.[3-5]

As expected, the mean free path of generated photoelectrons is much smaller in the solid material if its value is compared with the one in the vacuum environment. Therefore, most of the photoelectrons in a solid cannot survive due to inelastic collisions with other atoms. This is the reason why only a 10-20 nm depth length is accessible by the XPS technique. This also explains the power of the surface sensitivity of the XPS technique. In fact, 10-20 nm depth lengths are the best cases for the lighter atoms which have smaller atomic numbers. It diminishes to a 2-3 nm for heavy elements. This range is governed by the characteristic value of the attenuation length (AL) or inelastic mean free path (IMFP) of the substance, which is usually represented by "λ" symbol.[3-5]

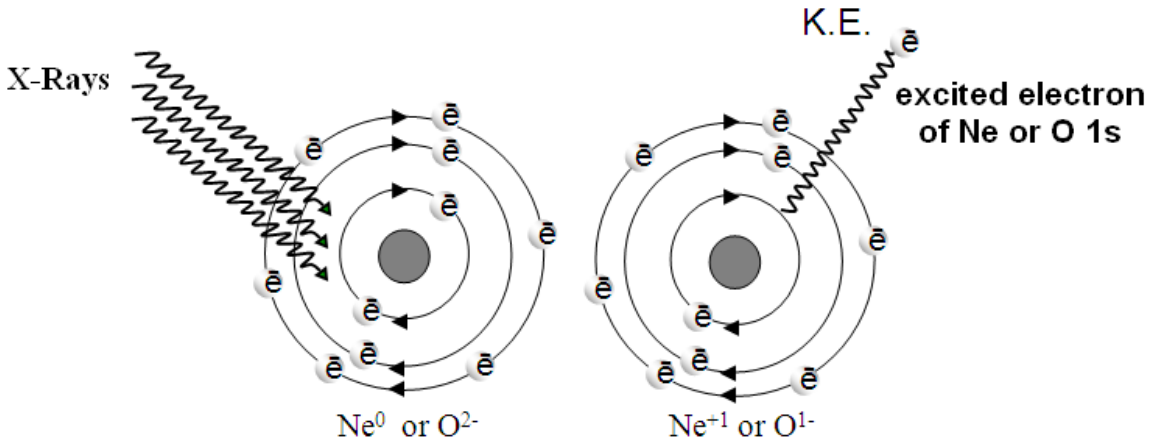

Figure 2. Schematic representation of the photoelectric effect.

The IMFP or AL can be defined as an average distance travelled by a beam of photoelectrons where the intensity decrease to 1/e factor of its initial intensity, due to both elastic and inelastic collisions which cause them to lose kinetic energy and/or to

change direction as demonstrated in Figure 3a,b. The relationship between final and initial intensities of photoelectron beam can be represented by the Beer-Lambert law[7], where is expressed in Equation 2 and demonstrated also in Figure 3b.

$$I/I_0=e^{-d/\lambda} \quad (2)$$

where I, I_0 are representing the transmitted and incident intensities, and d is the distance. This relationship helps us to evaluate overlayer thickness such as a silica (SiO_2) layer on a silicon wafer upto ca. 10 nm. In addition, the AL parameter can also be considered as a function of the kinetic energy of photoelectrons, so a simple empirical formula, the coverage percentage, chain length of overlayer molecule, etc. can be roughly derived between the kinetic energy and AL value of photoelectron for certain type of materials like organic polymers.[8-12] According to the above expression, after traveling along just one λ path length, 63% (1/e) of photoelectrons have already been scattered from their original route. Therefore, using XPS one has a chance to detect only the photoelectrons having a kinetic energy for traveling at least a 3 λ length or more in a solid to reach the surface of the sample.

Thus, with such an extremely short depth length (10-20 nm) XPS emerges as a crucial surface sensitive technique, and it perfectly matches today's demanded technologic requirements for investigations in the nanometer scale. Moreover, the surface sensitivity of XPS can be boosted up by changing the acceptance angle of photoelectrons with respect to the surface plane of the sample. This technique is named as Angle Resolved XPS.[3-5, 13] However, such a surface sensitivity may also become disadvantageous in some cases. For instance, a 10 nm depth length corresponds to just a few ten atomic layers

where one or more contaminant layers on each surface are always present. Hence, extreme care must always be practiced to ensure correct analysis.

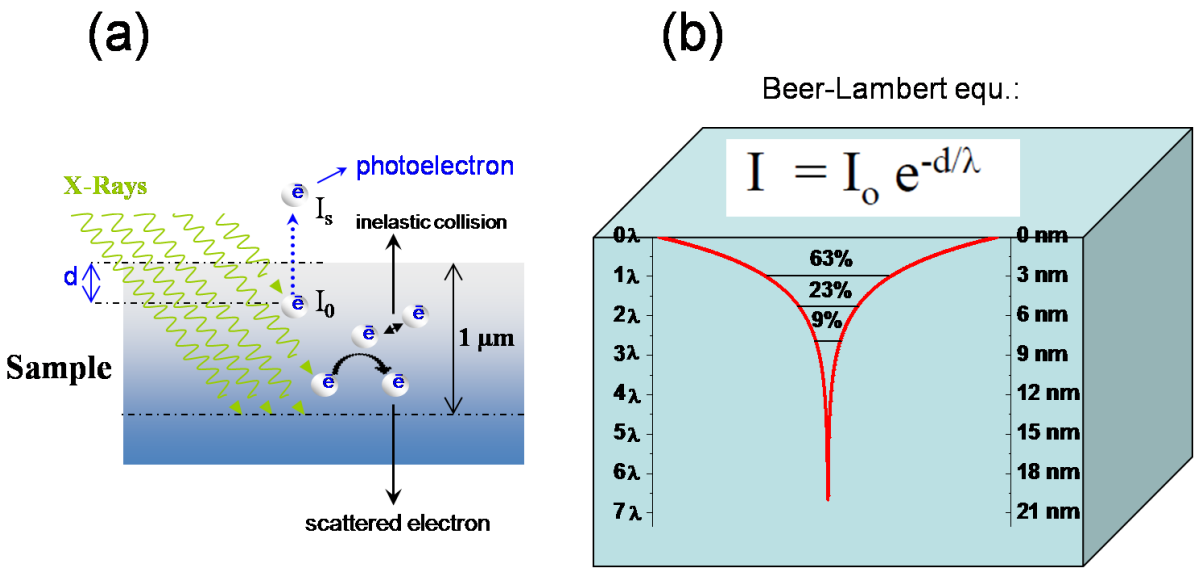

Figure 3. (a) Photoelectric effect due to x-ray radiation and elastic and inelastic collision of photoelectron (b) Beer-Lambert's relation and depth profile of XPS with calculated values of corresponding intensity distribution from first three attenuation lengths.

XPS is a commonly used investigation technique for many researchers in surface science. Even a simple survey analysis of XPS recording in just one minute experiment gives qualitative and quantitative outcomes about the surface of the sample (except for hydrogen and helium) such as elemental identification and atomic concentration information, respectively. The value of peak position (binding energy) of a particular photoelectron provides straightforward elemental identification of atom(s) from which electrons are emitted and have chance to survive till it reaches the detector. The value of binding energy not only provides information on classifying the identity of an atom, but also it provides information about type of atomic orbital such as s, p, d or f.

XPS technique is also an extremely sensitive technique for the determination of the chemical state of the atoms in the surface. Different chemical states of an element in a sample may create contrast as shifts in the binding energies positions. For example, different oxidation states present deviations in the energy levels of the core electrons and as a result in the kinetic energies of emitted electrons. A well known example is that different oxidation states of Si. Si2p peaks of silicon oxide (SiO_x) have chemical shifts as 1, 1,8, 2.7 and 3.5 eV for the oxidation states of Si from +1 to +4, respectively, when compared with metalic silicon which is assigned to have 0 oxidation state (Si^0).[14]

Furthermore, the XPS technique also provides quantitative analysis which is achieved by calculating the relative atomic ratios of the sample surface in a range of 1 to 20 nm using the intensity of the peaks. Other instrumental parameters contribute to this calculation as well. In general, the following formula is used for this purpose;[3, 5]

$$\frac{C_x}{C_y} = \frac{A_x}{A_y}\frac{\sigma_y}{\sigma_x}\left(\frac{E_y^k}{E_x^k}\right)^{\frac{3}{2}} \qquad (3)$$

Here, A is the area of the corresponding photoelectron peak, σ is the cross section of the corresponding orbital, and E^k is the kinetic energy. Equation 3 must also be corrected by individual transmission function of the XPS instrument along the entire kinetic energy axis of photoelectron to get consistent estimation of the atomic ratios. For our work, this feature helps us to check the stoichiometric ratio between elements of a chemical compound of the examined material. Last but not the least, as mentioned before the angle

resolved XPS offers both more surface sensitive information and also depth profile information about the sample by recording XPS data at different electron take-off angles of the sample with respect to the electron energy analyzer.

Lateral space information can also be collected via a series of XPS measurement on the sample at different positions. Then a correlation analysis between intensity information at a certain binding energy value of the photoelectron provides a chemically resolved 2D mapping image about the examined area of the surface of sample. This feature is especially helpful when the surface of the sample contains inhomogeneous overlayer(s). Therefore, a 2D mapping feature enriches our spectroscopic analysis.

The XPS technique has undergone some significant improvements during the last 2 decades. For instance, a differential pumping technique allows operating XPS at near ambient pressure levels (upto 10 mbar).[15-17] This enhancement is important especially for chemists because it moves from a chemically inert UHV chamber to a reactor chamber around the sample compartment containing a certain amount of reactive species. In addition, XPS can be furnished with recently designed two-dimensional (2D) detectors. For instance, while one of these 2D detectors provides a lateral spatially resolved spectrum, the other dimension provides energy resolution. The outcome is actually a 3D spectrum with energy, intensity and space axes.[18] The other type 2D detector provides a parallel angle resolved information without any tilt of the sample but with an energy resolution.[19] Therefore, this type of detector can provide atomically resolved depth-profiles.

1.1.1. Controlled Surface Charging

During XPS measurement, an electron current flows from the sample to the electron energy analyzer as illustrated in Figure 4. As a consequence of this, the emission of photoelectrons from the sample may cause a positive uncompensated charge accumulation, which is referred as "surface charging" in the literature.[20-22] Actually this event also causes a binding energy variation in the XPS spectrum, if the sample is not grounded or a poorly conductive one as modeled in Figure 4. A number of methods have been developed for charge compensation.[23, 24] However, previously published works by different groups including ours, confirm that if the surface charging is properly utilized, it can be a valuable tool for obtaining extra information about the surface electrical and chemical structure of the sample in the nanometer scale and at the molecular level.[22, 25-42] This technique is named as the "controlled surface charging".[6]

In general, the measured binding energy, i.e. the peak position, may vary due to the presence of internal and external factors such as creation of photoelectrons, size[43] and morphology,[44, 45] orientation[46, 47] of specimens and the surrounding electrostatic conditions of the examined atoms. These factors can be considered as internal parameters. External parameters include; applying voltage stress, exposing to stray, and low-energy electrons, ions, photons, chemical spices, etc.[22, 28, 30-33, 35, 38-42, 48-51] These intentional and unintentional variations in peak position (or the binding energy shifts) have been tried to be controlled or compensated by employing a variety of techniques. A completely neutralized experimental condition during XPS analysis is only an ideality because the charging process is a dynamical one and is usually governed by more than one parameter, and/or might be influenced by more than one time domains.

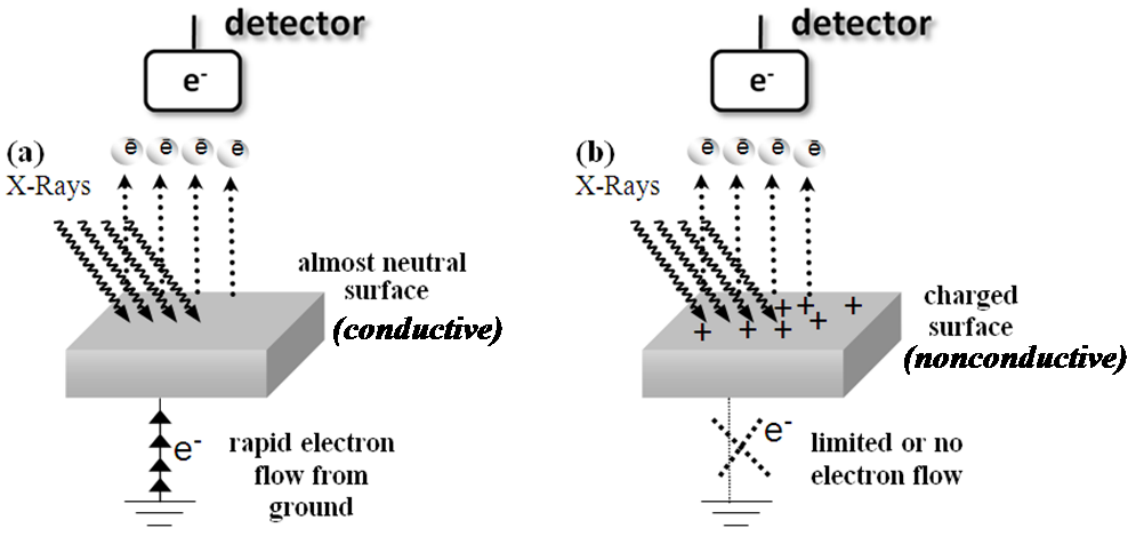

Figure 4. Charging processes in (a) a conductive and (b) a nonconductive material during recording of XPS data.

Applying an external bias potential is one way to vary the positions of photoelectron peaks. For this purposes, a DC stress can be employed to create a potential contrast between different dielectric domains of a sample. In addition, the operation of the flood gun during XPS measurements provides focused low energy electrons on the sample with a specific spot size, intensity, and kinetic energy as illustrated in the inset of Figure 5. For demonstration of this effect, a Si wafer which has a thermally grown oxide layer of a ca. 8 nm will be used. The Si2p region of the SiO_2/p-Si sample is recorded while the sample is grounded, and while it is also subjected to negative and positive 10 V bias potentials. When a -10 V DC bias is applied to the sample, the corresponding peak shifts to a lower binding energy because the applied potential also affects the kinetic energy of emitted photoelectrons. If the sample is a nonconductive one, an additional small shift appears toward the higher binding energy due to a positive charge accumulation on the sample. For the positive DC potentials an opposite situation takes place, since the low energy

electrons are pulled by the sample, to create negative charge accumulation on the sample. The repelling and pulling of the low energy electrons can also be monitored by measuring the total current passing from the sample under varied DC potentials as demonstrated in Figure 5b. When the negative potentials are employed, the current is limited to a 10-20 nA value due only to the presence of a x-ray induced photocurrent, which is not affected by the applied bias. When the applied bias changes to positive values, the sample attracts low energy electrons, so a larger current starts to pass through the sample around μA levels which increases linearly by the amplitude of the applied DC bias. The biased spectra are corrected as much as the amplitude of the external potential to make better comparison among the three spectra. Under normal conditions, the Si2p peak of the metallic Si (Si^0) appears at 99.5 eV, and that of the silica domains (Si^{+4}) at 103.2 eV which correspond the zero-point-charge (ZPC) states.[25, 52] As shown in Figure 5a, the Si2p peak of the pure Si is not affected from the applied bias, once the correction is carried out. This means that the pure silicon has enough-conductivity for our measurements. However, the peak of the silica domains is shifted in opposite directions and is broadened due to accumulation of inhomogeneous charges at different conditions. To determine the amount of charging on the silica domain, the value of corresponding peak position must be compared with the value of the ZPC. A measured peak position higher than the ZPC means that a positive charge is accumulated, and a negative charge accumulation causes a shift to lower values. As shown in Figure 5a, the sample at all three different conditions has positive charges, but the magnitude of the positive charge is different. At -10 V DC bias, it accumulates a larger amount of positive charge compared with the grounded and at +10V. Therefore, the DC biased XPS technique is a simple way

to determine the presence of surface charging. For example, using with this method one enhances the dissimilarities of different dielectric domains.[6, 25, 42]

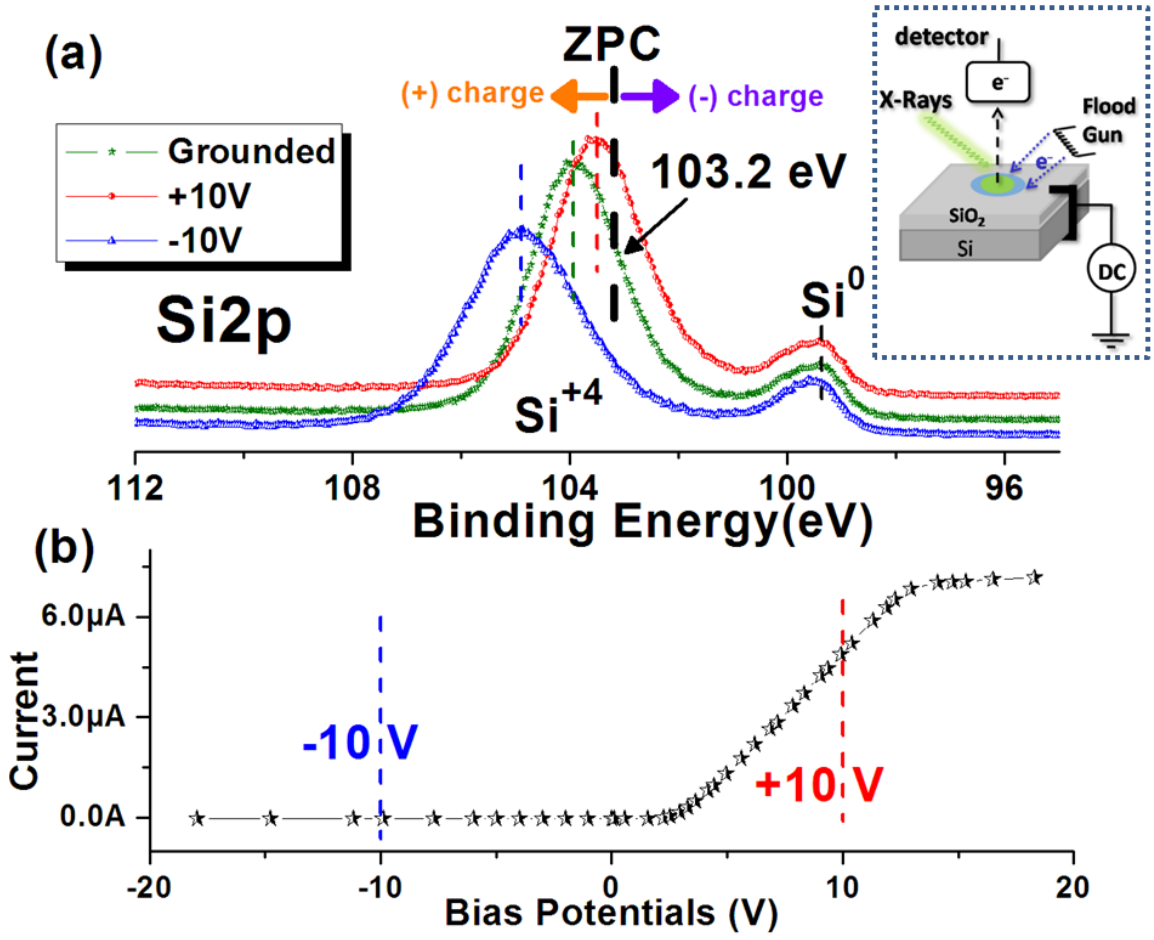

Figure 5. (a) XPS spectra of the Si2p region of a SiO_2/p-Si sample connected to ground (green) and to +10 V(red) and – 10 V (blue) external DC stresses. The thickness of the silica overlayer is ca. 4 nm. (b) The variation of the current passing through the sample under various bias potentials. The inset on the top right depicts the experimental setup.

Similar experiements can also be carried out using a squarewave electric excitation for probing the controlled surface charging in a time-dependent or dynamic fashion. To illustrate the methodology, a Au metal strip is chosen as the sample, and an externally introduced resistor and capacitor pair to impart a dielectric type of a behavior to it.[6] As

Au is one of the best conductive materials, the binding energy positions of photoelectron peaks are equally altered by application of the squarewave stress in the absence of resistor-capacitor pair. This result can be monitored by XPS as represented in Figure 6a,b. Grounded Au metal has an $Au4f_{5/2}$ spin-orbit doublet peak at 84.00 eV and the squarewave electric stress twins the peaks because the sample is subjected to a positive potential during one half of the SQW cycle and to a negative potential during the other half. Therefore, peak separation between the twinned Au4f peaks is always 20.00 eV as demonstrated in Figure 6b. Measurement of exactly a 20.00 eV binding energy difference (B.E. Diff.) translates to the absence of any charge accumulation and/or dissipation. The B.E. Diff. only deviates from a value of 20.00 eV when an external resistance exists in addition to the system: (Au+R). Hence, a less than 20.00 eV B.E. Diff. of the Au+R system is measured at any frequency, with no time dependence as illustrated in Figure 6c. The time dependence is observed only after incorporation of a capacitor to the system: (Au+RC). Therefore, the Au+RC system has a less than 20.00 eV B.E. Diff. at low frequencies while the half duration of the squarewave stress is long enough for ensuring a fully or partially charged and/or discharged state. But, the deviation from 20.00 eV B.E. Diff. recovers at high frequencies because the sample does not have enough time to charge and/or discharge as depicted in Figure 6d. Therefore, by applying external electrical stress and controlling the flow of the low energy electrons, the charge on the sample can be controlled and electric parameters similar to resistance and capacitance values can be extracted from a set of dynamic XPS measurement at different frequencies.[35, 38-42]

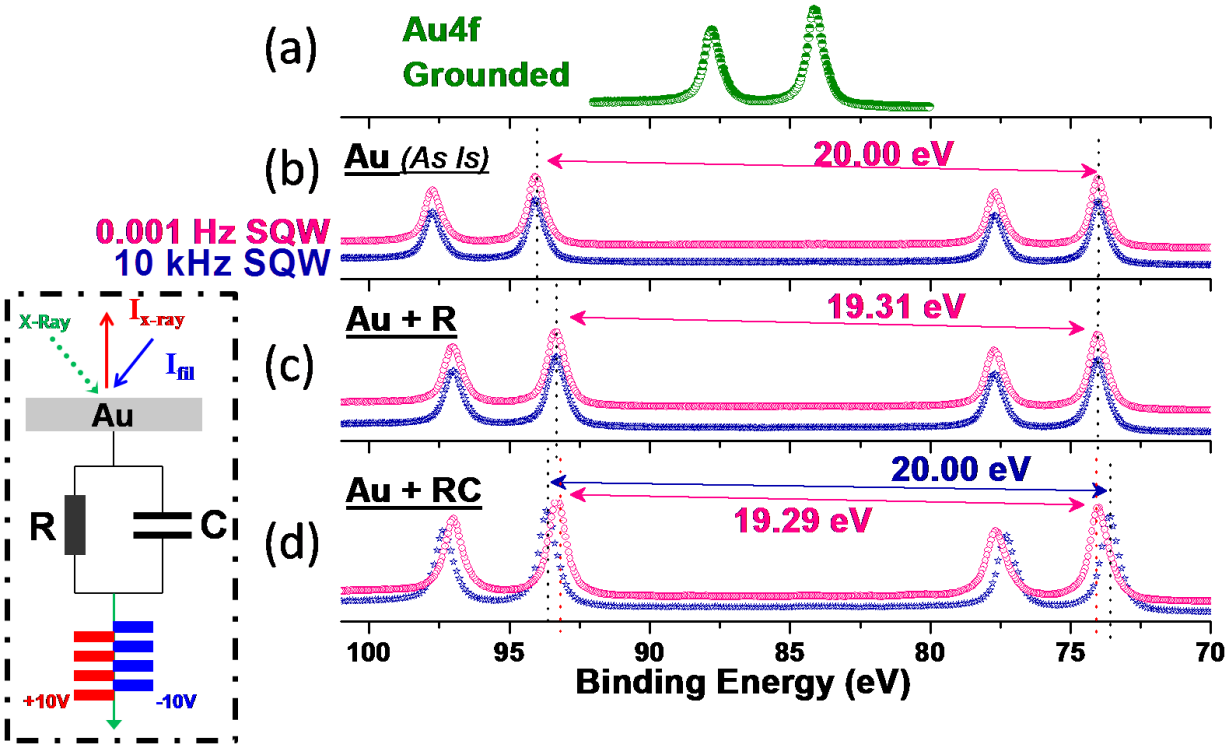

Figure 6. XPS spectra of the Au4f region, when the metal is connected externally to; (a) ground; (b) SQW excitation of ±10.00 amplitude and at frequencies of 10 kHz (navy spectrum) and 0.001 Hz (magenta spectrum). The same spectra are reproduced after connecting to an external circuit, consisting of; (c) a series resistor (R=220 kΩ); (d) a series resistor and a parallel capacitor (R=220 kΩ, C=500 nF). A schematic diagram of the experimental set-up is given as an inset, where $I_{X\text{-}ray}$ represents the electron current due to photo and secondary electrons generated, and I_{Flood} is the current due to the flood-gun used.

1.2. Photoconductivity

Photoconductivity is an optically induced electrical phenomenon for some of the semiconductive materials, which can basically be described as a conductivity enhancement or resistivity reduction of the semiconductor under photoillumination with an appropriate energy.[53] When adequate numbers of photons are absorbed by the

material, electrons are excited from their valance band to their conduction band and/or from mid-gap states such as trap, defect, surface, acceptor, and/or donor related ones, existing between the conduction and the valance band. This process creates an electron-hole pair in the semiconductor. If this event occurs in between or near a junction of n- and p- doped semiconductors, the generated electron and hole pairs are favorably separated from each other. This phenomenon is called charge separation as shown in Figure 7. The charge separation is an important topic and numerous works on this subject convey us that it has crucial potential in applications involving solar cells as a renewable energy source. In addition, the future projections about the energy production techniques indicate that it is one of the most promising technology to meet energy demand of the entire world in the near future.[54] Fortunately today's semiconductor technology assures us that generated electron-hole pairs can be separated from each other by applying proper potentials or well-designed devices with better band gap engineering.[55]

The conductivity of a semiconductor is defined as,[53]

$$\sigma = ne\mu \tag{4}$$

where n is the density of charge carrier, e is the elementary charge constant (1.602×10^{-19} Coulombs), and μ is the mobility of charge carrier at a certain temperature. Furthermore, from definition of photoconductivity any variation in conductivity can be expressed a summation of individual changes of independent variable as follows,[53]

$$\Delta\sigma = \Delta ne\mu + ne\Delta\mu \tag{5}$$

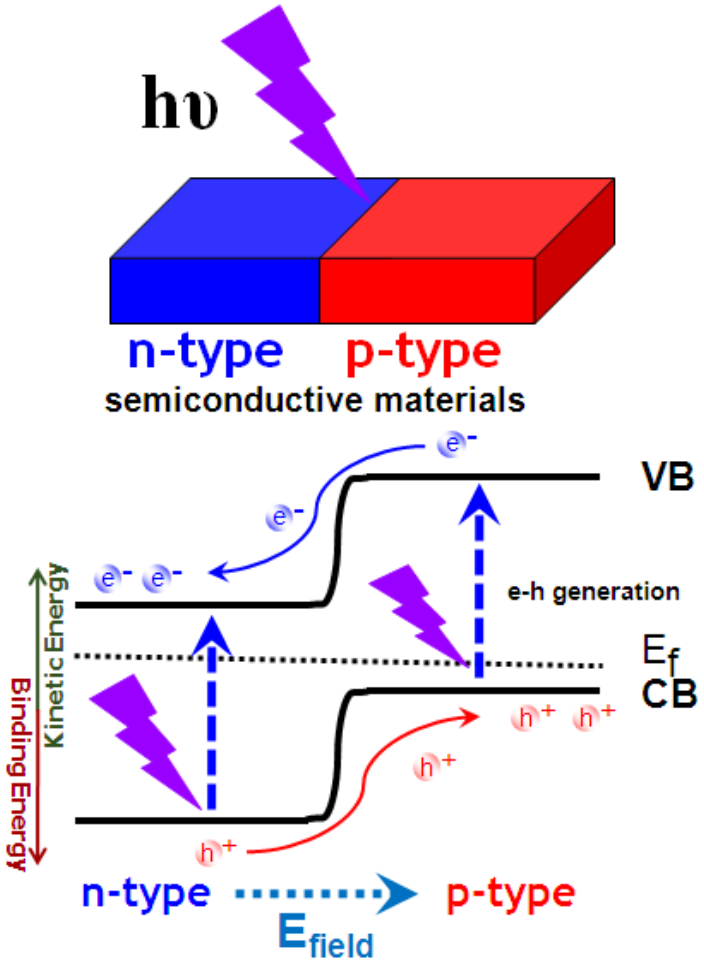

Figure 7. Photoinduced electron-hole generation and separation in between n- and p-type semiconductor.

For our experimental setup, the number of charge carriers can only be affected by introducing a light source or changing its intensity level in certain ways. However, an increase in the intensity level of the light source causes also an increment in the level of the density of charge carriers if the recombination rate of electron-hole pairs is slower than its generation rate. When this condition is fulfilled, we can assume that there is a correlation between the intensity of the light and the variation in the density of charge carriers in the absorbed region of the semiconductor. The mobility of charge carriers is another important parameter for the conductivity of semiconductive materials, and it can

safely be assumed to be constant for our measurement system because the temperature of analyzed sample is around room temperature, and a few degree variation in the temperature of the sample under both laser and x-ray irradiations is not expected to create a significant electrical conductivity change.[55, 56]

1.3. Surface Photovoltage

Surface photovoltage is a surface related phenomenon for semiconductive materials and occurs due to presence of band-bending phenomenon at the surface of the semiconductor.[57-60] The band-bending on semiconductive materials has both intrinsic and extrinsic factors. While doping type and amount, dangling bonds, and surface defects/states can be considered as intrinsic factors, the deliberately or unintentionally absorbed surface species and external stresses such as temperature, electric and magnetic field, etc. are possible extrinsic factors.[58, 61] Under the effect of these factors the surface states of a semiconductor converges to an energy value which promotes a certain amount of charge rearrangement between its surface and bulk. For example, an additional electron accumulation at the surface of n-Si gives rise to an upward band-bending in dark conditions as illustrated in Figure 8a. Under photoillumination, electrons are excited from the valance band to the conduction band. This process might cause a reduction in the extent of the band-bending or even a flattened band condition in the presence of under a sufficient photoillumination as demonstrated in Figure 8b and 8c, respectively. In contrary, a downward band-bending is present for p-Si, which will be elaborately in detail in the following passages

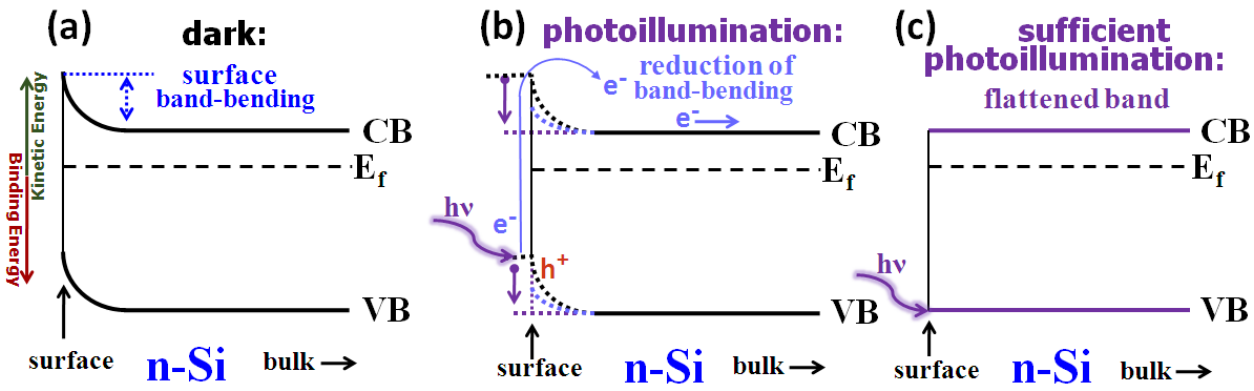

Figure 8. The band diagram of n-Si (a) in dark (b) under photoillumination and (c) in flattened conditions. Adapted from the references 57, 58, 59, and 60.

The surface photovoltage phenomenon becomes a more intensely concerned subject day by day as a result of inventible size shrinkage of electronic device, so previously negligible surface-related effects become more dominant at smaller scales. Measurement of surface photovoltage involves determining both magnitude and type of polarization of trapped charges or built-in potentials at the surface under light illumination. Usually the surface photovoltage corrects the accumulation of charges due to the band-bending by diminishing the built-in electric field. Kelvin Probe (KP) has been the commonly employed technique to evaluate surface photovoltage so far due to its simplicity.[58, 61-63] However, the KP technique does not have any chemical specificity, and it is not more than a well designed surface-compatible electrometer. Previously reported works show that XPS is another technique to directly monitor surface photovoltage with a certain reliability and chemical sensitivity.[57, 59, 64-70] Moreover, the modern XPS instruments have the ability to record the data in the snapshot mode, which provides a fast data acquisition with ca. 0.1 second time resolution for a narrow energy range from a few eV upto 40-50 eV energy window. While this speed of data acquisition is far away from the time domains of fast process involving electron excitation and electron-hole recombination

with the time constants of pico to nano seconds,[66, 67, 69-76] nonetheless, a sub-second time resolved spectroscopy still allows probing dynamics involving dipole and polarization type processes.[51, 77] For example, the time constants of some of the charge accumulation and dissipation processes in dielectric and insulator type layers are around or just below a time scale of second. Hence such process can easily be monitored with the fast data acquisition method of XPS.[42, 49-51, 78]

As discussed before the distinct surface electronic structure of semiconductors causes upward and downward band-bending for the n-type and p-type doped semiconductors, respectively.[57-59, 67] As it is well established, the different chemical properties of dopant atoms cause drastic changes on electrical properties of semiconductor. For example, if we assume that there is no surface related effect(s) on a Si wafer; namely no band-bending, then a n-type phosphorus, P doping into Si crystal introduces a stationary positive charge on itself and a mobile negative charge into semiconductor as illustrated in Figure 9a. For p-type boron, B doped Si, the stationary charges are negative and they are trapped onto dopant B atoms while the mobile positive charges are delocalized into the system as illustrated in Figure 9b.[55, 56] The upward band-bending of an n-type semiconductor is the result of the built-in electric field at the edge or surface of semiconductor due to mainly the discontinuity of the lattice, namely surface effect. This electric field is damped by pushing of the mobile negative charges to the surface of n-type semiconductor and remaining stationary positive charges onto dopant atoms inside the bulk of the solid. Meanwhile, the entire system has still a totally zero charge. However, the charges are different and vary from the surface to the bulk, which causes a depletion region (bended

band). The average length of the depletion region for Si was reported to be around 100 nm range as illustrated in Figure 8,10.[67]

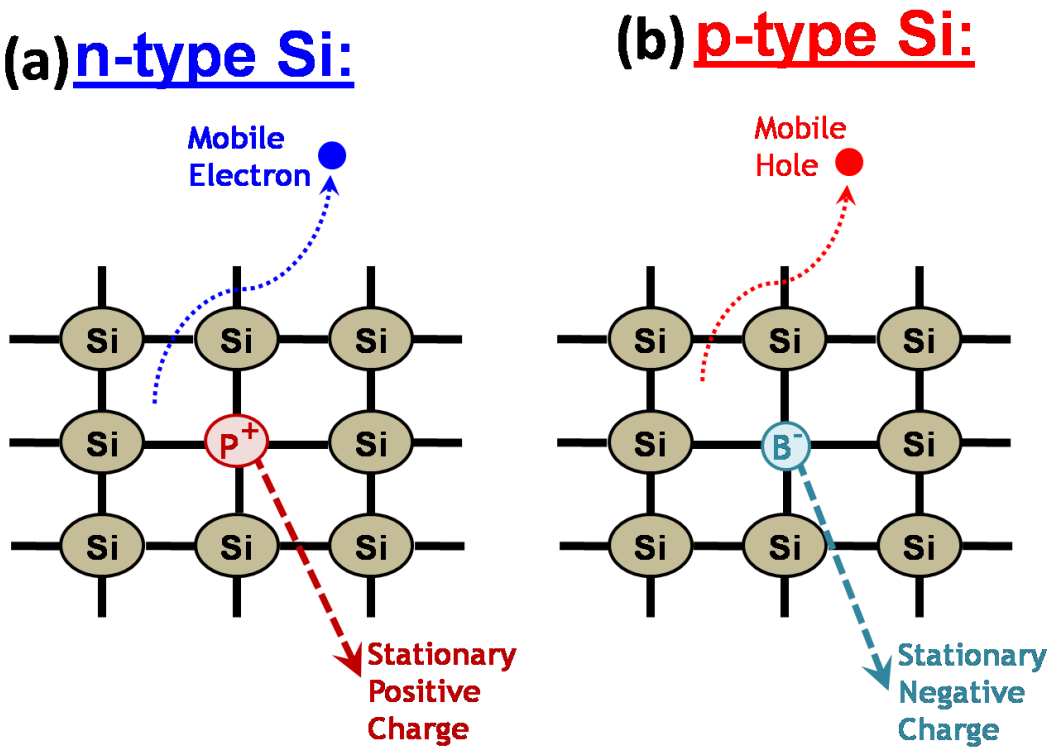

Figure 9. The representative Si lattice structures of the n- and p-type doped with (a) P (b) B elements. Adapted from the references 55 and 56.

Owing to the 10 nm depth sensitivity of the XPS technique, the charge accumulation at the surface of n- and p-type semiconductors can be measured by XPS. The band-bending of n-type semiconductor causes a certain amount of energy shift, which can be reduced by exposure to sufficiently energetic and intense photoillumination, which is also called surface band-flattening[58, 62] as measured and modeled in Figure 10a,b. As a result, the flattening of the upward band-bending of the n-type Si is monitored at a higher binding energy of the Si2p peak under photoillumination. Similarly, the downward band-bending of the p-type Si exhibits an opposite shift, and is called p-type surface

photovoltage shift as shown in the right panel of Figure 10. In other words, the surface band-bending effects of the n- and p- type doped Si might be reduced or entirely removed by proper photoillumination as they are measured by XPS to be +0.11 and -0.19 eV shifts, respectively. Unfortunately, the commercially available lab-based XPS instrument has an elemental sensitivity about ~0.1 atomic percent, and, it does not have sufficient sensitivity to probe directly the dopant atoms. However, the dopant dependent photoelectron peak shift can be traceable with XPS due to referencing or correcting of the peak position with respect to the pinned Fermi levels.

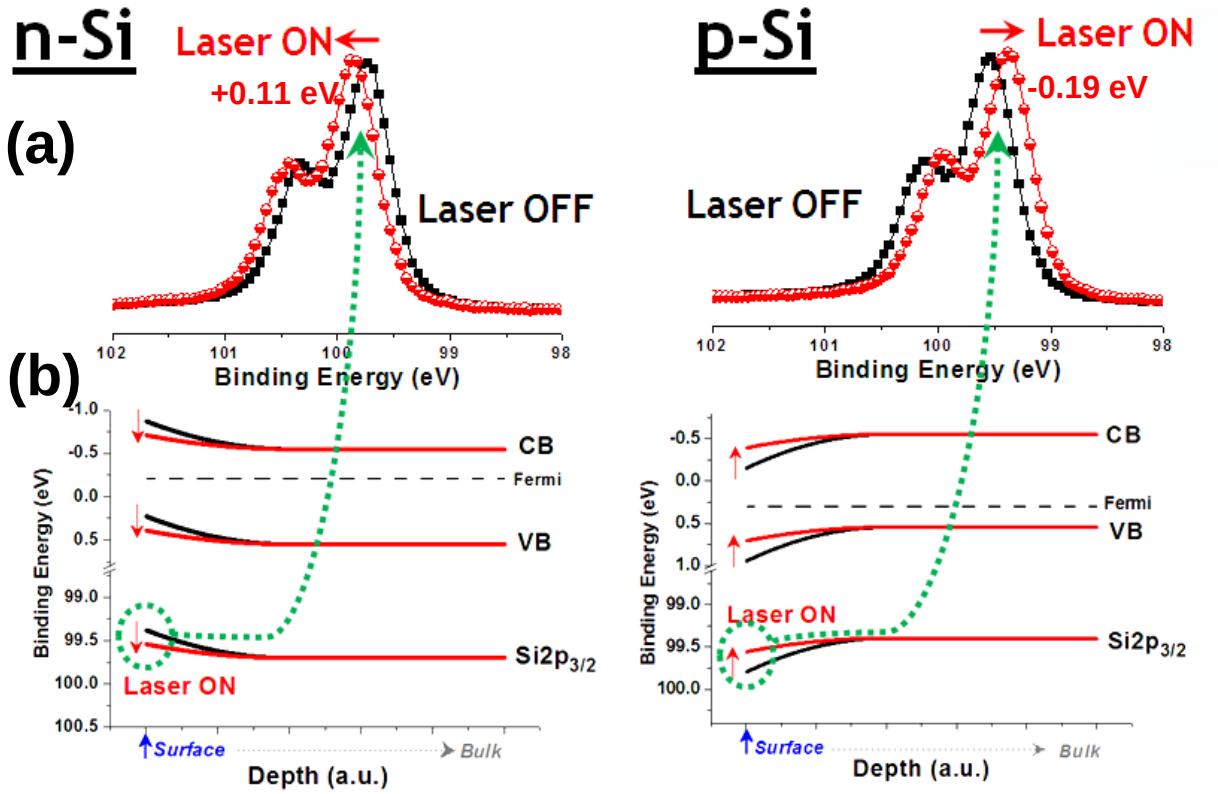

Figure 10. (a) The XPS spectra and (b) band diagram of n- and p-type doped Si without and with exciting light source (violet laser). While the left panel belongs to n-type Si, the right panel belongs to p-type Si. The dotted green circular and line indicates effect of light source onto both band diagram and XPS spectra of n- and p- type doped Si.[79]

2. Aim of Work

The electrical and optical properties of today's high-end technologic devices such as photovoltaics, photonics, optoelectronics, sensors, etc, become more crucial due to the required dramatic reduction in the size of such devices to reach faster processing powers with lower energy consumption. Moreover, the thickness of the semiconductor layer in such devices has already been downsized to few tens of atomic layers, so that the properties of the interfaces between different types of junctions and/or materials have become more pronounced. In this project we deal with a similar complexity for trying to distinguish voltage variations due to charging, surface photovoltage, and photoinduced conductivity changes developed in the semiconductive layers and/or at interface between different semiconductive layers as well as their substrates in a chemically addressed fashion.

SiO_XN_Y/Si,[37, 80] SAMs/SiO_X/Si,[52, 81, 82] polymer and/or metallic nanoparticles/SiO_X/Si,[28, 38, 39, 83, 84] HfO_X/Hf,[85-87] Al_YO_X/Al and WO_X/W,[30] GeO_X/Ge,[88] and SiO_X/Si,[28, 31, 34, 35, 78, 88-92] systems have been extensively investigated by Suzer's group for better understanding the nature and the mechanism of charging/discharging properties which are vital for developing next generation devices. For that, a technique has been developed for recording the shifts in the positions of the XPS peaks in response to different forms of electrical stimuli for probing dynamics of charging/discharging processes of thin dielectric films, which we have named as "Dynamic XPS". Modulation of the electrical signals in the form of square waves at different frequencies enables us to extract certain dielectric properties such as effective resistance and capacitance values in a chemically resolved fashion. This makes XPS a more powerful technique for

characterizing today's demanded nano or optoelectronic devices. Besides, these early published results have shown us the power of XPS as a charge sensitive technique.

In the present work, we have introduced photoillumination as an additional form of the external stimulus and investigated the combined optical and electrical responses of different semiconductive material such as n- and p-type Si samples and with thermally grown ca. 5 nm silica overlayer, as well as n- and p-type GaN, and CdS films samples which were grown using different routes. The present contribution is a continuation of our earlier work, where we try to distinguish between electric and photo-induced processes. Furthermore, these findings allow us to demonstrate that XPS is a surface characterization technique to track the potential variation on the sample under photoillumination. All these methodologies allow us to extend the Equation 1 and add new terms to extract potentials created by optical and electrical stimuli both in static and dynamic fashions, expresses as;

$$BE = h\upsilon - KE \pm e\cdot V \pm e\cdot Q/C \pm e\cdot I\Delta Rph \pm e\cdot SPV \quad (6)$$

where V, Q, C, I, Rph, SPV, and e are bias potential, accumulated charge, capacitance, current, photoresistance, surface photovoltage, and elemental electron charge, respectively. The use of this equation will be elaborated in the "results and discussion" part.

3. Experimental

3.1. Sample Preparation

The Si wafers (100) were purchased from the institute of electronic materials technology via the "www.universitywafer.com". Phosphor and boron doped n- and p-type Si wafers are one side polished wafers, and the values of resistivity are reported as 10-20 Ω·cm and 28-31 Ω·cm, respectively. The wafers are washed with acetone or ethanol to remove surface contaminants and dried under nitrogen flow. Then the wafers are left in a concentrated HF solution for 2 min to remove the native oxide layer on the substrate and other chemically bonded organic/inorganic contaminants. Afterwards, the wafers are washed again firstly with de-ionized water and subsequently with acetone to remove any unwanted species. Finally, they are dried under nitrogen flow one more time. This procedure provides a bare Si sample without much of a native oxide layer up to 30 min in atmosphere at room temperature.

The surface patterned Si wafers were manufactured with a high power fiber coupled near-infrared laser by the group of Dr. Ömer İlday (Physics Department of Bilkent University).[93-95] The doted, 2D scanned, and line shape patterned substrates were prepared for investigating with XPS. In addition, several patterned Si substrates were chemically cleaned with HF before the process to discriminate any laser induced chemical modifications by avoiding residual oxides. The usual laser patterning process was performed in atmosphere.

The CdS film was grown on the Si substrate by laser ablation technique and obtained from the group of Dr. Attila Aydınlı (Physics Department of Bilkent University). The successive ion layer absorption and reaction (SILAR) technique[96] was also performed to achieve ultra thin high quality CdS layers on Si substrate containing ca. 5 nm thermally grown oxide layer. Initially the Si substrate was treated with 0.01 M NaOH for further cleaning and obtaining chemically more active surface to increase homogeneity of the films. Subsequently, the substrate was immersed into sequentially Cd^{2+} cation (0.05M) and S^{2-} anion (0.05M) solutions successively to grow thin CdS films. A washing step of substrate with de-ionized water was followed after each ion bath step.[96] The ionic and washer solutions were frequently replaced with fresh solutions. The thickness of films can be controlled by increasing the number of immersion cycle, and we did not perform any annealing step.

A commercially available CdS based photoresistor (OEM) was used to probe a location depended resistance investigation. The encapsulated polymeric overlayer of the photoresistor for moisture-resistance, optical focusing and antireflection features were lifted off with acetone. An ultrasonic shaker treatment with acetone solution is employed for a further cleaning step during a 30 second period. After lifting off and washing processes, the photoresistor immediately was transferred into the ultra-high vacuum chamber to prevent oxidation and/or contamination. The virgin sample was analyzed without further ion etching, except for performing chemical depth profiling experiments.

The GaN samples were grown on double polished c-plane sapphire with a low-pressure metalorganic chemical vapor deposition (MOCVD) system (AIX 200/4 RF-S) in the group of Dr. Ekmel Özbay (Physics Department of Bilkent University). The Si doped

n-GaN had a thickness of 1 μm with ~ $1.2x10^{+13}$ cm^{-3} electron carrier concentration and ~300 cm^2/V.s mobility. The Mg doped p-GaN was ~0.5 μm thick with hole concentration of $4.5x10^{+17}$ cm^{-3} along with a mobility of 11 cm^2/V.s.

GaN is a wide band gap semiconductor and the band gap is reported as a direct one[97] and its value is reported as 3.4 eV.[98] For our photoillumination measurements we have employed four different lasers; violet (405 nm), green (532 nm), red (635 nm) and near-infrared laser (980 nm) the corresponding photon energies are 3.1, 2.3, 2.0, and 1.3 eV, respectively. Therefore, even with the violet laser, excitation is not band to band, but a sub-band excitation. The sub-band excitation has advantages and disadvantages which will be discussed in the "results and discussion" section.

CdS and GaN samples were etched with the Ar^+ ion gun of the XPS instrument employed to get rid of surface carbon and oxygen contaminants as much as possible till we reached a point that it was below the detection limit of our XPS instrument. Although, the kinetic energy of Ar^+ ions can be accelerated upto 4 kV, usually a low energy value (1-3 eV) has been chosen to avoid surface damage. This is a crucial point because even a small amount of damage can completely change electronic properties of semiconductors, so extreme care must be exercised during usage of the ion gun. For example, while Ar^+ ion etching of the CdS sample with a 3 kV kinetic energy for about one hour duration does not leads to Ar atom implantation into CdS sample, on the other hand significant amount of damage and insertion of Ar^+ ions could easily be incorporated into the Si wafers. For example, when Si wafers cleaned with Ar^+ even for a short time and a low kinetic energy power (such as a ten second exposure duration with 200 V kinetic energy),

the Ar peaks started to be detected with XPS. Therefore, for most of our measurements reported in this thesis Si based samples were not cleaned with ion gun.

3.2. Instruments and Technique

All of the XPS measurements were carried out using a ThermoFisher K-Alpha XPS instrument which is furnished with a monochromatic Al Kα (at 1486.68 eV) x-ray source. The operational chamber pressure is usually kept around 10^{-9} mbar. The X-ray beam is directed to the sample with a 55^0 incidence angle with respect to sample normal via a quartz crystal which also provides monochromatic filtration of the x-rays as demonstrated in Figure 11. The electron energy analyzer is located at the top of the sample with a 90^0 orientation with respect to the surface plane of sample. Hence the take-off angle is 90^0. An electrostatic lens system is employed to collect photoelectrons from a $\pm 30^0$ solid angle from the normal. The electrostatic lenses also collimate and re-focus the emitted photoelectron to the entry slit of the hemispherical electron energy analyzer, so the actual take-off angle from the sample surface is a 60^0 solid angle as illustrated in Figure 11. As a standard stability checking experiment of x-ray flux of the instrument with an Ag reference sample, the instrument yields >3 million counts per second at 200 eV pass-energy from $Ag3d_{5/2}$ line which also has one of highest x-ray absorption cross section. The spot size of the x-ray beam can be chosen from 30 to 400 μm diameter, but a 400 μm spot size is used for most of our measurements, unless otherwise mentioned. Three electronic CCD cameras (Bosch LTC0455/11) are mounted on the chamber of the K-Alpha system to assist sample transportation and to ensure superimposed intersection of the sample for x-ray, ion and flood guns with a better than 1 μm precision.

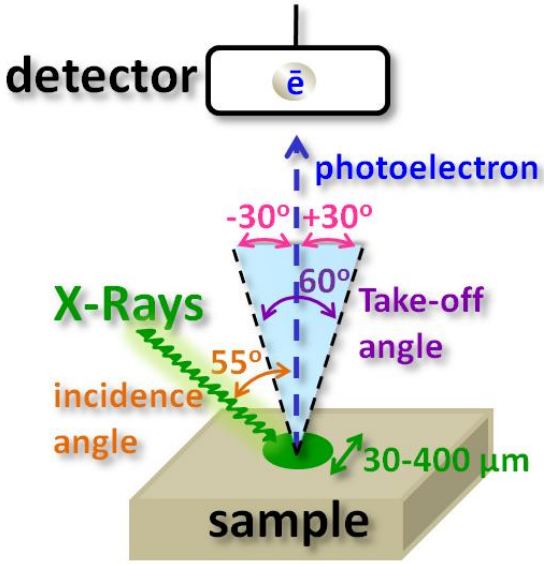

Figure 11. The arrangement of experimental setup of the K-Alpha instrument.

The instrument has a resistive array detector with 128 individual channels. In a normal scan mode, all energy channels of detector are used for averaging output to improve signal to noise ratio, so the required experiment time significantly decreases for a reasonable resolved spectrum in this mode. The detector also provides an energy resolution that is better than 0.02 eV.

In the snapshot mode, the detector can make parallel counting for different energy windows and allows recording a narrow range spectrum at only one dwell time of ca. 0.1 s. We recognized that this duration was not consistent with real experimental measurement time. After an efficient collaboration between the Surface Analysis Department of the ThermoFisher Co. and our team, this lag-time is now reduced to 50-70 ms by avoiding assigning of same settings for successive snapshot measurements. Now the fastest data acquisition speed between successive snapshots is shorter than 0.1 s with reasonable energy resolution and signal to noise ratio. This speed is important for us

because some charging/discharging processes have time constants in this time scale. Therefore, these types of processes can now be traced for the first time with a lab based XPS instrument, although, the synchrotron type sources and special multi-channeltron based detectors can have been reported to record data much faster than our speed (0.1 s) due to both higher brightness of the light sources and dedicated detector systems.[70, 74]

Several other modifications were also made on the standard sample holder of the K-Alpha system to achieve an electric connection port. Now, the sample holder can be externally connected either to the ground, a DC power supply, or to a pulse generator from both top and bottom sides of the sample as illustrated in Figure 12. Our electrically isolated sample holder can also provide an extra ground connection on the sample, so devices can now be analyzed during a more realistic electrical operation conditions by driving a sufficient amount of current to extract electrically resolved and chemically addressed data with just one probe. Stanford Research System DS340 is used as the pulse generator for our dynamic XPS measurement. In addition, Stanford Research System DS345 is used to generate sweep frequency of the squarewave function to gather faster impedance type measurements.

The K-alpha spectrometer is equipped with a flood and an ion gun unit. The ion gun can be operated to generate energetic Ar^+ beams at kinetic energies between 200 V and 4 kV to clean the sample and/or to obtain depth profiles. The flood gun is used to neutralize sample's surface during the measurements. The flood gun generates fluxes of low-energy electrons and Ar^+ ions at 0-2 eV and around 20 eV kinetic energies, respectively. The kinetic energy of low energy electron and Ar^+ ion fluxes can also be controlled.

Moreover, the leak valve of Ar gas can be manually closed and the flood gun can be operated to generate only a low-energy electron flux.

XPS peaks are fitted and deconvoluted by both a third-party free program, XPSPEAK95 (version 2.0)[99] and a dedicated program, Avantage® which is provided by the ThermoFisher Co. The binding energy scale of XPS instruments are calibrated using the reference peak positions of Au $4f_{7/2}$ (84.00 eV), Ag $3d_{5/2}$ (368.26 eV) and $Cu2p_{3/2}$ (932.67 eV).

3.2.1. Method and Model of Photo-Dynamic XPS

The dynamic XPS method is based on recording XPS spectra while the sample is subjected to an electrical stimulus with different forms and frequencies under the flood of low-energy electrons and/or Ar+ ions. A MATLAB® routine is used to simulate the dynamical XPS spectra. This program plots the calculated B.E. Diff. between the twinned peaks vs. the value of the corresponding pulse frequency for any arbitrarily assigned resistance and capacitance values. The solution is obtained by trial of a set of arbitrarily chosen R and C values in order to find the best match between the calculated and the experimentally measured B.E. Diff. vs. the frequency of the external electrical stimulus. Detailed information about the experimental method and software is available from our previously published articles.[35, 38, 40-42, 48, 88, 100]

In addition, different electrical models are also used to calculate the variation in the value of photoresistive materials under different forms of optical stimuli. An external

photoillumination with different laser sources is incorporated to probe the photo-dynamic processes as illustrated in Figure 12. Three visible and one near infrared lasers are used in the continuous wave (CW) mode as the excitation sources. The visible lasers have wavelengths of emission peaks at 405 nm, 532 nm, and 635 nm, and from now on they will be named as violet, green, and red lasers. The violet laser (CrystaLaser BCL-180-405) is a solid state laser and has a 180 mW nominal power output. The green laser (noname) has a nominal output power of more than 200 mW. These two lasers have a well defined circular spot about 1x1 mm size. The red laser (noname) has a maximum power output around 150 mW, and it has an approximately 4x2 mm rectangular shape. The near infrared laser (Oclaro LU980N-R) has a peak wavelength of 980 nm with a nominal 180 mW power output. Furthermore, the power output of near infrared (NIR) laser can be tuned by adjusting the current of the power supply. The spot size of the near infrared laser is around 1x1 mm, and the shape of its spot is circular. The shape and size of spots of lasers are captured by the digital camera of the K-Alpha as shown in Figure 13. Total individual spectral output powers of the four lasers are also measured with a Melles Griot Broadband Power Meter (13PEM001). If we compare intensity of four lasers, the red laser has a larger spot size, hence the intensity is at least one order of magnitude value less than the other three lasers. The corresponding energies of the violet, green, red, and near infrared lasers are 3.1, 2.3, 2.0, and 1.3 eV, respectively.[49-51] The characteristic parameters of the four laser sources are summarized in Table 1. Although we do not know the exact incidence angle of the laser sources, it should not be much different from 45^0 with respect to the sample normal because of the cross-sectional chamber design of the instrument.

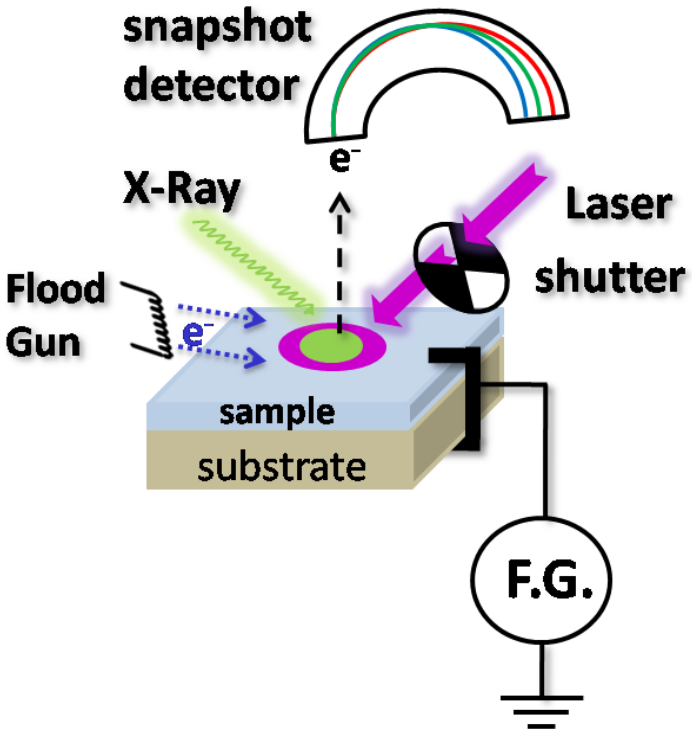

Figure 12. The method of the photo-dynamic XPS.

Table 1. The characteristic properties of the laser sources.

Name - Color	Wavelength *(nm)*	Energy *(eV)*	Power *(mW)*	Spot Size
Violet	405	3.1	180	1x1 mm
Green	532	2.3	>200	1x1 mm
Red	635	2.0	<150	2x4 mm
NIR	980	1.3	180	1x1 mm

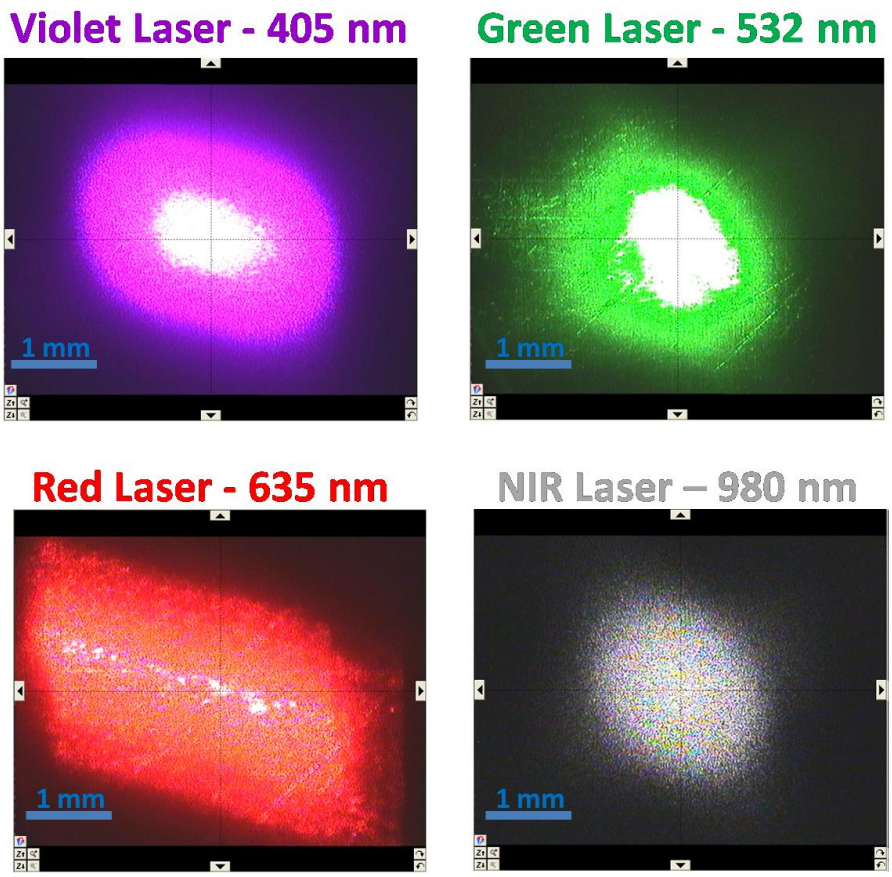

Figure 13. The snapshot frames of spots of violet, green, red, and NIR lasers. The frames are captured with the digital camera of K-Alpha.

The other optical accessories were purchased from Thorlabs Co., and all optical source and apparatus are built on an optic breadboard which has a 30x60 cm dimension as shown in Figure 14. The main optical path is designed for the violet laser, and its beam is approximately 11 cm above from the breadboard and is perfectly parallel-aligned to the breadboard. Two stationary aluminum coated mirrors are used to direct the beam of the violet laser to the sample in the vacuum system via a transparent optical port on the K-Alpha instrument. The optical paths of the green and red lasers are incorporated with the main optical path with additional one stationary and one flip

mounted aluminum coated mirror. The near infrared laser is integrated at an interposition of the main optical path with a flip, kinematic mount, and collimator. All mirrors also have their own kinematic mounts for a fine calibration of their light-paths on the breadboard and spot positions on the sample. The two digital cameras of the K-alpha instrument are focused to a 5x5 cm area on the sample, so the calibration of light spots on the sample can be achieved with sensitivity better than ca. 0.1 mm. The digital cameras are also sensitive to near infrared light to assist the alignment of the NIR laser, which is impossible with a human eye. A plano-convex lens with a 1 meter focal length is used to minimize the diffraction of beams and to achieve an intense and a small spot size on the sample.

A natural density filter (NDF) can also be inserted into the optical system. The NDF provides to control the intensity of light between continuously variable 1-4 optical density (OD) units, which corresponds to between 10% and 0.01% transmission of the incident light, respectively. A homemade mechanical shutter is also integrated to the optical system to allow experiments with successive laser on and off modes, without interruption of the state of the lasers. The speed of the shutter can be controlled with a squarewave function generator. The speed for the shutter can be controlled from 10 Hz to a small value as much as 0.0001 Hz: At higher than 10 Hz frequencies, the response of the shutter is not suitable, therefore, a MC2000 Thorlabs optical chopper can also be integrated into the optical system, which provides a chopped light source from 1 Hz to 10 kHz with three different blades. Consequently, while applying a squarewave electrical stress turns the XPS instrument to a dynamic one, integration of

photoillumination with a shutter or chopper component to our system results, in a photo-dynamic XPS measurement system.

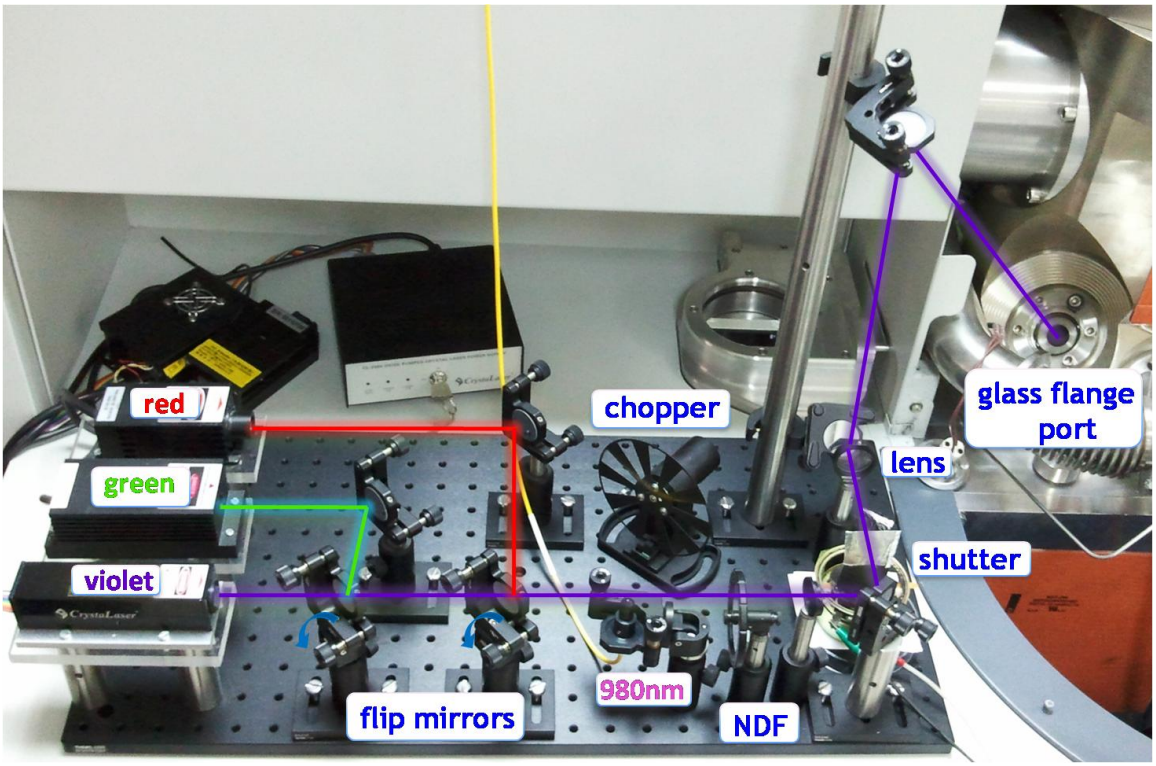

Figure 14. The optical breadboard and other optic component of photo-dynamic XPS system. The most of components are labelled and the pathes of laser beams are represented by properly colored lines.

The theoretical model of the dynamic XPS is based on a calculation of the corresponding XPS spectra by using numeric solutions of a simple lumped circuit as illustrated in Figure 15. For example, the Si substrate has a certain photoresistance (R_{ph}) value, and the SiO_X dielectric layer is approximated by a capacitor (C) and a resistor (R), and another parallel connected photoresistor, R_{ph}, and C unit represents a photoconductive CdS layer. The currents of I_{xray} and I_{fil} are modeled as a voltage controlled current source (VCCS).[35, 38-40, 42, 88] This lumped circuit is used to calculate the

response of the sample to each type electrical and optical stimuli and at any frequency. As a result, an effective resistance (and/or photoresistance) and capacitance value of the sample can be extracted using our model and experimental data for both laser off and on states.[41]

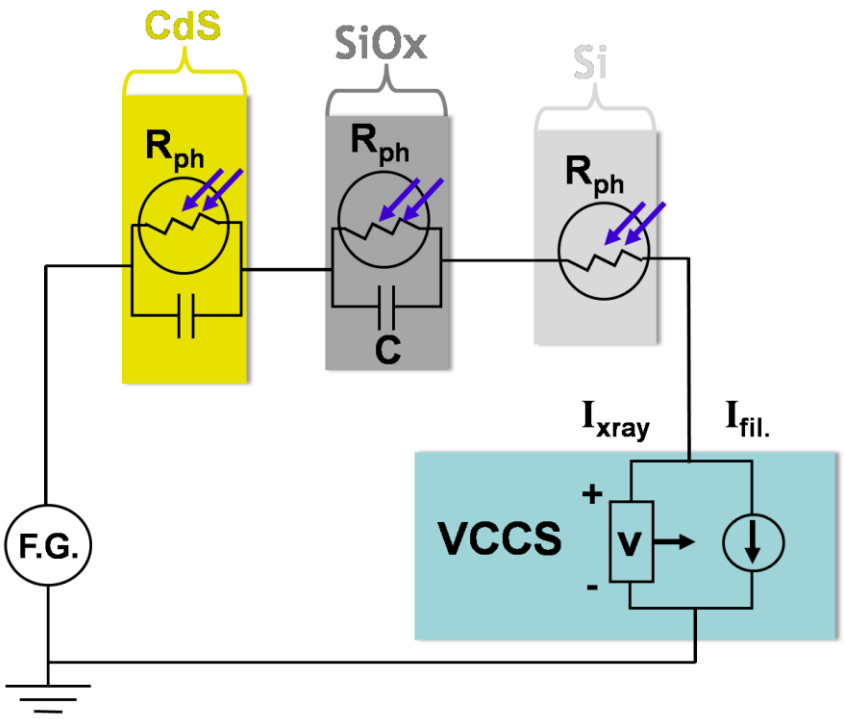

Figure 15. The model of the photo-dynamic XPS.

4. Results and Discussion

4.1. Surface Photovoltage and Band Offset Measurements on n- and p-type Si

The band-bending creates further complications in terms of device performances. Moreover, these effects become more pronounced for small size devices where the surface-to-bulk ratio increases significantly. For a better understanding of the nature of the surface photovoltage and the band-bending structure of semiconductors, n- and p-Si samples are investigated with the photo-dynamic XPS technique. As illustrated in Figure 10 and 16, n- and p-type doped Si samples have bands bended in opposite directions to reduce the energy gap between the mid-band intrinsic energy level (E_i) and the Fermi level at the surface. In other words, the surface related effects force the Fermi levels to pin around the E_i level. The possible reasons for this kind of surface related semiconductive behavior were mentioned before. Therefore, the band-bending effect at the surface of semiconductive materials changes to approach an almost undoped (intrinsic) Fermi level position. This induces a depletion region at the surface of semiconductive materials, which spans form the surface to the bulk as was shown in Figure 8 and 10b.

As a result of the Fermi level pinning, the peak position of the n-Si appears at a higher binding energy than the p-type Si, but in reality the opposite band-bendings bring the peak positions of the n- and p-Si to a closer energy as shown in Figure 10 and 16 *(see also Figure 21a for a better demonstration).* Therefore, the developed surface

photovoltages of n- and p-type doped Si samples under photoillumination have opposite polarities. The measured surface photovoltage responses of the Si2p peak with XPS are shown in Figure 16.[50]

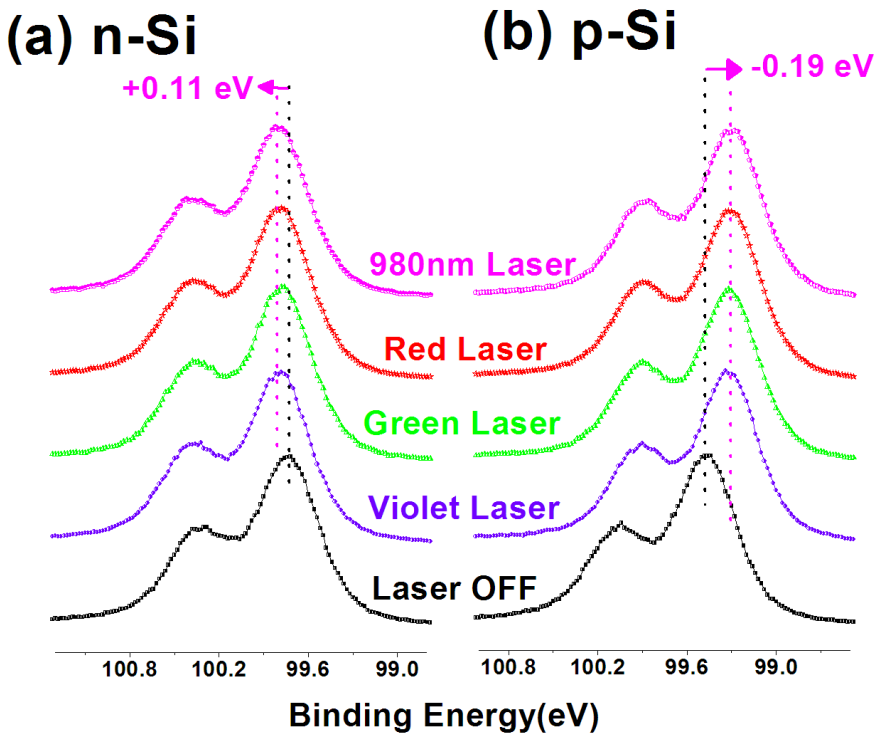

Figure 16. The XPS spectra of Si2p regions of (a) n- (b) p-type doped Si without and with violet, green, red and near infrared laser excitations.

The variation of the laser energy and intensity on the surface photovoltages of the n- and p-Si are also investigated with different lasers using NDFs. All of the four violet, green, red and NIR lasers are employed for this purpose. Note that, the photons generated by our four lasers have energies greater than the band gap of Si (1.12 eV)[101] at room temperature. Hence, they all produce an equivalent surface photovoltage shift on both n- and p-type Si wafers as shown in Figure 16. Tuning of laser intensities might help us to determine that whether the sample is already saturated by photoillumination or a further surface photovoltage shift may be possible. The optical density is also considered as an

extent of absorbance. The relationship between the optical density (OD), transmitted (I), and incident (I_0) light intensity is represented as:[56]

$$\frac{I}{I_0} = 10^{-OD} \tag{7}$$

This is a logarithmic relation between the optical density and the transmitted light intensity. Hereafter, instead of a value of light intensity, an equivalent of the OD will be used, and the surface photovoltage plots will be drawn in a semi-logarithmic fashion. As depicted in Figure 17, a low level filtration of the light with NDFs does not create any measureable variation in the XPS peak position of the sample, so the p-Si sample has already been saturated under this intensity level. As expected, further reduction of the intensities with the NDF exhibits an almost linear response between the logarithm of the intensity level of the light and the surface photovoltage response.[55, 56]

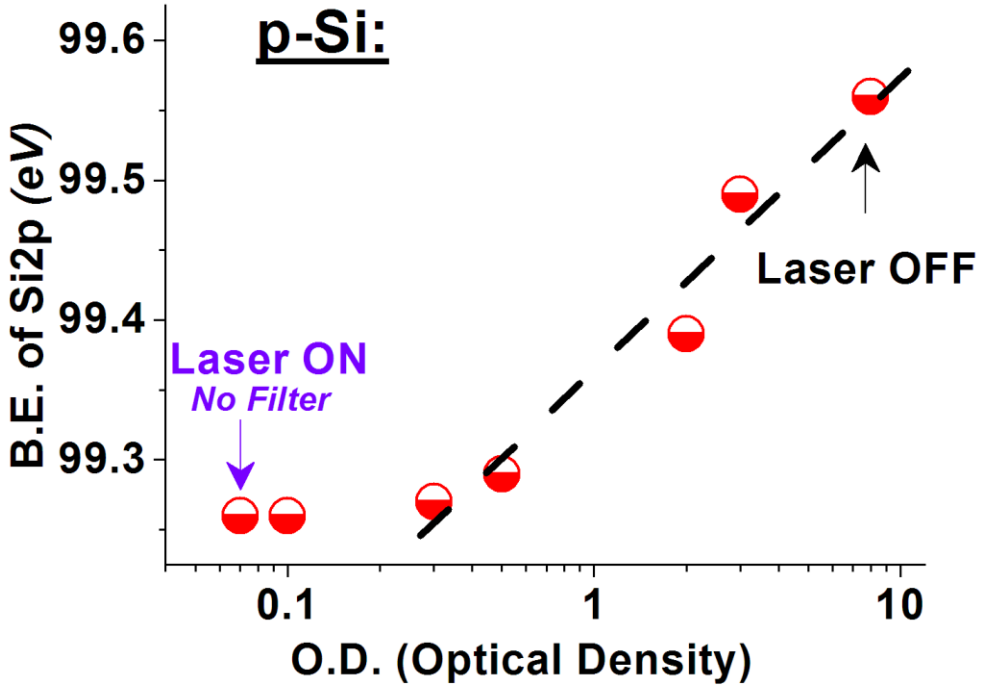

Figure 17. The response of peak position of p-type doped Si under exposes of violet laser with tuned photon intensities.

In the light of with previously discussed results about the building-up of the surface photovoltage on the n- and p-Si samples, it is obvious that under illumination the bended bands have been flattened. However, the next question might be "to what extent the bended bands of Si samples are flattened?" The question can also be answered with XPS, and it has already been reported.[57, 59, 64-70] However, it cannot be measured with a high degree of experimental accuracy because the semiconductor and metal contact between the sample and the instrument produces nonuniform and usually irreproducible contact potentials and/or Stocky barriers between the Fermi levels of instruments and semiconductors.[55, 56] Therefore, instead of measuring individual band-flattening of one sample with respect to an unstable and irreproducible reference point, we have attempted to measure the difference between the Fermi levels of two n- and p-type Si using a mechanical metal (Au) connection between them as shown in Figure 18. This strategy has already been utilized in many times to determine generally the band offsets/discontinuities between different semiconductive domains,[85, 87, 102-112] and it has various advantages. For example, the Fermi level along two semiconductors has a smooth and reproducible transition without interruptions or jumps as illustrated in Figure 7 and 20. In addition, this technique helps us to diminish some of the instrumental errors because an identical metal contact between both Si samples is expected to produce identical potential deviations on the samples and causes similar shifts in the peak positions.

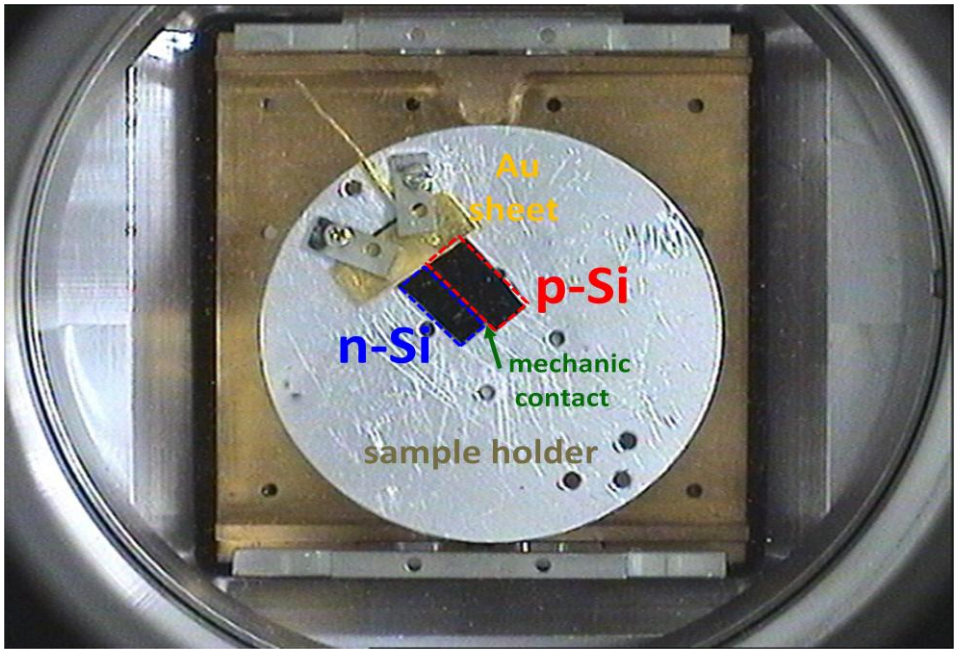

Figure 18. The picture of sample mounting with Au sheet for the photo-dynamic XPS measurement.

We also have to calculate their original (bulk) pinned Fermi level positions of the samples, using the resistivity values of the n- and p- Si reported to be 10-20 and 28-31 Ω·cm, respectively. From the resistivity (ρ) versus the doping level of the n- and p-Si plot, a formula of the ρ is expressed as:[55]

$$\rho = \frac{1}{en\mu_n + ep\mu_p} \tag{8}$$

$$n_i^2 = np \tag{9}$$

Where the doping levels of the n- and p-Si wafers are calculated as 2.8 x 10^{14} and 4.7 x 10^{14} cm^{-3} from Equation 8 and 9, respectively if the mobility of electron and hole carriers (μ_n, μ_p), and the intrinsic carrier concentration (n_i), in the Si lattice at room temperature are taken as 1500 cm^2 $volt^{-1}$ sec^{-1}, 450 cm^2 $volt^{-1}$ sec^{-1}, and 1.45 x 10^{10} cm^{-3}. The Fermi

levels of the n- and p-Si samples can be calculated with respect to the middle point of the band gap E_i, using Equation 10a and 10b:[55]

$$E_f\text{-}E_i = kT\ln\left(\frac{n}{n_i}\right) \quad (10a)$$

$$E_i\text{-}E_f = kT\ln\left(\frac{p}{n_i}\right) \quad (10b)$$

Where k is the Boltzmann's constant and T is taken as room temperature (300 K). Equation 10a,b yields that Fermi levels of the n- and p-Si as pinned at 0.26 eV above and 0.27 eV below the E_i, respectively as illustrated in Figure 19b,c.[50] From these pinning values we can construct a band diagram between them as shown in Figure 20a. The calculated band diagram produces a 0.53 eV band offset value between n- and p-Si for the bulk or for a hypothetical Si samples which are free from surface-related effects. However, the B.E. Diff. is measured by XPS without any photoillumination *(at a laser off state)* as 0.17 eV as modeled in Figure 20b and shown in Figure 21a. This measurement is taken from an intersection point of both the n- and p-Si as demonstrated in the inset of Figure 21, so the compound signal represents two different Si2p peaks which is deconvoluted by two Si2p envelopes. There is an obvious disagreement between the calculated and measured values of the band offset between the n- and p-type Si. This deviation is postulated to be due to the band-bending. The band-bending shields some of the bulk properties of semiconductive materials. On the other hand, photoillumination reduces the band-bending, such that the B.E. Diff. between n- and p-Si samples is measured as 0.49 eV. Now the calculated and the measured values are more or less in the same range. Moreover, the smaller

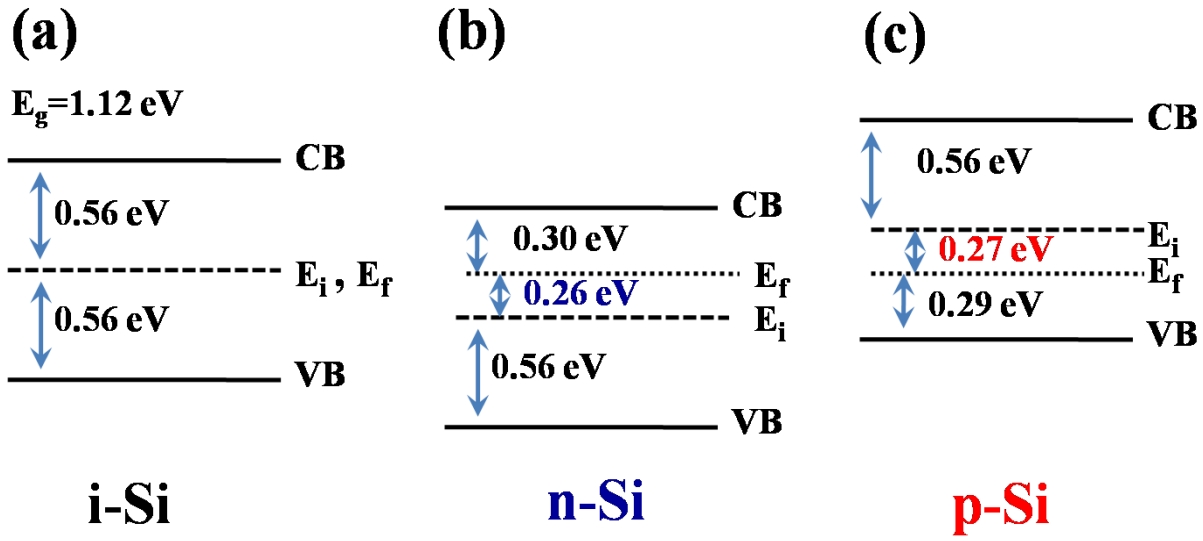

Figure 19. The band diagram of an (a) intrinsic (b) 2.8 x 10^{14} cm^{-3} of n-type and (c) 4.7 x 10^{14} cm^{-3} of p-type doped Si.

experimental value is also reasonable because it has been previously reported that x-rays also cause a certain amount of surface photovoltage on semiconductors.[59, 113, 114] This agreement between experimental and theoretically calculated results reveals important scientific implications. First of all, irradiation of semiconductive materials with a suitable light source causes band-flattening and allows a solid to recover its original band position even at its surface by eliminating or defeating surface effects. Therefore, the bulk band offset values can also be reliably measured by XPS. In addition, with this type of XPS investigation the nature of doping of semiconductive materials can be determined as to be n- or p-type. Another important implication is that the photoinduced XPS shifts enable us to assess the extent of doping in a quantitative manner.[50]

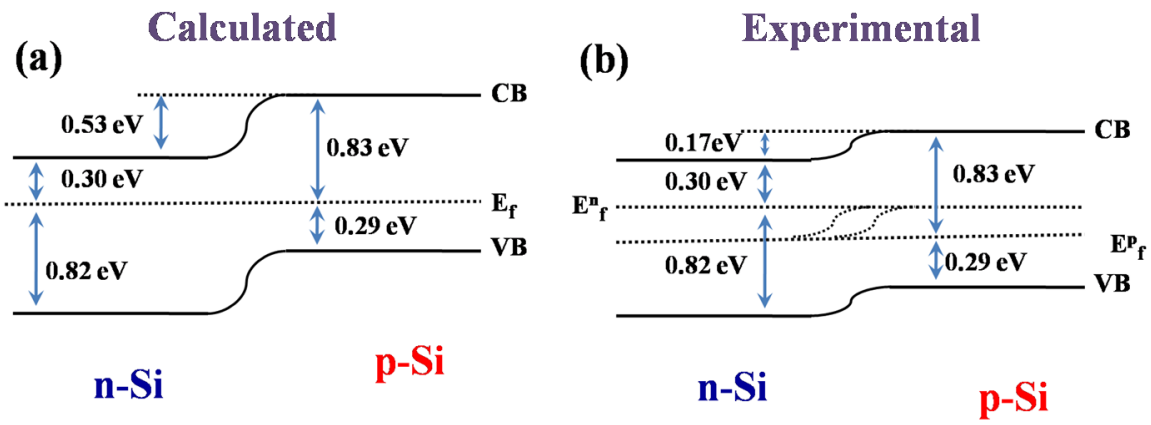

Figure 20. The band offset between n- and p-type doped Si (a) calculated, and (b) measured by XPS without light illumination.

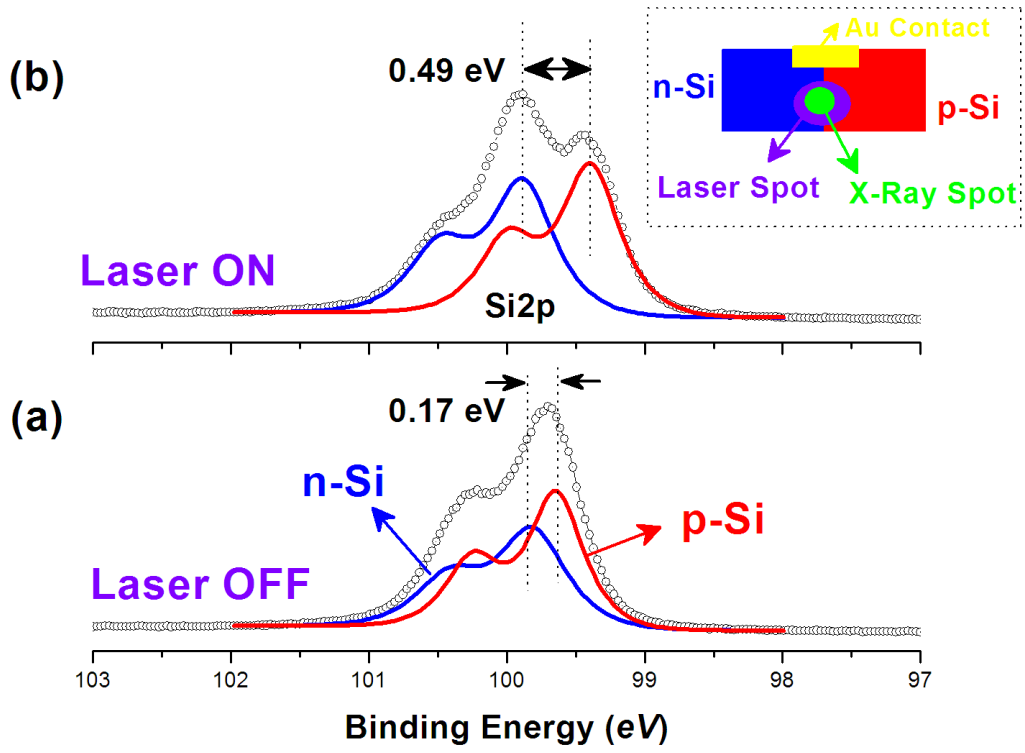

Figure 21. The experimental and fitted XPS spectra of Si2p regions of mechanically connected n- and p- type Si (a) without and (b) with laser illumination. While the dotted points represent experimental data, solid lines represent fit Si2p spectra of n- and p-type Si samples. Inset shows a simple model of experimental setup.

4.1.1. Inversion of the Surface Photovoltage of SiOx / n- and p-doped Si

Inversion of the surface photovoltage has also been extensively discussed in literature, but a unifying picture has not emerged. Surface photovoltage inversion is achieved under some conditions. For wide gap semiconductive materials the surface state/traps can be the source,[115] and it requires an energetic matching of the photonic excitation between the valance band and surface states, and/or surface states and the conduction band. This effect will be discussed in the GaN section. Applying or inducing a proper electric field is another way to convert, diminish or invert the band-bending at the surface of semiconductive materials.[116] However, the insertion of an induced electric field in a XPS experiment cannot be utilized because the emitted photoelectrons from the sample are also affected by the electric field. Another way to invert the surface photovoltage is by introduction of a new interface. For silicon, a thin silica layer can be used to invert the band-bending at the surface of the material,[117-119] since, the presence of a thin silica overlayer completely changes the surface photovoltage behavior of n- and p-Si samples.

As shown in Figure 10, 16, and 21 the energy difference between n- and p-doped Si is measured as 0.17 eV without any photo-illuminations and 0.49 eV under photo-illumination as a consequence of the surface photovoltage shifts of +0.11 and -0.19 eV, respectively. With the introduction of a thin oxide layer, a possibility to induce additional bending arises due to excess electron transfer from the silica layer to the Si substrate. This electron transfer has been frequently discussed in the literature to cause a positive charge build-up on the silica layer. This charging effect is also traceable by XPS as a shift towards a higher binding energy in the corresponding silica peaks. This shift occurs

identically in the both Si2p and O1s photoelectron peaks as demonstrated in Figure 22. It is obvious that an excess electron accumulation at the interface between the silica layer and Si substrate causes a further downward band-bending for both the n- and p-Si. Therefore, while the magnitude of surface photoresponse of the p-Si wafer increases, a completely reverse effect is observed on the n-Si because of its upward band-bending as shown in Figure 22 and 23, and demonstrated in Figure 24.[50]

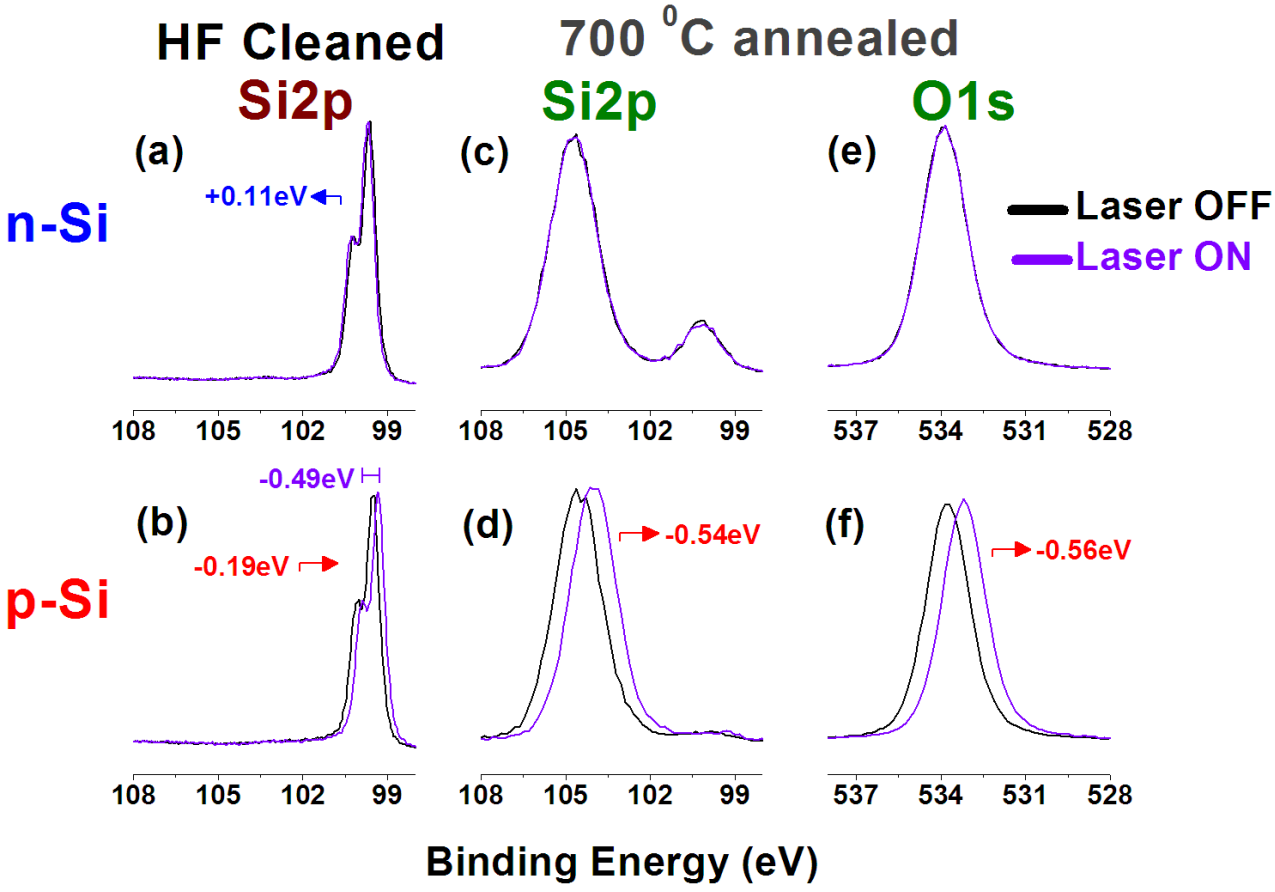

Figure 22. The Si2p XPS spectra of (a) n-, (b) p-Si of HF cleaned Si wafers. The Si2p (c,d) and O1s (e,f) spectra of n- and p-Si wafers which contain ca. 10 nm a thermal oxidized overlayers.

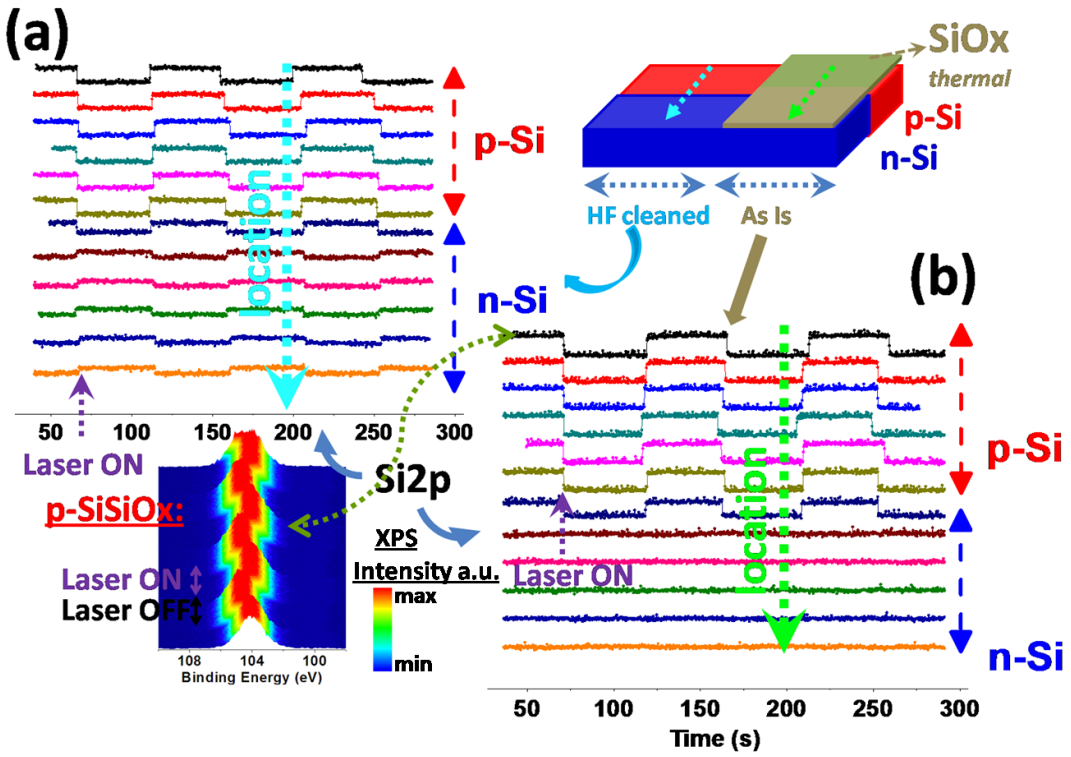

Figure 23. The corresponding surface photovoltage behaviors of (a) n- and (b) p-Si wafers which contain ca. 10nm thermal silica from Si2p peaks and under a chopped photo-excitation at 0.01 Hz rate. The first cycle of Laser ON states are indicated on the both two spectra. The upper inset configuration and composition of the n- and p-Si samples and the bottom inset shows a single frame of the XPS snapshot experiment form p-Si.

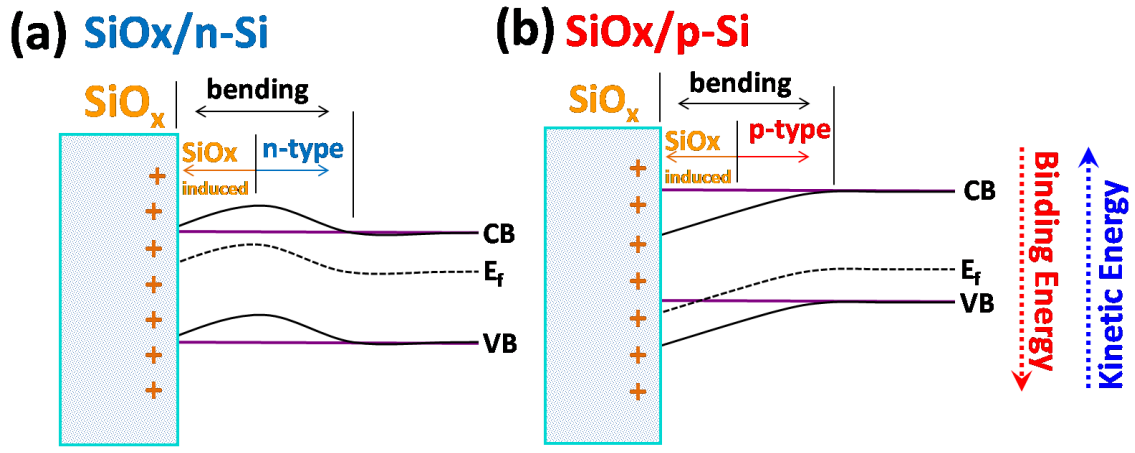

Figure 24. A model of inversed surface photovoltage interface between the silica overlayers and (a) n-, and (b) p-Si.

4.1.2. Dynamical Photoconductivity and Surface Photovoltage Response of a SiO_x / p-type Si Surface Structure

Both electrical and optical excitation dependence of on HF cleaned p-type Si is probed by recording Si2p regions with XPS as shown in Figure 25a-c. A -0.19 eV peak shift between laser off and on states is measured at three different electric conditions; (i) the sample connected to the ground, and (ii) subjected to a 1 kHz and (iii) a 0.001 Hz squarewave electric stresses. Identical results but in opposite direction (+0.11eV) are obtained for the n-type Si as shown in Figure 10, 16, and 22 for the ground case. Therefore, the developed surface photovoltages of the n- and p-Si wafers do not have any bias and/or frequency dependence.[40] The responses to photoillumination are instantaneous in the vacuum environment as expected[66, 67, 69-74] and time constants of the surface photovoltage transients are much faster than our probe speed *(<0.1 s).*

However, when a thermally grown ca. 4 nm thin silica dielectric layer is incorporated as an overlayer on the Si substrate, the response to both external electrical and optical excitation sources becomes more complex as shown in Figure 26. As discussed before, the bipolar electric squarewave pulse excitation twins and separates the peaks from each other as much as the amplitude of the stress. Each of the twinned SiO_2/Si system has two separated envelopes of the Si2p peak due to the presence of different oxidation states. The broadened envelopes belong to the silica layer, where silicon atoms have mostly +4 oxidation states and the B.E. Diff. between the two envelopes is about 4 eV.[25] The well resolved and a 0.61 eV spin-orbit split Si2p peaks represent the Si^0 domain.[50]

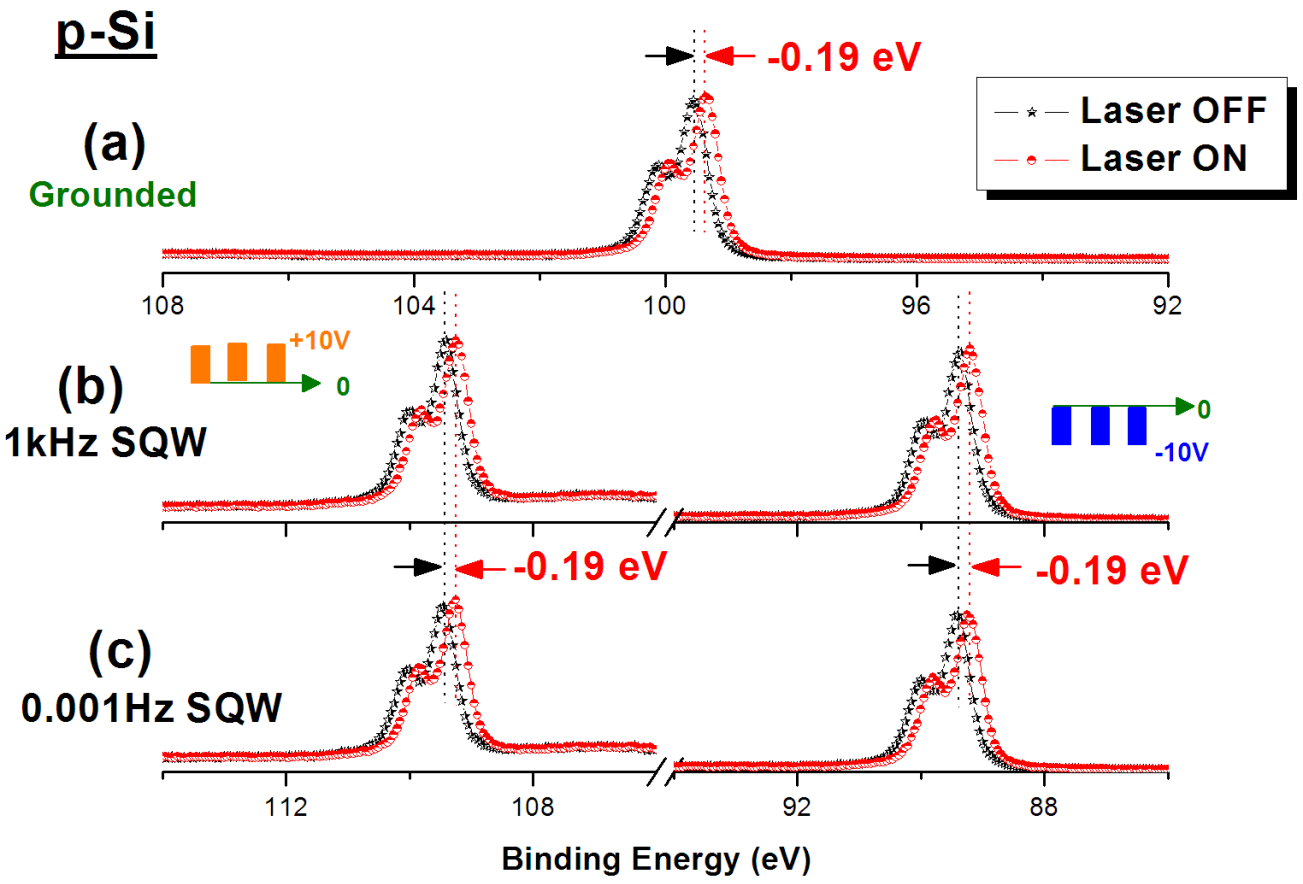

Figure 25. The XPS spectra of Si2p regions of p-type doped Si (HF cleaned) with and without light illumination and while connected to (a) ground, (b) 1 kHz, and (c) 0.001 Hz squarewave electrical stress.

At the higher frequencies the SiO_2/p-Si system exhibits a 20 eV symmetric peak separation corresponding to the electric stimulus as shown in Figure 26a for the bare Si sample, which indicates that there is no change in charging and/or discharging states on the sample or within the interface of the silica and the Si substrate. Optical stimulus imposes an additional -0.50 eV shift for both of the Si2p peaks. The reason for a higher photoresponse of the SiO_2/p-Si system due to the oxide induced additional band-bending was discussed in the previous section. On the other hand, at the lower frequency the system exhibits asymmetric shifts for the silica overlayer while the substrate peak is not

affected. As discussed above, a fast transient response must be due to the surface related processes such as surface photovoltage, and the slower transition must be due to the bulk related phenomena such as charging, discharging and/or change in the photoconductivity. When we focus on the peak shift responses of the silica overlayer and follow them from lower to higher frequency at the laser-off mode, we observe a 20 eV B.E. Diff. due to freezing of charging and/or discharging processes at high frequencies, and the charge storage capability (capacitance) of the dielectric silica layer is by-passed by the faster electrical excitations. Moreover, if we compare the silica peaks with and without photoillumination at low frequency, we observe a bigger shift between the laser off and on states. This process is a photoinduced process and has one slow component which responses to both electric and optical stimuli, and one fast component which responses only to optical stimulus. Furthermore, the two processes are different from each other and have different time constants, but the time constant of the fast response is beyond our time resolution.

However, a crucial point arises that, since silica has a band gap around 9 eV and is a good insulator,[120] the excitation with the violet laser (3.1 eV) should in principle be impossible. The explanation must be related with the fact that the silica layer has certain amount of defect states in its mid-band gap region, and absorbs visible and ultraviolet light to excite electrons or holes from the valance band to the defect states, the defect states to other defect states, or the defect states to the conduction band. All of these processes increase the charge carrier density and induced conductivity.[117, 121] Therefore, we probe this conductivity changes with XPS under photoillumination and/or electrical stress and can distinguish them from the fast surface photovoltage effects.

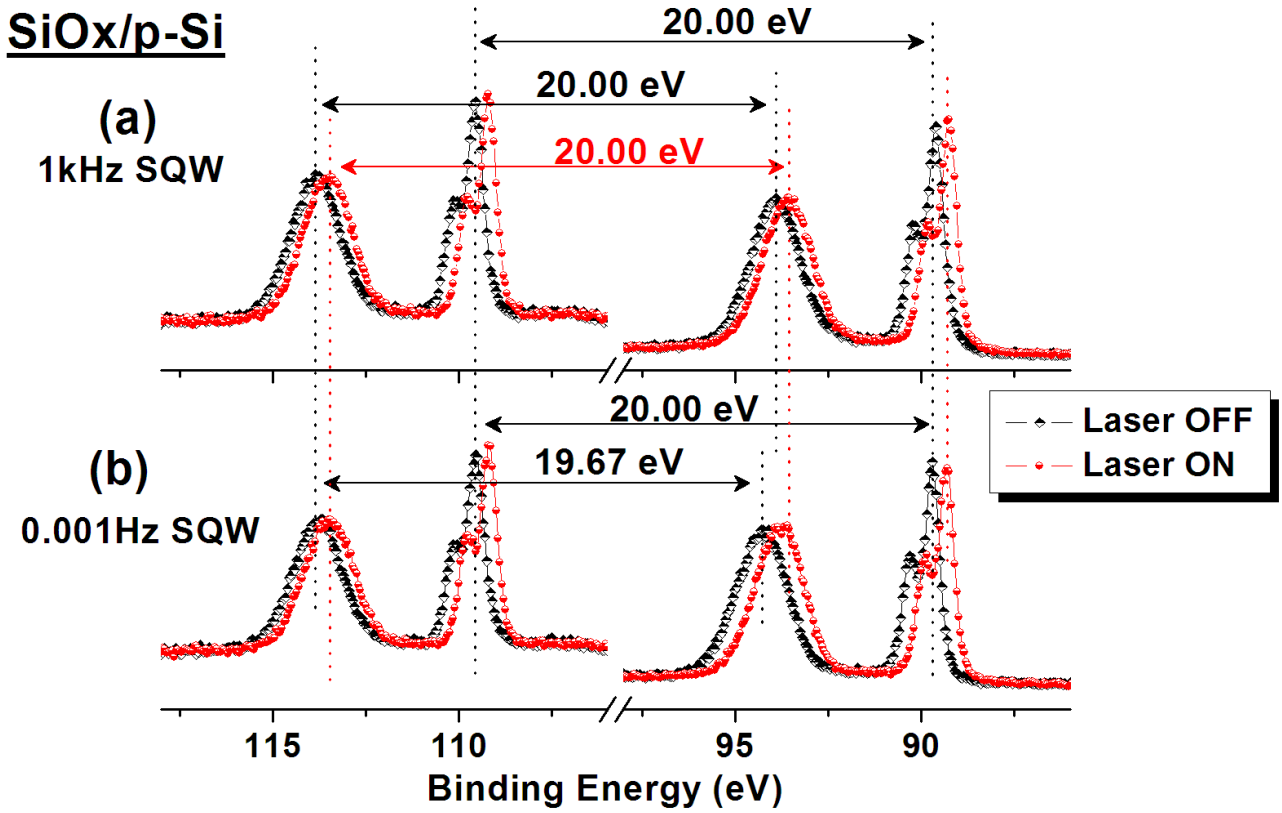

Figure 26. The XPS spectra of Si2p regions of ca. 4 nm silica layer and p-type doped Si substrate with and without light illumination and while connected to (a) 1 kHz (b) 0.001 Hz squarewave electrical stress.

4.1.3. Elemental, Chemical, and Electrical Investigation of a High-Power Fiber Laser Patterned Silicon

Application of a high power laser radiation for surface patterning on silicon as well as other materials dates back to more than four decades.[122-124] This method is one of the easiest and cheapest way to produce sub-micron and nanometer size patterns on materials. Our attempt at this point is to understand the chemical modifications which occur on the surface of the Si wafer during this process and to measure possible

consequence of the chemical modification on electrical properties using the dynamic XPS technique as a chemically and spatially resolved method.

The short and highly intense fiber coupled near-infrared laser by the Si wafer causes a locally heated and/or melted region on the substrate. A significant temperature increment makes Si atoms more reactive with oxygen molecules from the atmosphere. In addition, explosive events also occur during the processing on the surface of Si and cause volcano type surface features. The volcano type structures also consist of a cavity at the center of the hill which is also the center of the laser irradiation spot. These features are easily noticeable in their scanning electron microscopy (SEM) images[95] in the reference 95.

Elemental XPS analysis of the doted patterned Si with 200 μm steps as shown in the inset of Figure 27 is performed on an intersection area between the laser patterned and non-patterned regions. The analysis reveals two distinct silica domains, therefore, three different Si2p peaks occur at the binding energies of 99.60, 104.02, and 106.91 eV. The Si2p peak at 99.60 eV corresponds to metallic Si^0. The higher binding energy peaks correspond to oxidized Si domains, and the one at the 104.02 eV is a slightly positive charged peak position of Si^{+4} as previously discussed. The Si2p peak of second silica domains can only be explained by the presence of a very high differential charging on them. It is important to note that a similar binding energy shift with a same direction also appears on the O1s peaks as shown in Figure 27b and as indicated in the inset of in Figure 27. The same directional shifts in both Si2p and O1s peaks of the second silica domain imply that an additional positive electrical charge accumulation arises on this domain instead of a chemical variation. Since chemical processes might include electron transfer between at least two atoms, this event must cause an opposite binding energy

shifts on the corresponding atoms. The quantification analysis from Si2p and O1s regions point out that both silica domains have almost a 1:2 atomic ratios between their corresponding Si and O atoms, so the two distinct silica domains are chemically identical.

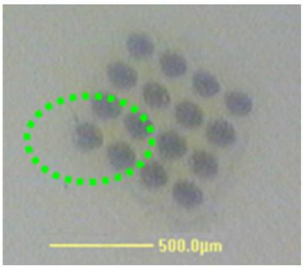

Name	Peak BE	FWHM eV	At. %
Si2p metalic	99.6	0.67	10.3
Si2p native	104.02	1.63	13.4
Si2p patterned	106.91	2.84	17.3
O1s Scan native	533.51	2	26.0
O1s Scan patterned	536.58	2.93	33.1

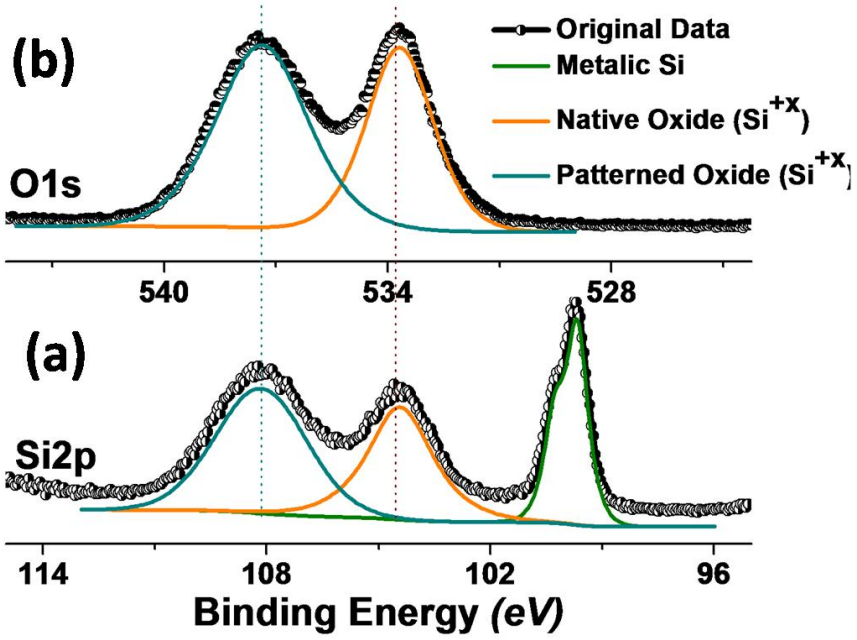

Figure 27. The elemental XPS survey of the laser patterned Si (a) Si2p region and (b) O1s region. The left panel of inset is an optical image of the sample and shows the analyzed features and the x-ray spot (green circle) on the sample. The right panel of the inset shows chemical compositional analysis between Si and O element of the analyzed region.[125]

An XPS line scan over the patterned region with a smaller x-ray spot size provides a more detailed picture. While in the non-patterned region only one silica domain is observed, over the patterned region both O1s and Si2p peaks start to broaden and

gradually shift to higher binding energies as shown in Figure 28a,b as depicted in Figure 28a,b. The location dependent line profiles of Si2p and O1s peaks have identical binding energy variations along both the laser patterned and the non-patterned regions. Therefore, the high-power laser processing creates electrically different, but chemically identical domains on the silicon substrate, and both chemical and electrical properties are traceable using either the Si2p or O1s peaks.

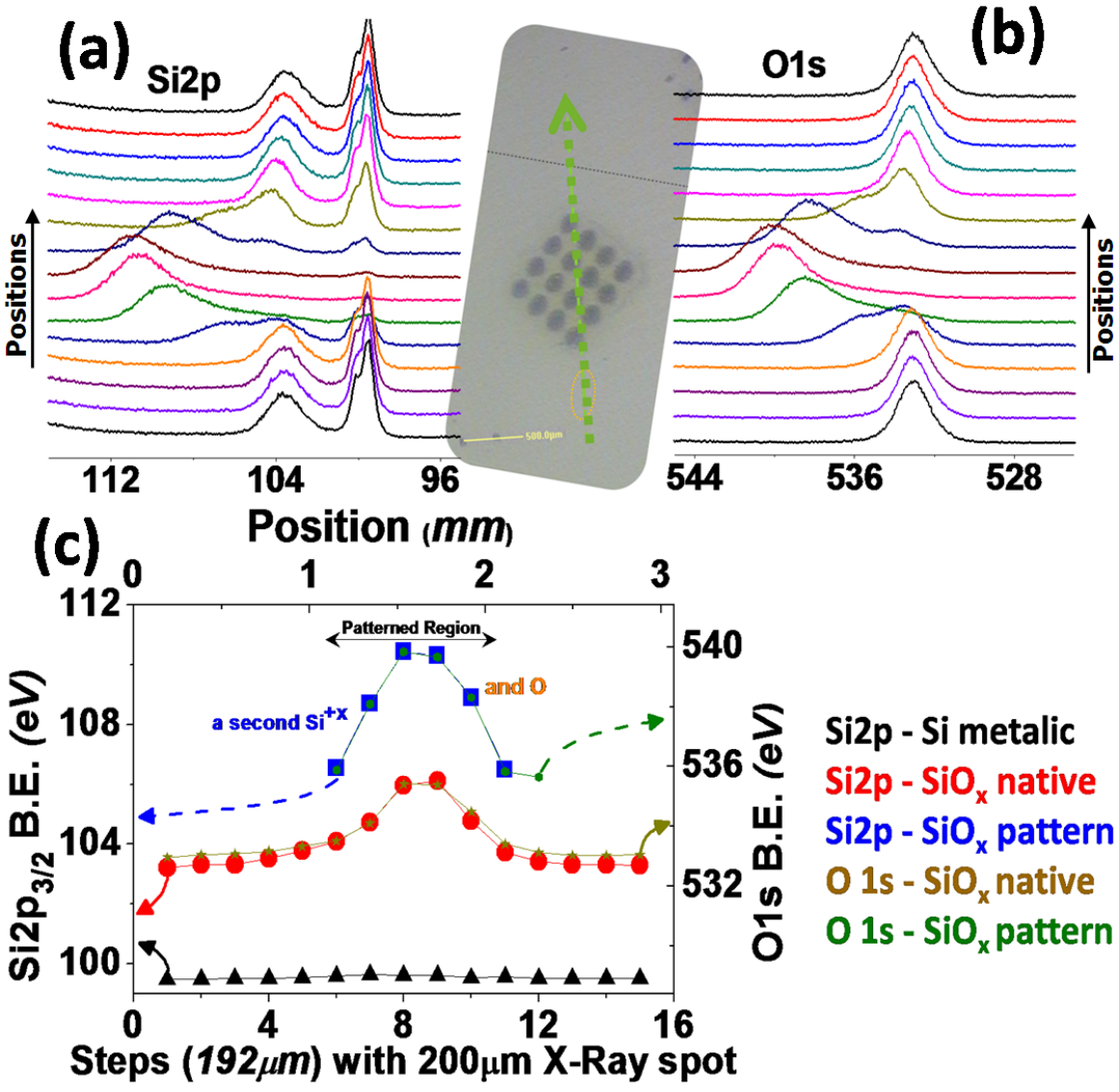

Figure 28. A XPS line scan of (a) Si2p (b) O1s region on the patterned Si. (c) the fitted peaks lines of both Si2p and O1s peaks vs. positions.[125]

To obtain further electrical properties of the laser patterned Si domains, we have used a triangular waveform with ±10 V amplitude and at 0.01 Hz frequency. The potential sweeps from +10 V to -10 V in 50 seconds in one direction, and then sweeps in the reverse direction for another 50 seconds. The O1s region was followed to record in a fast data acquisition with the snapshot mode to create a time resolved behavior of the two domains, since the O1s peak has a higher cross-section. Under triangular excitation the O1s peak of the lower binding energy resembles to that of a typical silica. The position of this peak follows faithfully the variation of the external potential between +10 V and -10 V, with only a small amount of charging/discharging. Following the external potential faithfully means that if a +2V potential is applied, the O1s peaks appear at 535.5 eV shifted from the grounded O1s at 533.5 eV as depicted in the inset of Figure 29. However, the O1s peak of the second silica domain does not follow the external potential faithfully. At the positive cycle of the external potential (from 0 V to +10 V and as well as in the reverse direction, the O1s peaks of two silica domains shift together as a response to the applied potential, so their charging behaviors are also similar with each other. During the negative cycle (from 0 V to -10 V and as well as in the reverse direction), the O1s peak of the second silica domain starts to accumulate large amount of positive charge, so that as much as 18 eV peak separation is present between the O1s peaks of two domains. Explanation of this odd behavior of the second silica domain must be related with the laser patterning process, during which volcano-type silica features are produced, and these structures do not have proper electrical connection to the Si substrate. As a result, these features have larger contact-resistances between the silica

domains and the substrate. This resistance causes large differential charging and later on a breakdown under certain condition, in the presence of low energy electrons of the flood gun and the applied external potentials. After the breakdown the second silica domains follow the external voltage like the other silica domain as shown in Figure 29.

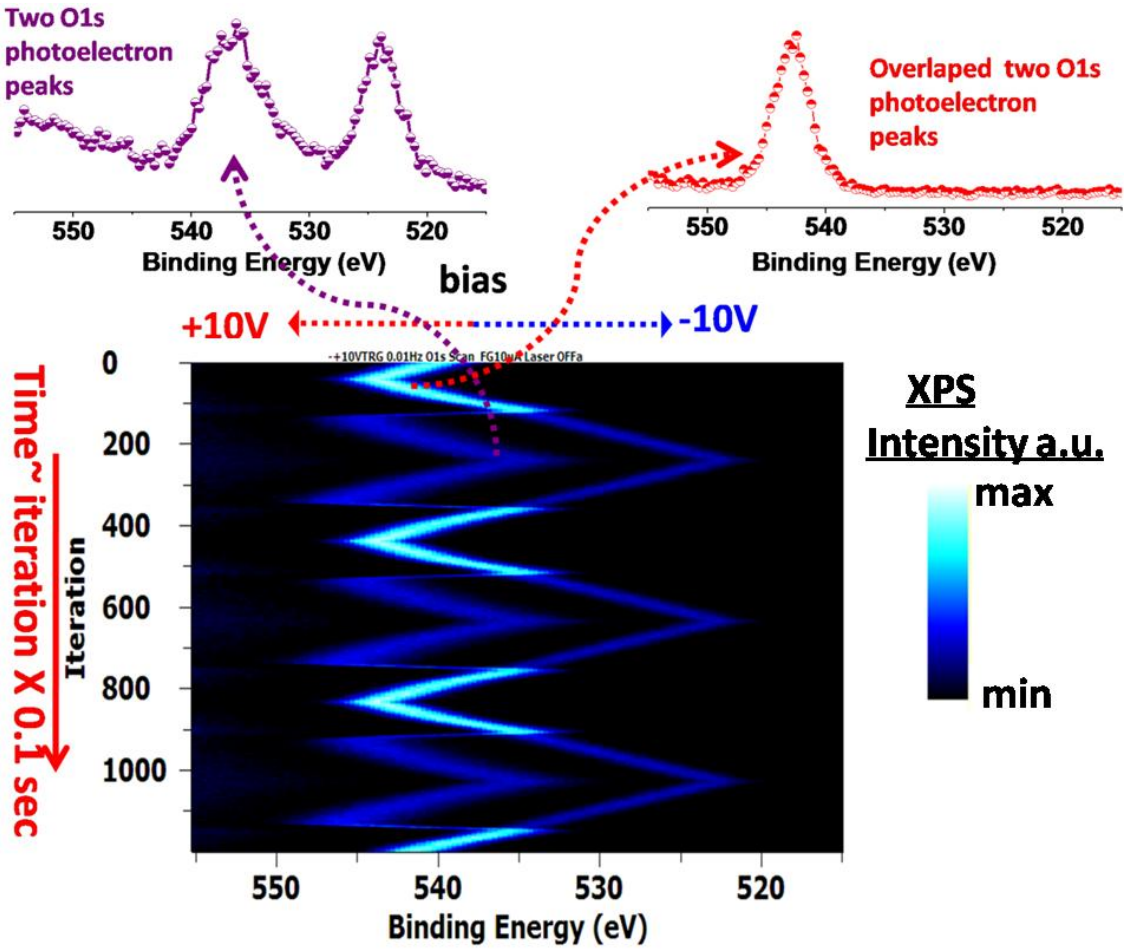

Figure 29. A 2D false color contour map of the sequential snapshot O1s spectra of the laser patterned Si under a triangle (±10 V) electrical stimulus at the 0.1 Hz frequency. The inset shows two O1s snapshot spectra under -10 V (left) and +10 V (right) bias.[125]

Application of the triangular electrical stimulus (±10V) assists to us to perform additional electric characterization with XPS. It is obvious that two silica domains have different electrical characteristics. The patterned region collects large positive charges which can be tuned by adjusting the parameters of the flood gun as shown in Figure 30b.

In addition, there is a remarkable hysteresis among charging and discharging paths. It is obvious that further detailed analyses are necessary to understand the nature and dynamics of complex processes in order to obtain better material characteristics of these laser created features.

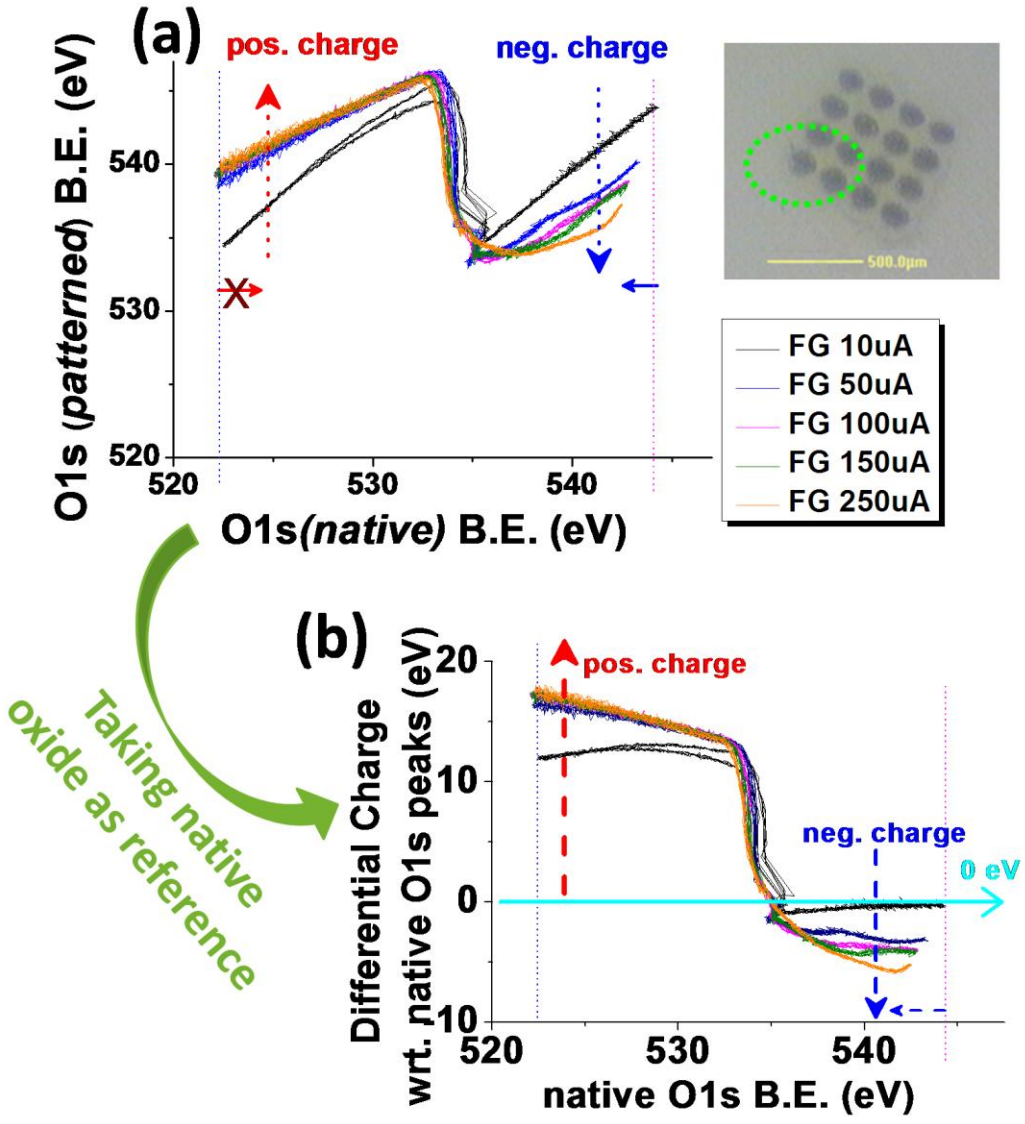

Figure 30. The variation of snapshot spectra of the O1s peaks of two silica domain (a) vs. each other and (b) the B.E. Diff. between them vs. the O1s peak of the first silica domain.[125]

4.2. Photoresponse and Electrical Parameters of CdS Film

CdS is one of the well known photoconductive semiconductor and is also employed in solar cell devices due to its ideal photosensitivity and photoconductive performance with the visible light.[53] The band gap of CdS is reported as a direct one[126] at 2.4 eV.[53] The CdS is naturally n-type semiconductor due to sufficient amount of sulfur vacancies[127, 128] However, p-type CdS have also been prepared with doping different metals such as Bi,[129] Cu[130] and Ag.[131]

This part of work is dedicated to follow a similar approach to the SiOx/p-Si system and to investigate the CdS films with the photo-dynamic XPS. When the sample is connected to ground, upon photoillumination the peak of Cd3d is shifted to a +0.2 eV higher binding energy as shown in Figure 31. The response of CdS can be attributed to both an n-type surface photovoltage shift and a photoconductive response due to change of conductivity of the sample.

The photoinduced response of the CdS film is reduced under green laser excitation, and in the case of red laser the shift almost disappears or sometimes shifts slightly in the opposite direction as shown in the inset of Figure 31. The lack of a response to a red laser can be explained by postulating that CdS does not have enough sub-band photoconductivity,[132] however, in the response of the CdS film to green laser does not have a reasonably explanation.

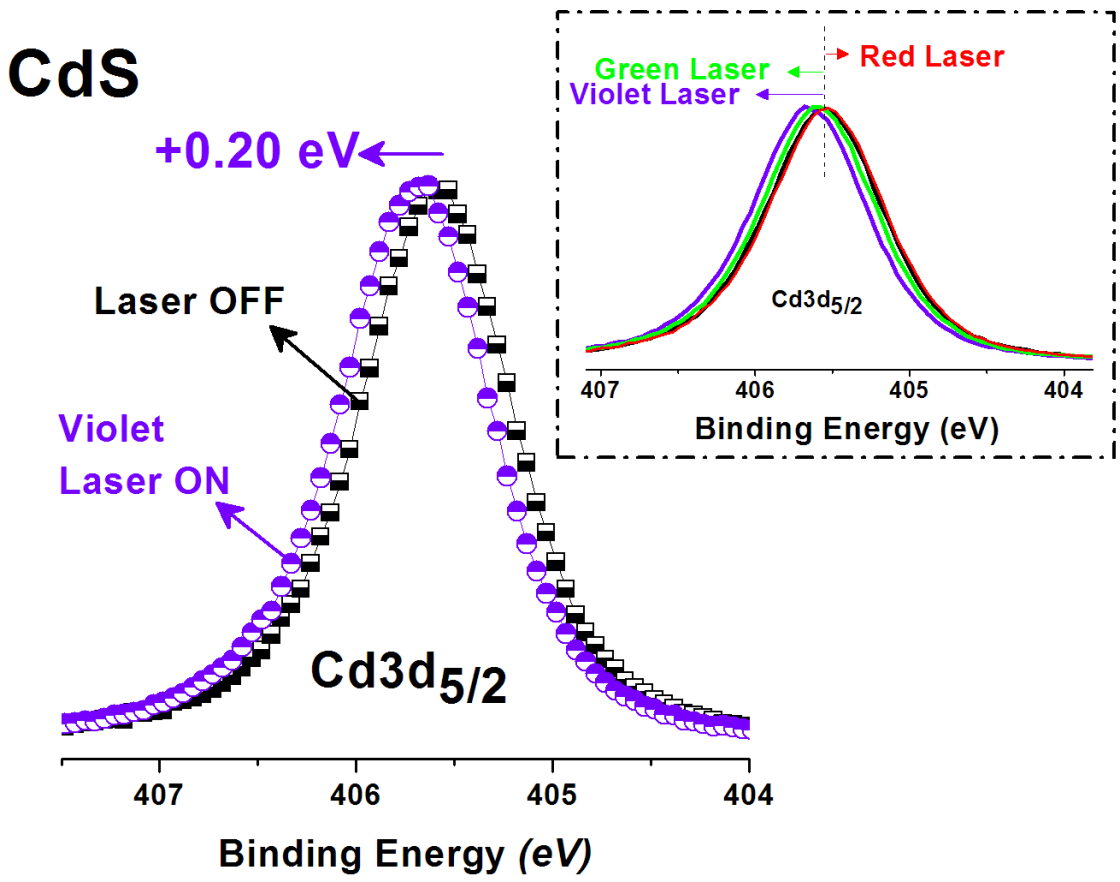

Figure 31. The XPS spectra of $Cd3d_{5/2}$ of the CdS film without and with violet laser excitation. Inset shows the responses of CdS to violet, green and red lasers.

The relationship between photoconductivity and intensity of light is nonlinear as was indicated in earlier published studies.[53, 133] The explanation of this phenomenon is that photoconductivity is a bulk related property rather than a surface one. For that reason, an efficient absorption of light through photoconductive material may cause an exponential intensity decay of the incident light along penetration path. Therefore, the relationship between photoconductivity and the intensity of light is expressed as;[53, 133]

$$\Delta\sigma = I^n \tag{11}$$

where **Δσ** represents the change of conductivity (or the photoconductivity), **I** is the intensity of the incident light, and **n** is a number smaller than 1. Of course, **n** is a material specific parameter and might be governed by some intrinsic parameters such as doping type and level, defect/trap states, charge mobility, temperature, charge generation and recombination rates, etc.[53, 133]

For establishing a relationship between photoconductivity and intensity of incident light from an electrically grounded sample using NDF is not convenient, because connecting the sample to ground does not produce a suitable reference point due the uncontrolled charging and discharging processes as was represented in the inset of Figure 31. Therefore, this effect was measured using the controlled charging technique with squarewave electric stress. The data set was chosen from the 10 kHz squarewave applied spectra while the intensities of violet or green laser are varied by the NDF. A high squarewave frequency is preferred to eliminate charging/discharging of the sample. As depicted in Figure 32 the result is quite impressive, and CdS has a very different behavior when compared to the response of the Si sample. The photoconductivity response of the CdS film is extremely sensitive to even a small change of intensity of light, e.g. a 50% power reduction via a 0.3 OD filtration creates a measureable deviation on the sample, while the surface photovoltage of Si did not exhibit any change in this range. Therefore, we can declare that the CdS film does not reach a saturation point even at the highest power of photoillumination of our system and it might even exhibit a further shift if a higher intensity of light could be utilized.[40]

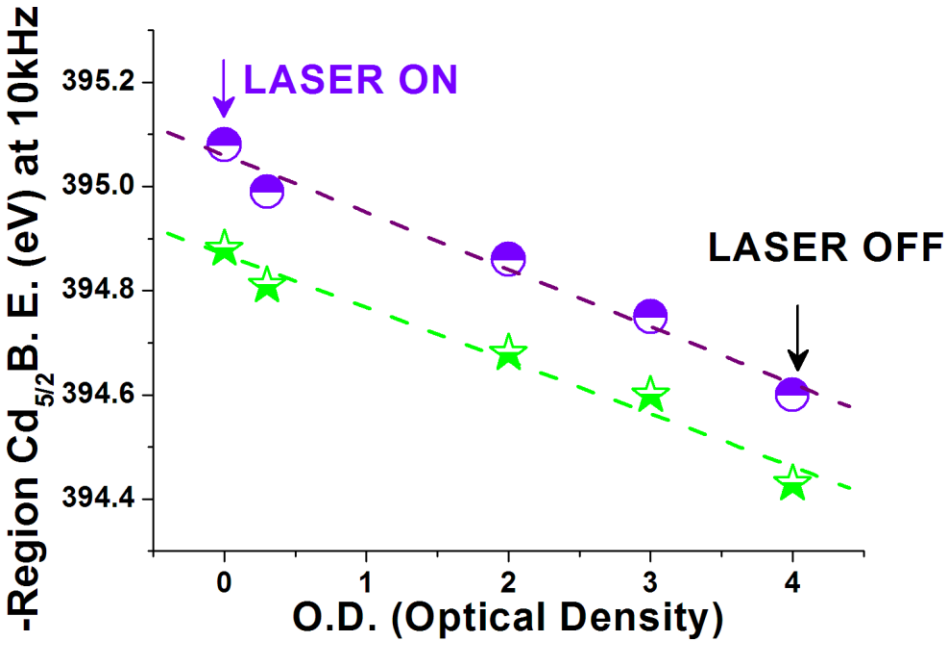

Figure 32. The relationship between the photoconductivity of the CdS film and intensity of the incident light beam of violet (violet dots) and green (green dots) lasers. The dot points are experimental data and dashed lines are linear fits.

XPS spectra of CdS films are measured under the squarewave electrical stimuli at a high (10 kHz) and a low (0.001 Hz) frequency, and under violet and green laser (not shown) illumination and different intensities via NDF as shown in Figure 33. At the higher frequency, the twinned Cd3d peaks symmetrically shift due to an I·R drop as a result of photoconductivity change and an upward band-bending of the surface photovoltage effect is also observed. However, at the lower frequency the charging effect is also asymmetric similar to the dielectric silica overlayer, and it exhibits a more complicated behavior as shown in Figure 33b. Under a +10 V potential stress of the low frequency squarewave electric excitation, the sample is forced to accumulate a negative charge from the flood gun electron without photoillumination, while under a -10 V stress the sample might accumulate a positive charge. Under photoillumination, the resistance value of CdS is reduced which causes a certain amount of charge dissipation in both

positive and negative cycles. While dissipation of a negative charge causes a shift of the Cd3d peaks to higher binding energy, the dissipation of a positive charge has a reverse shift. Therefore, the directions of photoconductivity, surface photovoltage and negative charge dissipation have the same direction at the + 10 V cycle of the squarewave excitation, and so they produced larger photoinduced shifts. On the contrary, the charge dissipation of a positive charge and the n-type surface photovoltage have a reverse direction and they cancel each other as shown in Figure 33b. The photoconductivity value for this case is extremely small because all stray electrons are ejected by the sample by the negative bias potential. As a result, only a very small current passes through the sample as discussed in the controlled surface charge section.[40]

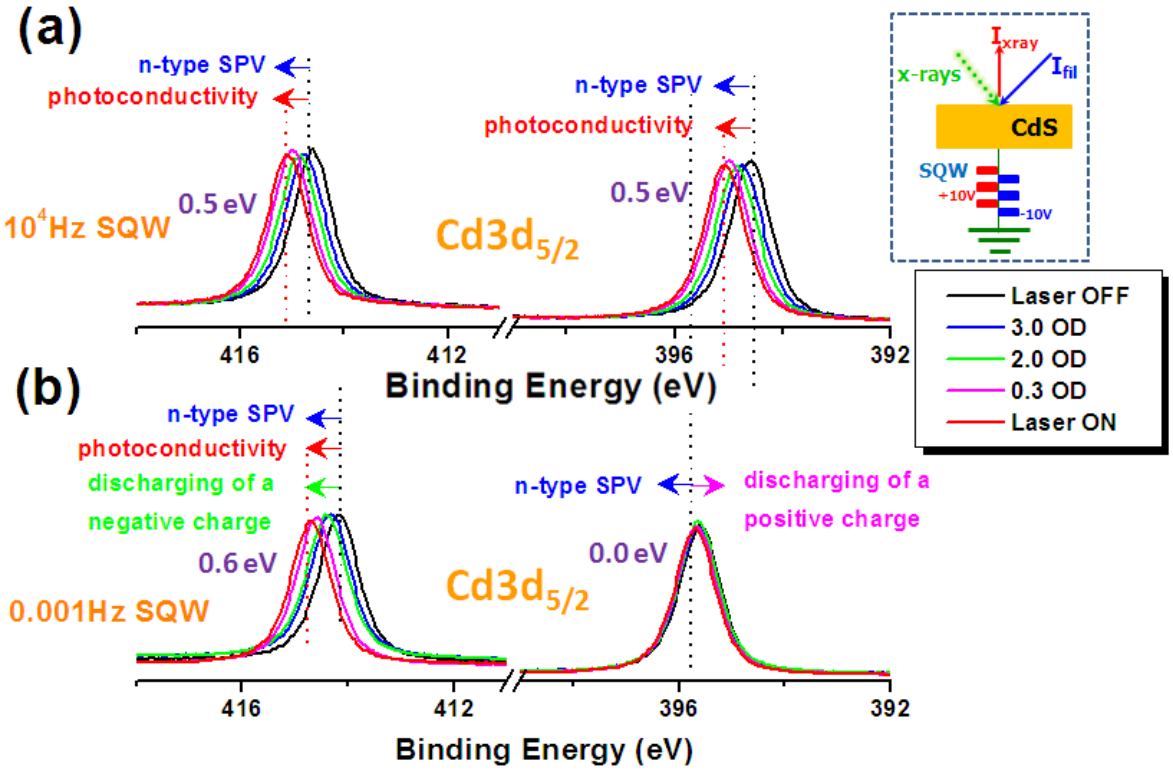

Figure 33. XPS spectra of Cd3d peak of CdS film with and without photoilliminuation and at a (a) 10 kHz and 0.001 Hz squarewave electrical stress. As shown in caption the intensity of excition source is tuned with NDF. The inset shows the experimental setup.

A more detailed investigation is employed to extract the electrical properties of CdS film with the photo-dynamic XPS, using squarewave electrical excitation of different frequencies in the range from 10^{-3} to 10^{4} Hz, both with and without photoillumination. The spectra are fitted, and both the B. E. Diff. and full width half maximum (FWHM) values vs. the frequency of the squarewave electrical excitation are plotted for both the laser-off and on states, as shown in Figure 34a,b. The effective resistance and capacitance values of CdS are extracted by fitting the frequency dependence of the measured and calculated Cd3d peak profiles as mentioned before by the numeric solution of an electrically simulated of XPS system. Yielding a good agreement between the experimental and calculated data for both values of the B.E. Diff. and the FWHM means that a successful simulation is carried out. Accordingly, the effective resistance and capacitance values are obtained as 250 kΩ // 300 nF and 210 kΩ // 300 nF for laser-off and -on states, respectively. The effective C value of the photoconductive CdS layer does not change, but the effective resistance value decreases significant under photoillumination as expected. Furthermore, the value of the FWHM increase indicates that around 1 Hz an inhomogeneous charging is developed on the upperlayer of the CdS films without photoillumination. Under photoillumination the inhomogeneous charges become both lessened and more uniformly distributed into the CdS film (Figure 34b).

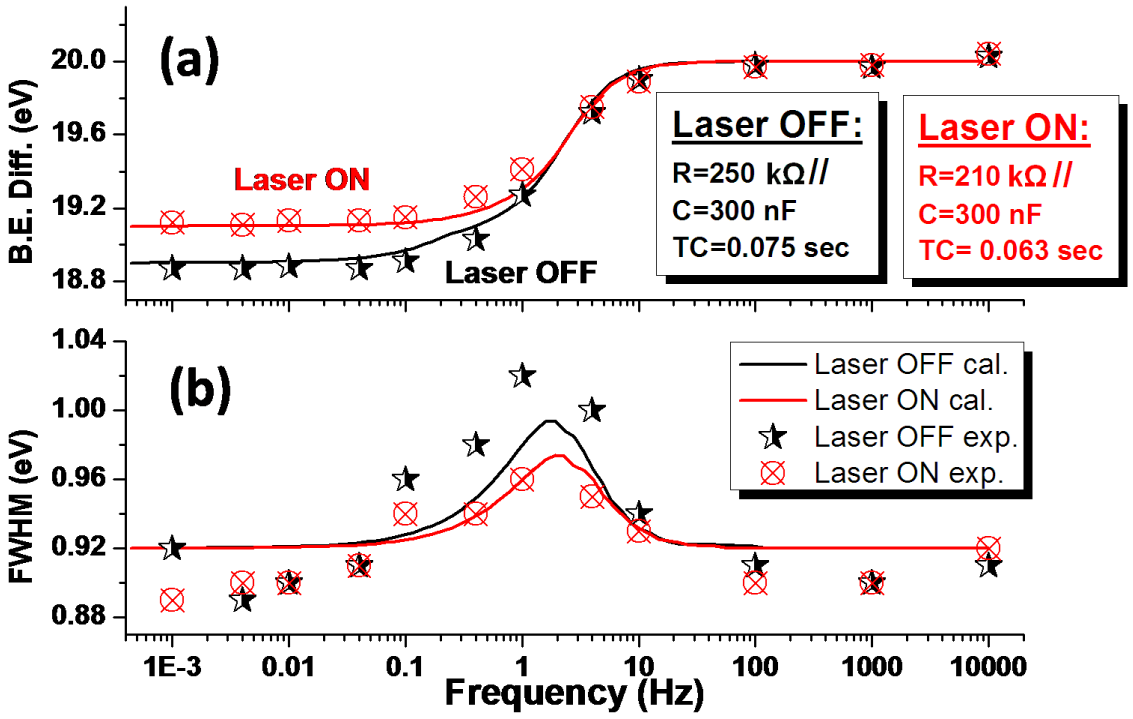

Figure 34. The frequency dependence of (a) the measured and calculated B. E. Diff. and FWHM values of CdS film under saquarewave electric stress between 10^4 and 0.001 Hz with and without photoillimuniation. Inset shows allined values of resistance and capacitance value for both two laser off and on states.

4.2.1. An XPS Investigation of CdS Based Photoresistor under Realistic Operational Conditions

Recently, XPS is becoming a versatile technique for performing spatially resolved *in-situ* and in *in-operation* type chemical and electrical measurements under realistic conditions.[18, 134, 135] In parallel with these recent developments, in this part of the thesis we will present a spatially resolved chemical and electrical analysis on a commercially available CdS based Light Dependent Resistor (LDR) under realistic operational conditions with XPS. The technique involves extractions of chemical and location

specific surface potential variations as a shift in the XPS peak positions. The main advantage of the technique is to provide an element specific surface electrical potential of an actual semiconductive device during operation. The system is also modeled to extract certain electric information. The location dependent electric profile analysis with this model yields data in two dimensions (location and energy) for a line scan and three dimensions (two locations and one energy) for an area measurement.[53, 136] A numerical analysis is executed to reveal spatially revolved resistance information without and with photoillumination. Morphologic defects are also examined under different electrical and optical conditions to assess their effect on the performance of the device.

In the past, the Scanning Auger Spectroscopy (SAS) has been employed to get a spatially resolved chemical analysis of semiconductive electronic devices.[137-141] Although, the SAS has provided a sub-micrometer lateral resolution for three decades ago, this technique is not suitable for the required energy sensitivity of the current semiconductor technologies. In addition, while other conventional scanning techniques such as atomic force microscopy, scanning tunneling microscopy, Kelvin Probe, etc. provide nanometer size space resolution, they have an important drawback that they do not have any chemical specificity. Therefore, XPS technique emerges as a strong candidate for providing both chemical and spatial information.

The CdS photo-active region of LDR is usually intentionally doped with tin, lead, and silver elements to widen the spectral response and/or conductivity, and also to enhance the response of the device.[131, 142, 143] The LDR has a regular patterned photoresistor design as can be seen from the inset of Figure 35. It has both chemically and electronically distinct regions. The brownish zigzag line is an almost pure CdS

photoconductive material which is supported by a ceramic substrate. The two gray regions on the top consist of heavily Sn and Pb doped CdS, and are electrically conductive and function as electrodes for the device.

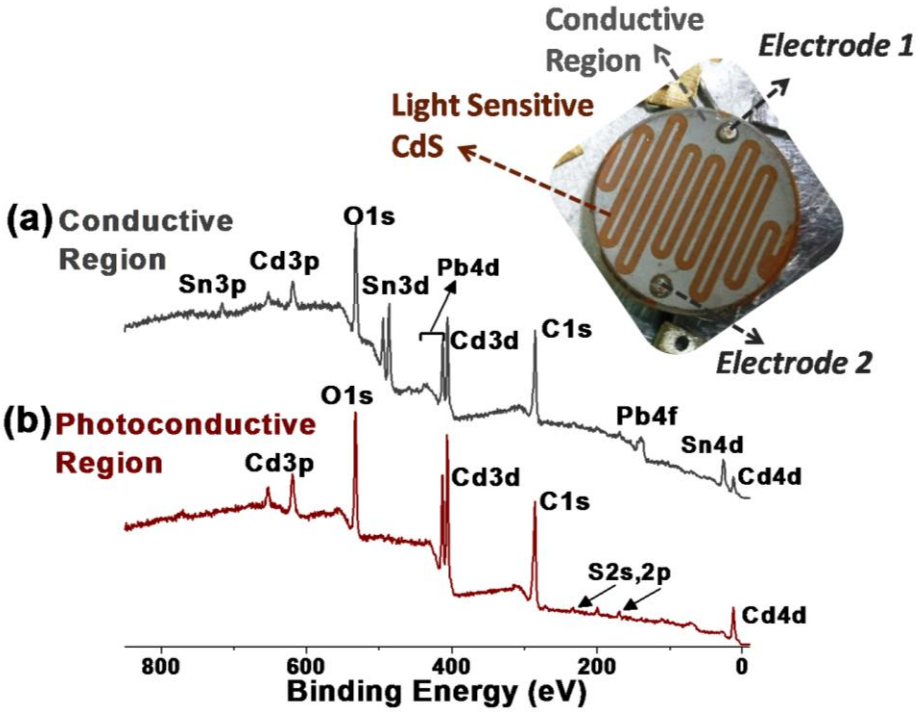

Figure 35. The XPS Survey spectra of (a) the conductive and (b) the photoconductive regions of a CdS based LDR. The inset is an optical picture of the device and electrical connection.[79]

The chemical composition of the conductive and photoconductive regions can be determined using XPS elemental analysis. As mentioned above, while the conductive region includes Sn and Pb elements with high concentrations as well as Cd metal, the photoconductive region consist of only Cd metal as depicted in Figure 35a,b, respectively. Because of the relatively small photoelectric cross-section of the S2s and S2p peaks, S content of the regions is barely visible in the survey spectra before Ar^+ ion etching. Both conductive and photoconductive regions contain a certain amount of carbon and oxygen species, which can be attributed to possible contaminations and residues from

the protective resin. A more realistic chemical analysis can be conducted after a certain amount of Ar^+ ion etching to get rid of any chemical contamination and residues. XPS depth profiles of two regions are achieved by sequential cycle of ion etching, the atomic percentage values of each element are plotted vs. time in Figure 36. While the concentration of the O1s peak is almost completely diminished, the C1s peak decreases, but cannot be eliminated completely. Variations in the concentration of Cd3d and S2p peaks for both conductive and photoconductive regions are identical to each other, and their concentrations gradually increase with the increase of etching time. The concentrations of the dopant elements of Sn and Pb in the conductive region initially increase due to removing contaminations, and start to decrease afterwards.

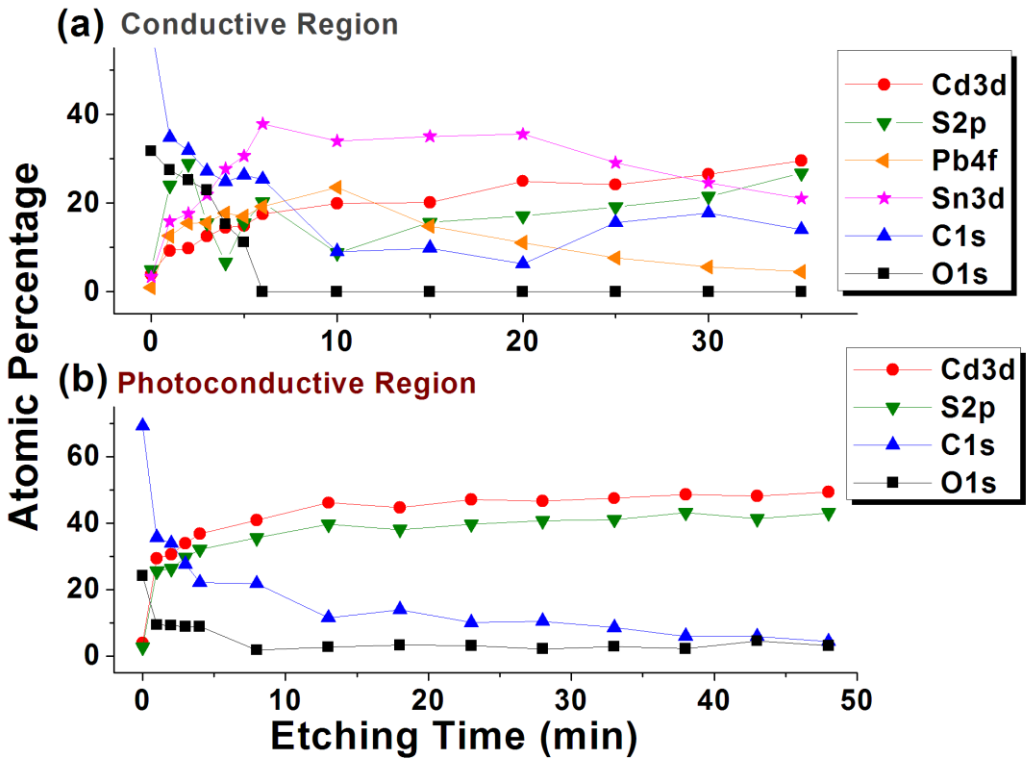

Figure 36. XPS depth profiles of CdS based LDR from (a) the conductive and (b) the photoconductive regions.[79]

In order to achieve a laterally revolved potential distribution of the LDR, the measurement has been performed under an external bias to reproduce more realistic operational conditions during gathering XPS data. Two metal contacts of the LDR provide electrical connections to the electrodes (and conductive regions), so the LDR can be integrated in a complete electrical circuit to operate by driving an electric current. For this reason, one of the electrodes is connected to the power supply over an external resistor, and another one is grounded to the instrument as demonstrated in Figure 37. An external ballast resistor is employed to control the flow of the current and to avoid saturation of the photoconductive region by injection of excess charges into the LDR. Note that, due to a high doping concentration of the two conductive regions, these regions are electrically highly conductive. Therefore, any applied potential from two electrodes can be distributed in the entire part of gray regions without potential drop. As expected, an applied potential along the photoconductive region starts to deviate due to its finite resistance value.

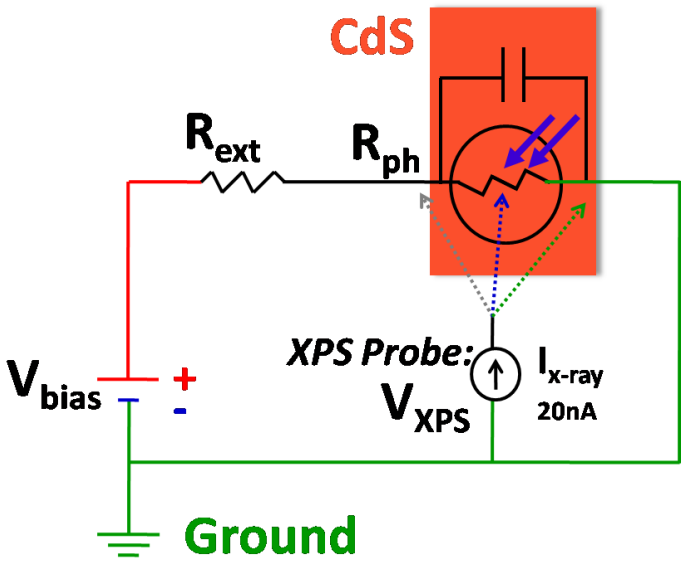

Figure 37. An electric circuit model of the experimental setup to simulate location depended resistance behavior of a CdS semiconductor under realistic conditions.[79]

XPS line scan results of the LDR along a defined pathway without and with violet laser illumination are shown in Figure 38a,b, respectively as a false counter-colored plot, and in Figure 38c as peak positions of the Cd3d. The measured surface potentials extracted from the Cd3d peak positions are similar to the structure of the optical picture which confirms the consistency of our measurement technique. A +6 V (0 V, grounded) of the applied potential starts to decrease or (increase) only along the photoconductive regions depending on the direction of the movement and the position of the XPS probe as shown in Figure 38a, b, and c. Along the conductive regions the measured surface potential remains constant at +6 V or 0 V (ground) as much as the applied potential on the two electrodes. The location specific surface potential variations can be modeled as;

$$\left(\frac{V_{bias}}{(R_{ext}+R_{max})} + I_{xray}\right) R_{ph}(x,y) = \Delta V_{XPS}(x,y) \qquad (12)$$

where V_{bias} and R_{ext} are the magnitudes of the externally applied potential and the ballast resistor, and R_{max} is the maximum resistance value of the photoconductive region. $I_{x\text{-}ray}$ is a minor current source due to the photoelectron effect of x-rays which is constant and taken as 20 nA as measured independently. The $R_{ph}(x,y)$ is the unknown location depended photoresistance value. The $\Delta V_{XPS}(x,y)$ is the location depended measured surface potential, obtained by subtraction of the grounded peak position of the Cd3d peak from the measured binding energies of the Cd3d peak at any position. The Equation 12 can be rearranged to;

$$R_{ph}(x,y) = \frac{\Delta V_{XPS}(x,y)}{\frac{V_{bias}}{R_{ext}+R_{max}} + I_{xray}} \qquad (13)$$

Equation 13 includes two unknowns; $R_{ph}(x,y)$ and R_{max}. The R_{max} can be obtained from the boundary conditions. For instance, when the x-ray probe is on an edge of the photoconductive region of the first electrode *(at a +6 V biased contact),* the $R_{ph}(x,y)$ and R_{max} must be equal to each other and the value of R_{max} can be determined. Accordingly, a Matlab® routine solves first the boundary situation and obtains the R_{max} value. Then it executes Equation 13 for each point with the measured surface potentials to obtain location specific $R_{ph}(x,y)$ as shown in Figure 39a.

The characteristic photoconductive performance under photoillumination with different lasers and the spectral responses of the LDR are shown in Figure 38c and 39a. The violet and green lasers have higher and an almost equal photonic energies with the band gap energy of CdS *(2.4eV).*[53] For that reason, upon illumination the response of the CdS exhibit almost a zero resistance and only the grounded potential is measured at all locations, which means that the circuit is shorted by the photoillumination with violet and green lights. The photoillumination with the red laser also causes a similar photoresponse with violet and green laser, due probably to the preference of other dopants and defects. However, the NIR laser provides a limited photoconductivity effect on the LDR, which is reasonable because of its lower energy. Moreover, any surface potential variation is an indication of a potential build-up on the device. While the small slopes or fluctuations imply small lateral electric fields along the line direction (mostly in the conductive regions), the larger slopes indicate a larger field generation over the device (mostly in the photoconductive regions). Therefore, the measured surface potential profile could be converted to a laterally generated electric field data as shown in Figure 39b.

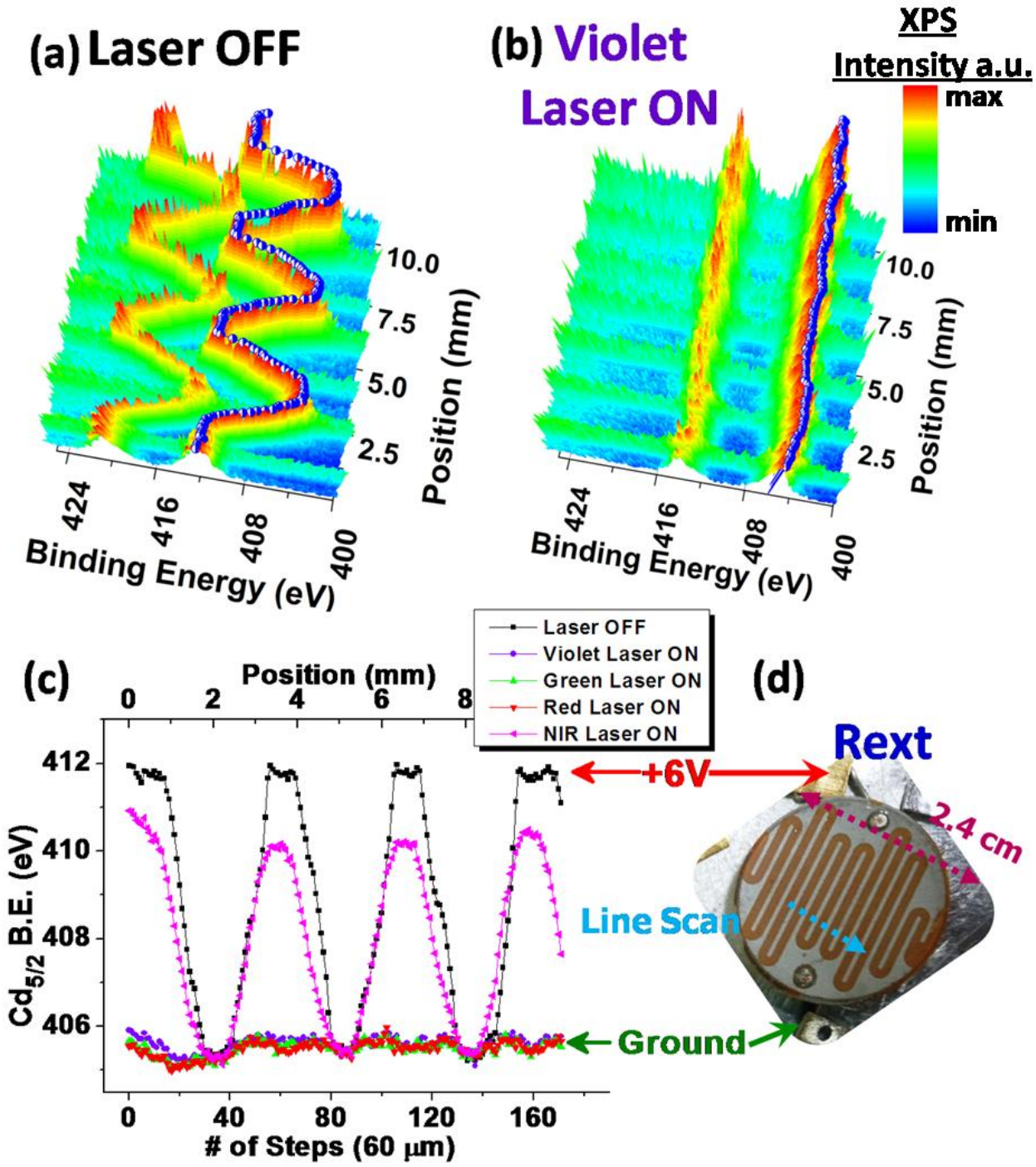

Figure 38. A false contour color plot of XPS line scan spectra along both the conductive and the photoconductive regions of the device at the (a) laser off, (b) laser on states. (c) The measured binding energy position along the line scan without and under violet, green, red, and near infrared lasers illumination. (d) The position of the XPS line scan on the actual device.[79]

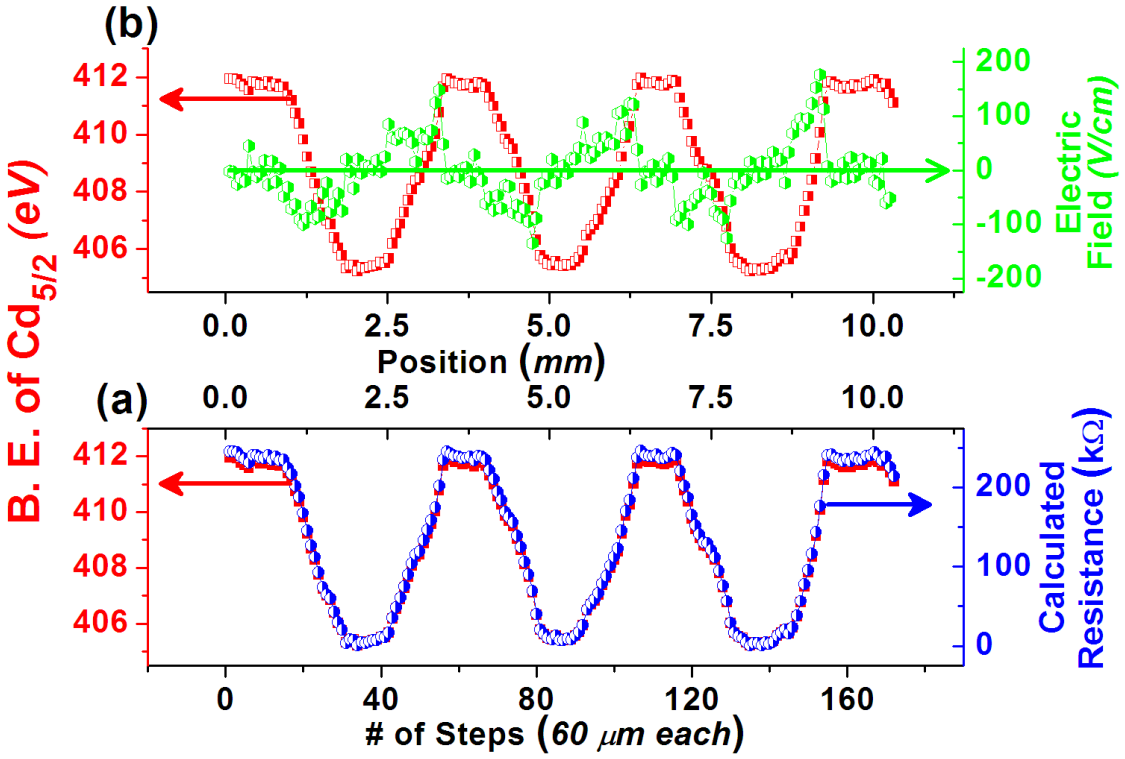

Figure 39. (a) The measured binding energy positions of $Cd_{5/2}$ peak and (b) corresponding calculated location depended resistance values along the XPS line scan.[79]

XPS mapping of survey spectra can also be recorded for a defined area with equal steps along the lateral horizontal and vertical axes. A similar potential deviation with the line scan is measured now as a three dimensions output as shown in Figure 40. The graph has two lateral space dimensions and one binding energy (chemically resolved) dimensions, which reveal critical information about the variation of the surface potentials. A false-color contour plot is used to emphases the extent of the potential variations. In this plot, the top of hills correspond to a +6 V biased conductive regions (Electrode 1), so the Cd3d peak is shifted to about 411 eV, which is almost constant with small fluctuations over the corresponding conductive region. These domains appear in red or reddish colors. The valleys correspond to the grounded conductive region

(Electrode 2), and their color is chosen as green. The downhill side potential variations between the reddish (411 eV) and green (405 eV) territories surface the variations in the potentials of the photoconductive region due to its finite and location depended photoresistance value.

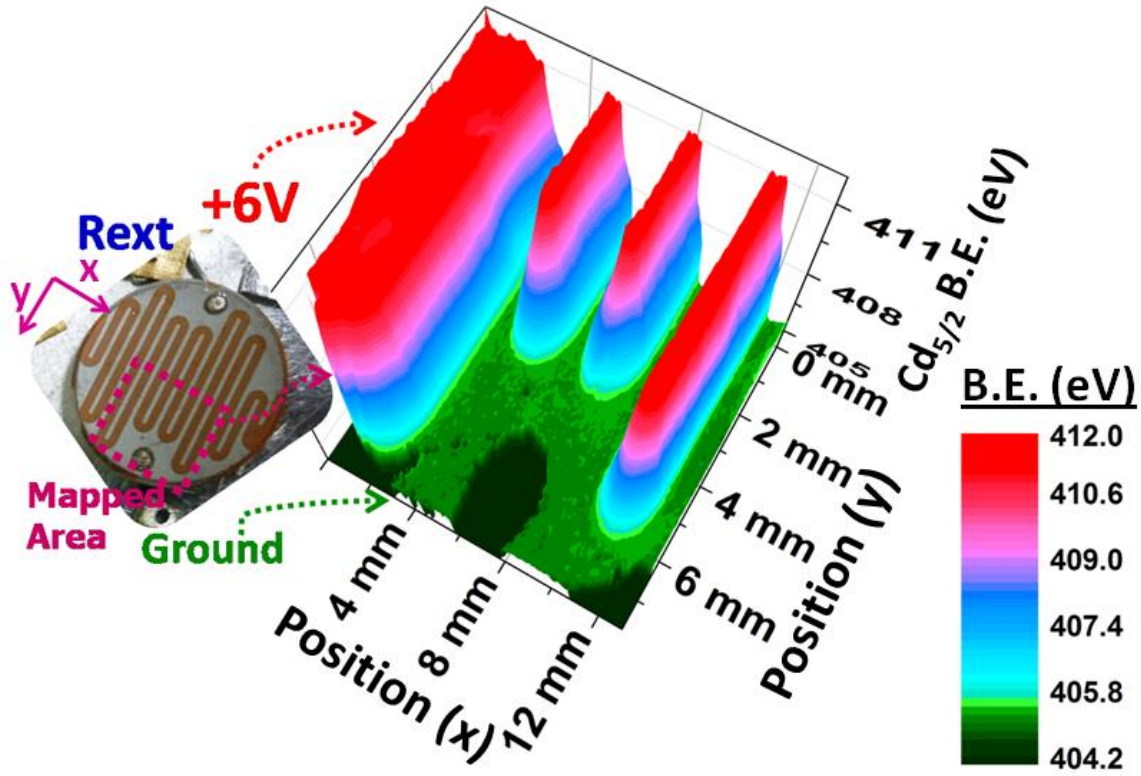

Figure 40. A false contour color plot of XPS area mapped spectra of the LDR device with two lateral space dimensions and one energy dimension.[79]

To obtain chemically and electrically resolved output, we have to fit all of the XPS data sets with the Cd3d envelop. This set consists of 10,010 *(130x77)* individual Cd3d spectra, and requires time and computer power to fit and handle. At the end, rich chemical and electrical contrast between the conductive and photoconductive regions of the LDR can be obtained during its operation. It is rich because the XPS peak positions have more detailed, albeit complex information, since the position of XPS peak can be affected by elemental, chemical, physical, electrical, optical, mechanical, etc. parameters.

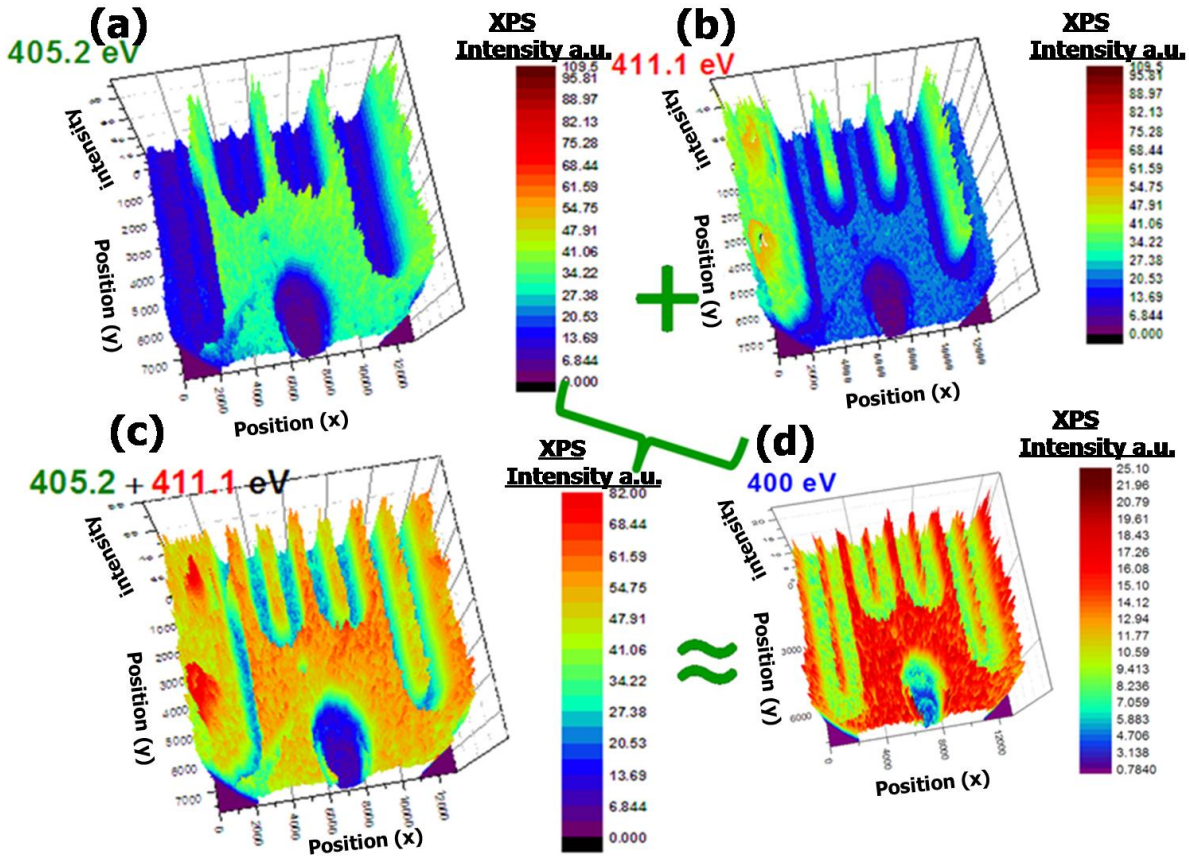

Figure 41. X-ray photocurrent maps with two dimensional space resolved spectra at (a) 405.2 eV, (b) 411.1 eV, (c) a summation of the intensities at 405.2 and 411.1 eV and (d) at 400 eV.[79]

The chemically contrasted information can also be obtained in simpler fashions. For example, the simplest chemical information can be extracted by just following the x-ray photocurrent information without any fitting as demonstrated in Figure 41. In this procedure, one follows the x-ray photocurrent at the peak positions, 405.2 and 411.1 eV, corresponding to the peak positions at +6 V biased and grounded Cd3d peaks, respectively. The resulting picture is not a complete chemical contrast, and has only half of the information about the LDR. Therefore, the sum of these two data sets yields a full chemical composition map as shown in Figure 41c. Interestingly, similar chemical composition information can also be extracted using a baseline position data, for

example, at 400 eV as shown Figure 41d and 42. This unexpected result can be directly related with the chemical contrast between the conductive and photoconductive regions. Doping with Sn and Pb increases electrical conductivity and in turn causes an intensity enhancement on the baseline of the conductive regions. As a result, x-ray photoconductivity mapping provides a full chemically contrasted compositional map at position for away from a peak position. This trick is almost an effortless exercise to obtain certain compositional analysis from chemically different domains, and it drastically reduces data processing time.

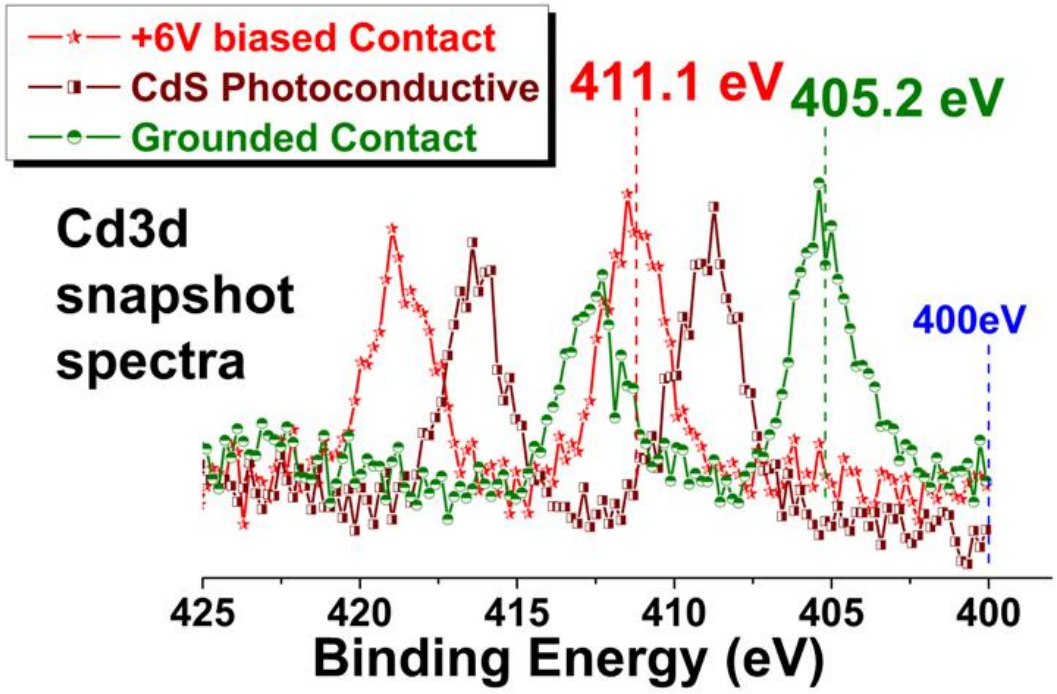

Figure 42. Intentionally selected XPS snapshot spectra for comparison of x-rays photocurrent at 400 eV binding energy.[79]

The CdS based LDR used in this work has also defected regions, as shown in detail in Figure 43. These defects are probably created during the fabrication process. In the defective site the conductive region extends over to the photoconductive region, so the measured voltage is smaller than excepted. However, as shown in Figure 43d under violet

light photoillumination the electrical contrast between the defect region and the normal region disappears, since the violet light almost completely eliminates all resistive characteristic of the LDR. But since the NIR laser causes only a limited photoconductivity on the device, as demonstrated in Figure 43c the defect site becomes more pronounced under NIR light photoillumination laser. Hence, XPS with proper photoillumination provides unique information for assessing defect and/or device performance.

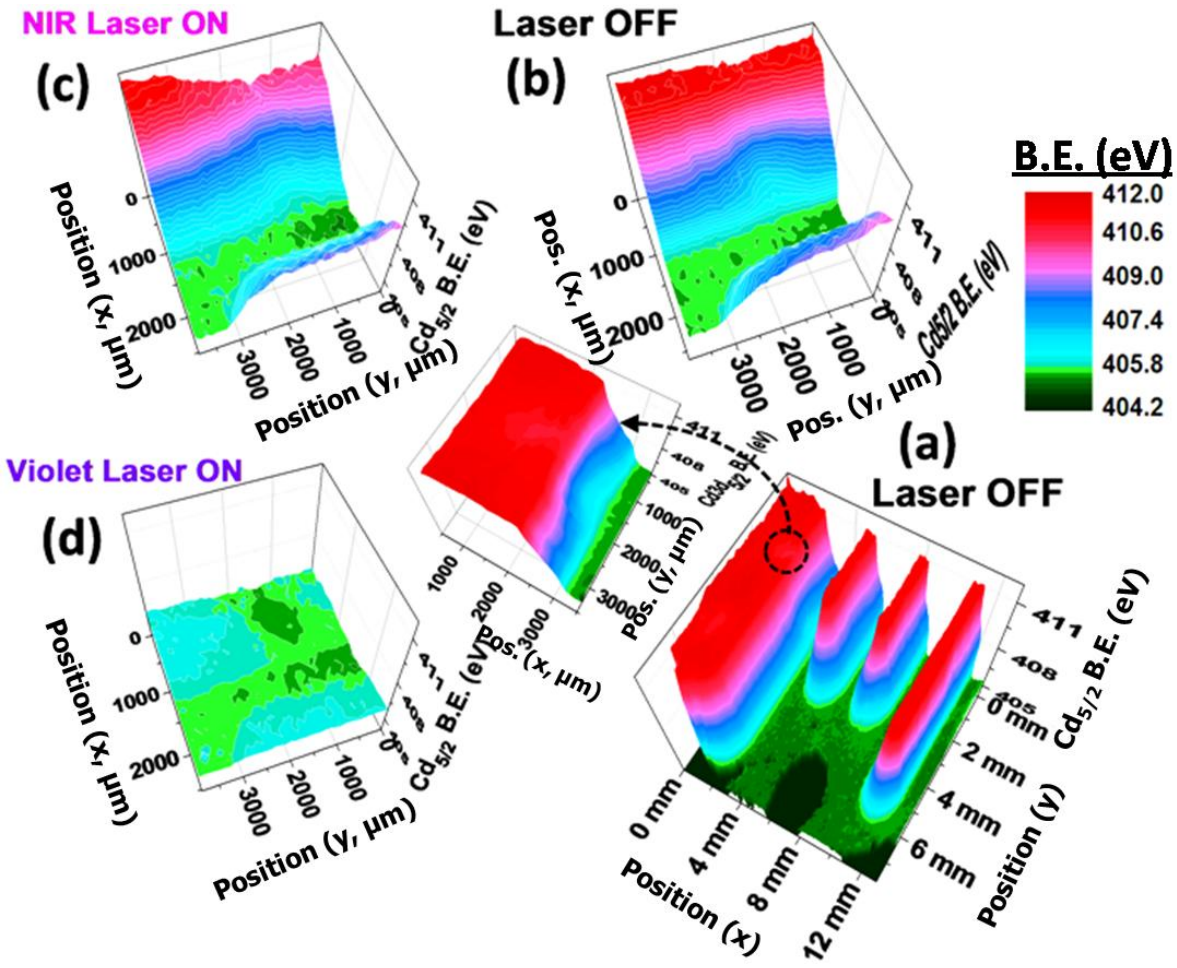

Figure 43. The defect region analysis of XPS mapping. (a) A big area Laser OFF, (b) defect specified small area scans Laser OFF state (c) NIR Laser ON, and (d) violet Laser ON with iso-energy line to emphasize energy steps (0.2eV).[79]

4.3. Surface Photoresponse and Transients of n- and p-type GaN

n- and p-type doped GaN samples are also investigated with the photo-dynamic XPS. A survey spectrum of the p-type GaN has an intense $Ga2p_{3/2}$ peak at 1118.49 eV and 3d, 3p, 3s peaks at 20.15 eV, 106.48 eV, 161.41 eV, respectively as shown in Figure 44.[2] In addition, Ga has a number of LMM Auger lines spanning the interval from 380 to 630 eV.[2] Unfortunately, a broad LMM auger line of Ga at 397 eV is overlapping with the N1s peak, so it is not possible to follow individual N1s region with our XPS instrument using AlKα x-rays. We generally follow the Ga2p if we need high intensity which is required for snapshot type fast data acquisition mode. The Ga3d peak is recorded for a better resolution due to a sharper energy distribution of the d-orbitals when compared to the p-orbitals.

The $Ga2p_{3/2}$ spectra of the n- and p-GaN are recorded with and without violet laser illumination, as shown in Figure 45a,b, respectively. The highest steady state surface photovoltage responses of the n- and p-GaN are measured as +0.15 eV and -0.39 eV, respectively, while the flood gun is not employed. When the flood gun is functioning, the response of especially the p-type GaN is significantly altered and provides additional information about the band diagram of the semiconductor, as will be discussed later in this section.

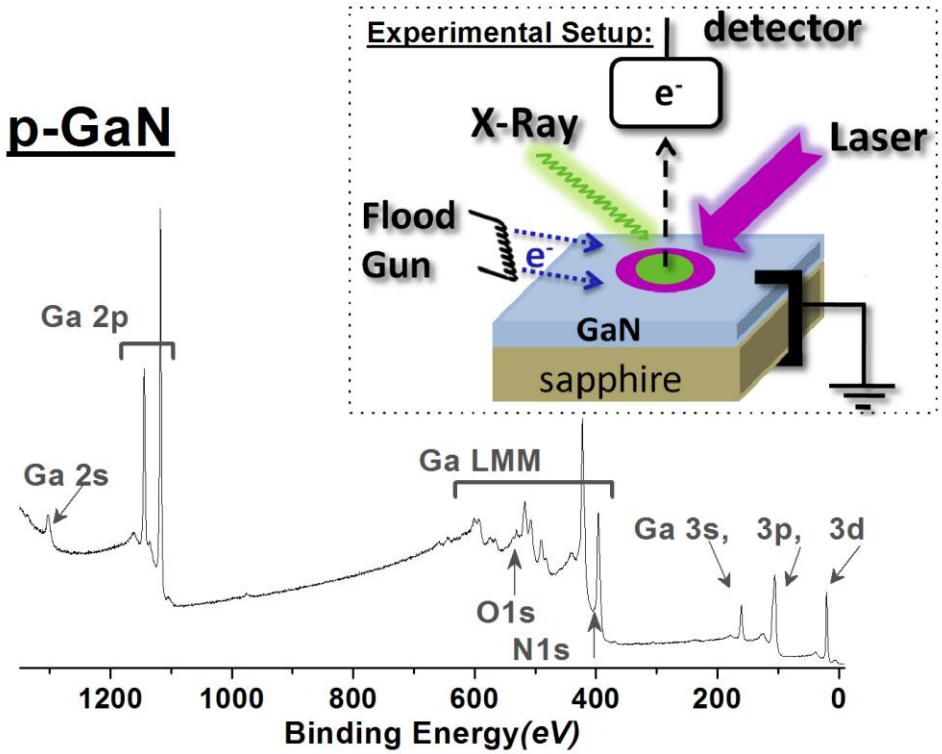

Figure 44. Survey XPS spectrum of p-type GaN sample. Inset demostrates the experimental setup.

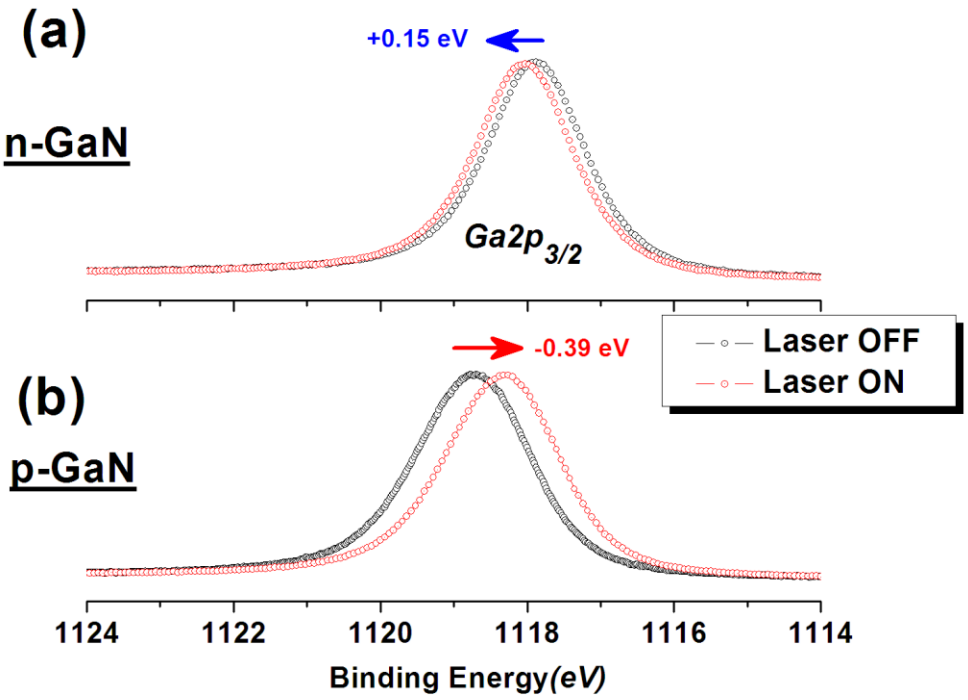

Figure 45. The XPS spectra of the (a) n- and (b) p-type GaN with and without photoillumination.

As mentioned before, an illumination with the violet laser (3.1 eV) is a sub-band gap excitation since the band gap of GaN is 3.4 eV. Although the sub-band gap surface photovoltage value of the p-type GaN has not been reported before, the earlier reported works point out a higher surface photovoltage for the n-type GaN than our measured value.[59, 61, 63, 144, 145] The possible reasons for the measured lower surface photovoltage of the n-type GaN can be explained by reasons related to our measurement system. Firstly, x-ray irritation can be considered as a pumping source for building up of a surface photovoltage as has been reported before.[59] The other possible explanation is that the previous surface photovoltage measurements were carried out in an ambient atmosphere with the Kelvin Probe technique, so the interaction between the sample and the ambient gas has a significant effect on both the magnitude and the dynamics of the surface photovoltage. A comparison between ambient and vacuum measurement indicates a reduction for the measured surface photovoltage in the vacuum environment.[146] In addition, contribution from the sub-band gap photoexcitation is also an important factor for measuring a decrease of the surface photovoltage in the n-GaN sample.[63] These sub-band gap surface photovoltage processes of the n- and p-GaN under violet laser photoillumination are depicted in Figure 46a,b, respectively. These processes involve a resonant excitation of an electron and a hole from surface states into bulk for the n- and p-GaN, respectively. For example, for the assumed surface photovoltage processes during the laser-on state one electron (hole) of the surface state of the n-GaN (p-GaN) is excited to the conduction (valance) band. At the laser-off state the excited electrons or holes must return back over a potential barrier. Usually thermal excitation can provide this energy, but for our measurements the generated charge carriers can be re-excited by x-rays, too.

Further investigation is necessary to determine the effect(s) of x-rays on the surface photovoltage transients.[49]

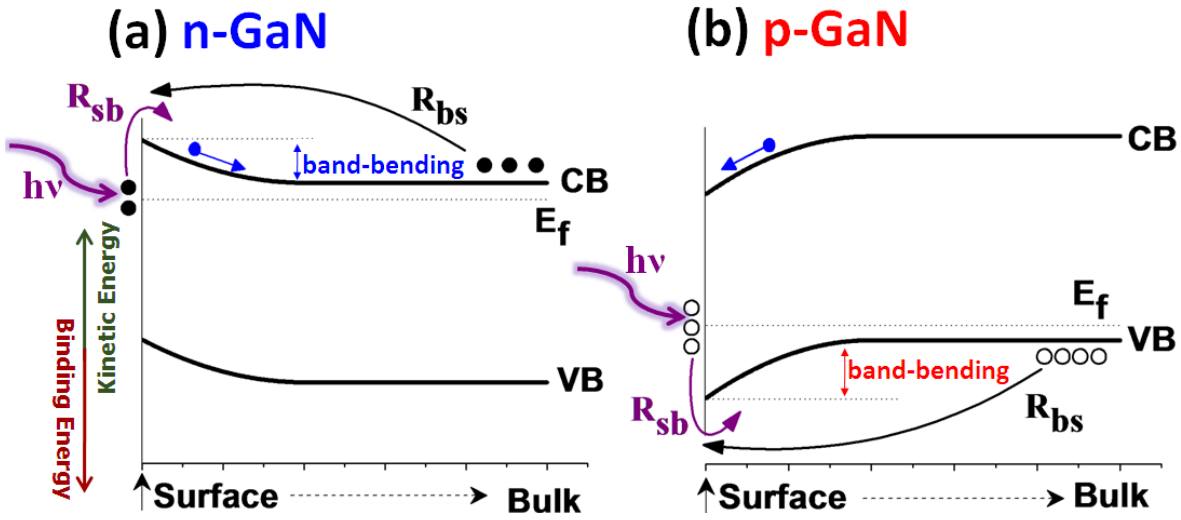

Figure 46. The bended band diagrams and possible sub-band gap photoexcitation processes of (a) n-GaN (b) p-GaN.

As in the case of the Si sample, we have also carried out measurements by varying the intensity of the excitation source to obtain a relationship between the measured value of the surface photovoltage and the logarithm of the intensity of light as given in Figure 47. It also exhibits a saturation behavior in the region of high intensity, which indicates that the response of the p-GaN sample must be mostly due to surface related processes. In addition, photoconductive response of the GaN to the excitation light source as in the CdS film are also observed from the dynamic XPS investigations as shown in Figure 48. The n-GaN sample has enough dark conductivity, so there is a small charge accumulation and dissipation processes under the external electrical stress as shown Figure 48a. The p-GaN has a significant resistance and capacitance to allow us to observe a strong frequency dependence to the squarewave electrical stress as shown in Figure 48b and

47a. The frequency dependence of the p-type GaN is different from that of the CdS. The laser illumination causes only a symmetric shift for both higher and lower frequencies of the squarewave electric excitation. A clearer picture comes out when the B.E. Diff. vs. frequency plots are constructed as shown in Figure 49b. All of shifts of the p-GaN at all frequencies produce similar amounts of offset. As a result, the binding energy difference vs. the frequency plot eliminates this offset type shifts between the laser off and on states and produces identical differences at every frequency as shown in Figure 49b. In the light of these results, we can say that the photoconductivity of the n- and p-GaN samples under the sub-band excitation might be lower than the energy resolution limitation of our instrument.

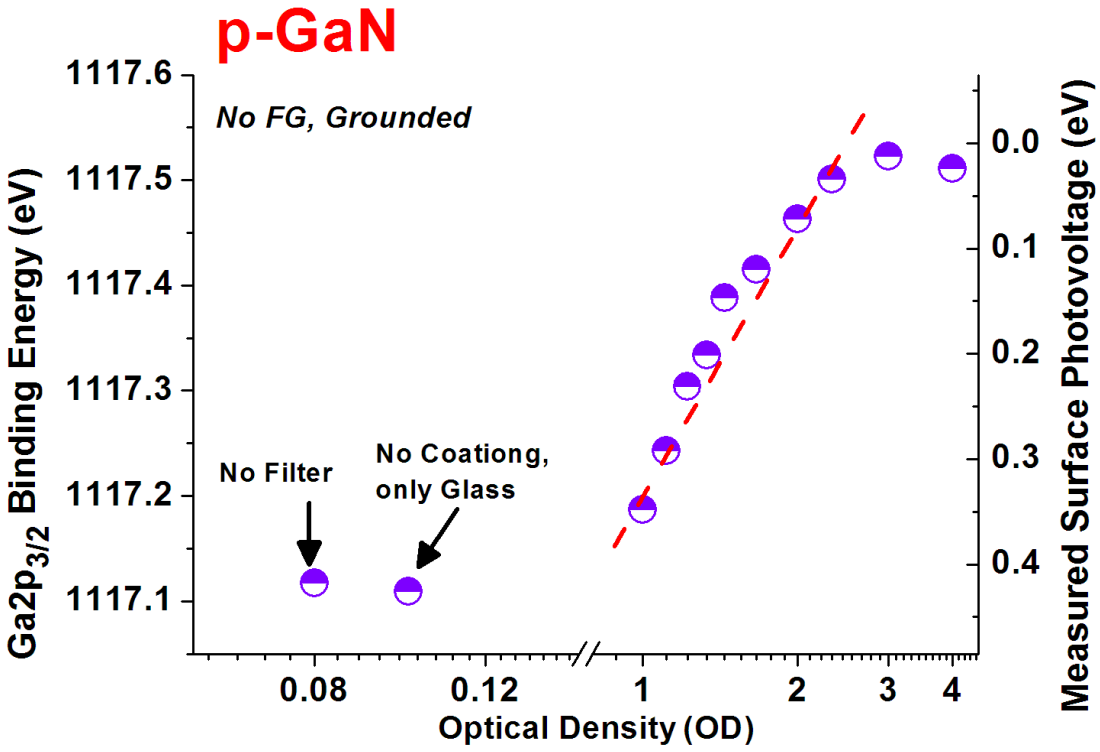

Figure 47. The relationship between measured binding energy variation or build-up of the surface photovoltage of p-GaN and the intensity of excitation source.[79]

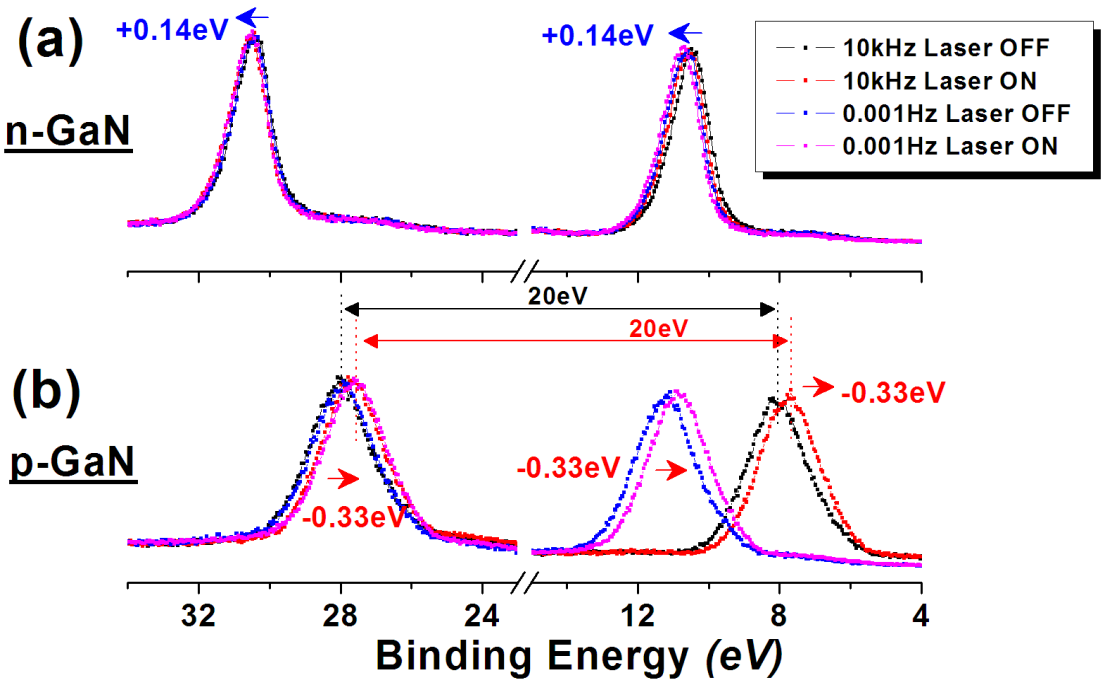

Figure 48. XPS spectra of Ga3d peaks of the n- and p-GaN with and without photoillimination, at (a) 10 kHz, and (b) 0.001 Hz squarewave electrical excitation.[79]

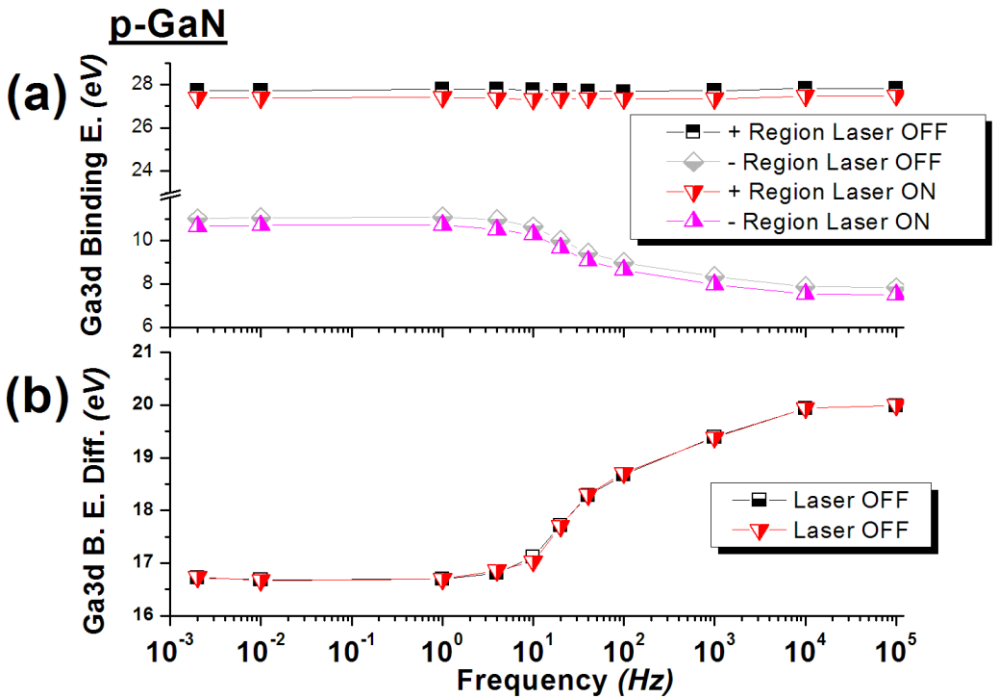

Figure 49. Frequency dependence of (a) the measured binding energies and (b) binding energy difference of the p-GaN under different squarewave electrical excitation frequencies with and without photoillumination.[79]

The transient type surface photovoltages as well as steady-state ones are also measured as illustrated in Figure 50 under shuttered photoillumination. The successive snapshot spectra of the $Ga2p_{3/2}$ peak are recorded with 0.1 s intervals, and the data are fitted with a 50:50% Gaussian+Lorentzian mixture to determine the peak positions using the Avantage® program. When the flood gun is not operating, the transients of the n- and p-GaN are very fast, instantaneous and are +0.15 eV and -0.39 eV, respectively. The low energy electron flood-gun facility of the XPS instrument was utilized to gather additional information about the nature and the mechanism of the sub-band gap surface photovoltage. It is known that the low energy electrons can penetrate to a significant depth and can also be incorporated to the conduction band of semiconductors. As shown in Figure 50, the cyan lines are the surface photovoltage behavior of n- and p-GaN with low energy electrons. The presence of low energy electrons leads to a small shift of ca. 0.2 eV for the n-GaN due to its relatively higher conductivity, and ca. 1.2 eV for the p-GaN due to its limited conductivity. The use of the flood gun did not affect the transient surface photovoltages of the n- an p-GaN, but an additional process for the p-GaN also appears as depicted in the inset of Figure 51. This can be explained as follows. The p-GaN develops a certain magnitude of downward band-bending at its surface. This downward band-bending at the laser-off state provides a proper well to capture the flood-gun electrons at or near the conduction band, as schematically illustrated in the inset of Figure 51, to cause an opposite shift to lower binding energy as expected and measured. When the state of the laser is changed to the laser-on, the downward band-bending is immediately flattened and is no longer a well. Hence, the accumulated electrons during the previous state are quickly swept away to the bulk, because now the conduction band

of the bulk has many favorable energy levels for the electrons as also shown the inset of the Figure 51. This event is observed as a further shift to a higher binding energy.[49, 51]

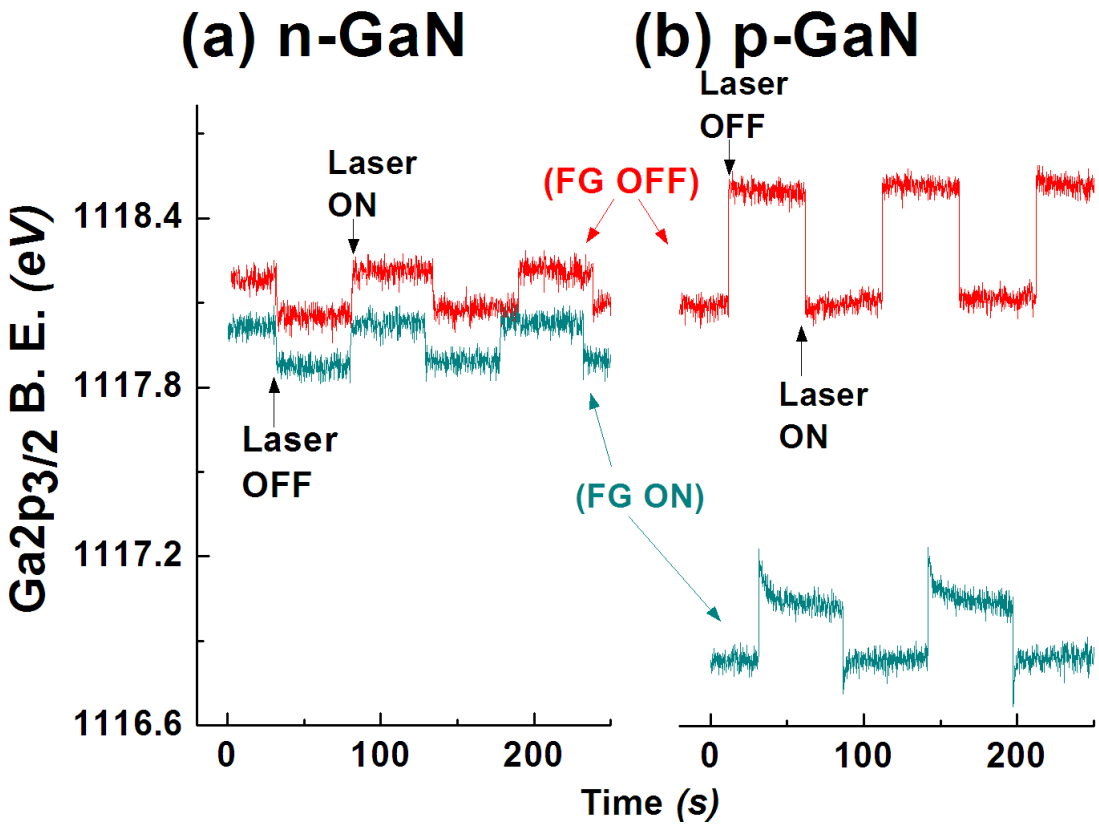

Figure 50. The meaured binding energy changes recorded in transient mode of $Ga2p_{3/2}$ peak of (a) n- (b) p-GaN whit and without low energy electrons.

Moreover, the time constants of the electron accumulation and sweeping of the p-GaN are quite different from each other and are measured as 6.3 and 0.85 s respectively as shown Figure 51. This difference is reasonable because two mechanisms have different natures. The impinging electrons takes longer time to be accommodated, since each accumulated electron contributes to the build-up of the negative sheet of charge at the surface, which in turn reduces the rate of accumulation of further negative charge.

However, when the laser is turned on, the sweeping of accumulated electrons to the bulk is very effective and quick due to its large volume compared to the surface.[49, 51]

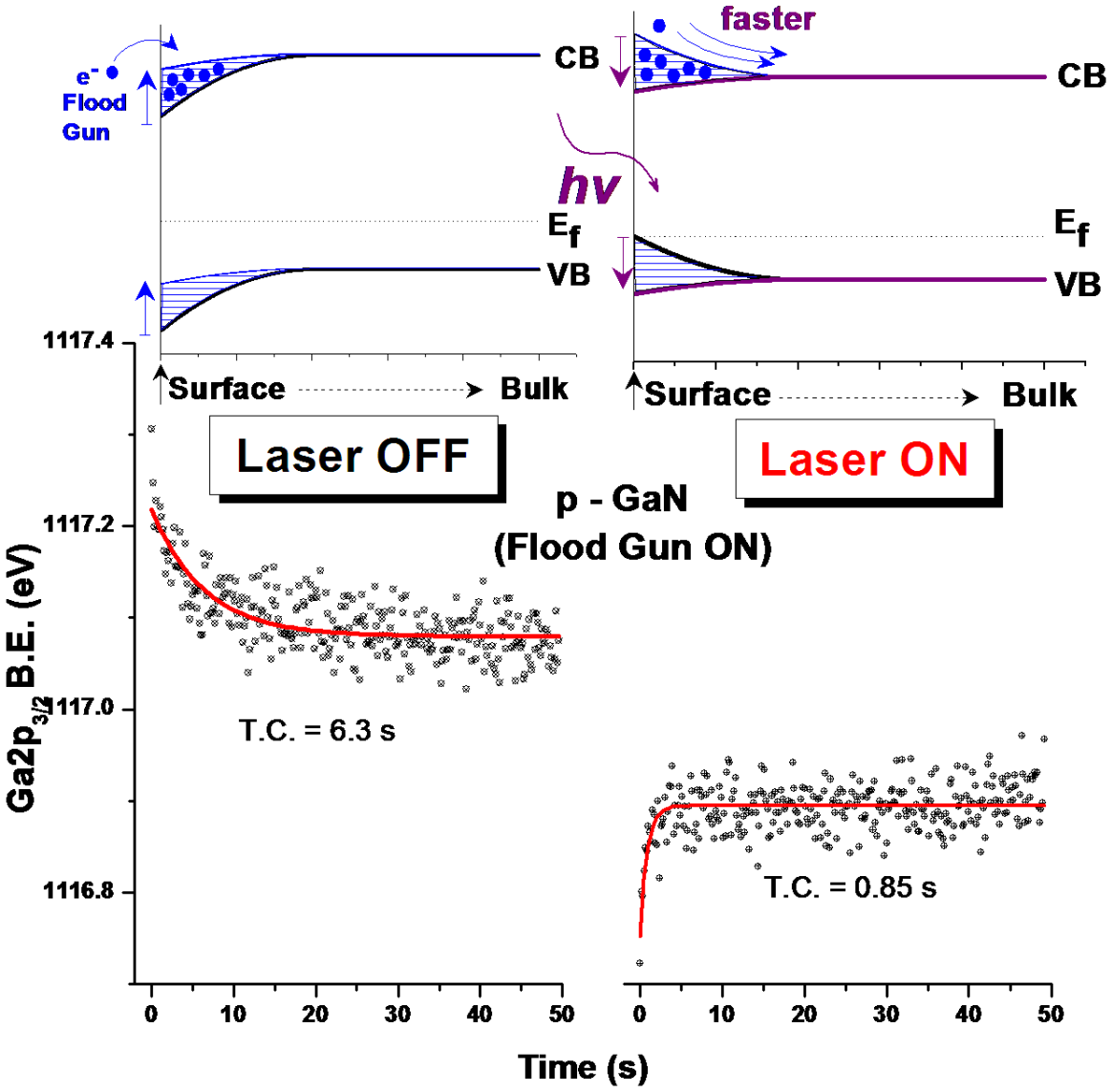

Figure 51. The exponential fitting of the laser on and off transients of the p-GaN. The inset demonstrates possible slow and faster mechanisms of the electron accumulation and sweeping in and from the conduction band.

4.3.1. Inversion of the Surface Photovoltage of p-type GaN

As discussed before, band-to-band or other energetic transitions yield a surface photovoltage measured as a red-shift in the binding energy of a p-type semiconductor. However, under certain conditions an opposite surface photovoltage shift can also be obtained. As GaN is a wide gap semiconductive material, the p-GaN has surface defects, traps, etc. Previously published reports predict the pinned Fermi level is about 1 eV above the valance band and presence of surface states which act as a donor or an acceptor in p-GaN.[63, 144, 147, 148] Therefore, the strong downward band-bending of the p-GaN is expected to lead to band inversion as schematically displayed in Figure 52a,b.

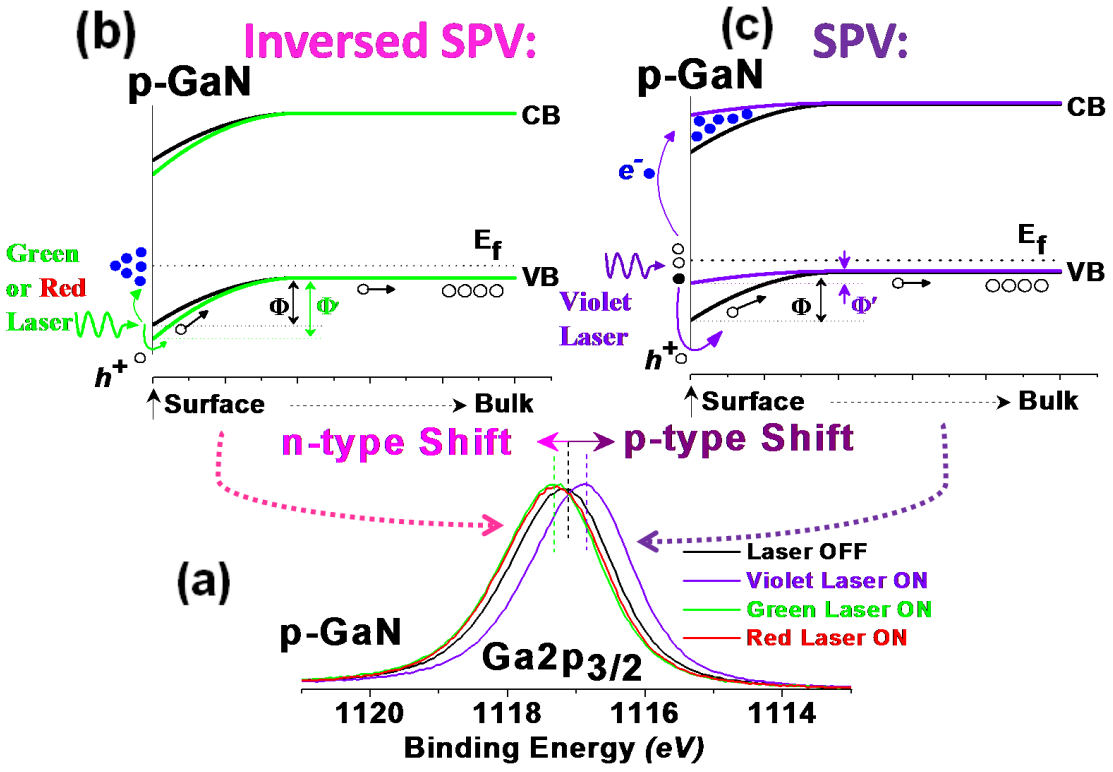

Figure 52. (a) The surface photoresponse of the p-GaN under violet, green, and red laser illumination and possible mechanisms of (b) inversion of the surface photovoltage of p-GaN for green and red laser sub-band gap excitation and (c) the surface photovoltage for violet laser sub-band gap excitation.[79]

The green light *(2.3 eV)* excites electrons from the bended valance band to the surface state(s) of p-GaN as displayed in Figure 52a,b. As a result of this, the valance band is bended to a further lower kinetic energy (as measured a higher binding energy shift with XPS) position as shown in Figure 52a,b. Under red light photoillumination a similar result also appears as another example of the inversion of the surface photovoltage as also shown in Figure 52a,b. However, the more energetic violet laser excitation excites electrons from surface state(s) to the conduction band as demonstrated in Figure 52a,c. Therefore, the downward band-bending of p-GaN is now flattened due to accommodation of the excited electrons in the conduction band. The power of XPS stems from the fact that all of these excitations and the resulting potentials could be monitored as shifts in the core and valance peaks of the sample in a chemically addressed fashion.

5. Conclusions

The main emphasis of this work is characterization of photo-induced voltage variations in semiconductive materials, under electrical and/or optical excitation sources and probing with a noncontact and chemically resolved method; the photo-dynamic XPS. The electrical effects have been investigated by our group and different groups so far, but optical stimulus has not been extensively utilized to investigate the related phenomena with XPS. Our main strategy is based on the premise that different processes are triggered by different stimulant sources, and the corresponding responses manifest to different extents and in different time domains. As a result, we can distinguish these differentiated responses via appropriate form and combination of the excitation sources.

Using our photo-dynamic XPS we have determined that n- and p-type Si samples under photoillumination exhibit opposite polarity surface photovoltages due to band-flattening process, and this technique can be used as a method to determine the type of doping of Si wafers. By providing appropriate reference point between the n- and p-Si samples and correcting with respect to their surface photovoltage values, the dopant dependent peak shifts are assessed by XPS. Varying the intensity of the incident light provides us further information about the nature of the surface photovoltage. The band inversion effects are monitored on the n- and p-Si in the presence of silica overlayers, and due to different charging behaviors of Si and Si^{+4} domains under photoillumination. We have also distinguished the faster surface photovoltage process from the slower photo-induced ones. From chemical and electrical characterization of the high power pulse NIR laser processed Si wafer with XPS, we have determined that the patterned and unpatterned domains are stoichiometrically identical (SiO_2), but are electrically very

different from each other. Moreover, an investigation with dynamic XPS enhances the electrical contrast between these two silica domains.

The electrical parameters of CdS are extracted by employing our photo-dynamic XPS technique with and without photoillumination. The photo-dynamic XPS technique also provides fruitful information by creating charge contrasts between different types of processes such as charging/discharging, photoconductivity, and surface photovoltage. Varying the intensity of the incident light and also recording the frequency dependence of CdS films reveal detailed characteristics about the surface photovoltage and the photoconductivity of these systems. The location dependent surface potential variations over the photoconductive and the conductive regions of the CdS based LDR is investigated under realistic operational conditions with the photo-dynamic XPS in a chemically specific fashion to probe the spatially resolved electrical information and to identify defect sites.

The photo-dynamic XPS method is also used to characterize the instantaneous behavior of the transient surface photovoltage of the n- and p-GaN samples in a dynamic fashion to probe the band-flattening mechanisms which involve sub-band gap photo-absorption. By incorporating low energy electrons, accumulation and sweeping of electrons in and from the conduction band of the GaN is observed as an additional interaction between surface states and stray electrons. Probing of these processes provides us a better understanding about the mechanism of the transient surface photovoltage of the p-GaN. An inversion of the surface photovoltage of the p-GaN was observed under sub-band gap photoillumination using different lasers.

6. References

1. Siegbahn, K. "Electron-Spectroscopy for Atoms, Molecules, and Condensed Matter." *Science* **1982,** 217, (4555), 111-121.

2. Moulder, J. F.; Stickle, W. F. and Sobol, P. E. **1992.** *Handbook of X-Ray Photoelectron Spectroscopy*. Minnesota: Physical Electronics Division, Perkin-Elmer Corp.

3. Briggs, D. and Seah, M. P. **1996.** *Practical Surface Analysis by Auger and Photoelectron Spectroscopy*. (2nd ed.). Chichester: Wiley.

4. Hüfner, S. **2003.** *Photoelectron Spectroscopy: Principles and Applications*. (3rd ed.). Heidelberg: Springer Verlag.

5. Watts, J. F.; Wolstenholme, J. and Wiley, J. **2003.** *An Introduction to Surface Analysis by XPS and AES*. Chichester: Wiley Online Library.

6. Sezen, H. **2008.** *Investigation on Electrical Charging/Discharging Properties of Thin PS/PMMA Polymeric Films by Dynamic X-Ray Photoelectron Spectroscopy.* Thesis (M.S.), Bilkent University, Ankara, Turkey.

7. Mitschele, J. "Beer-Lambert Law." *Journal of Chemical Education* **1996,** 73, (11), 260.

8. Powell, C. J. "The Energy Dependence Electron Attenuation Lengths." *Surface and Interface Analysis* **1985,** 7, (6), 256-262.

9. Bain, C. D. and Whitesides, G. M. "Attenuation Lengths of Photoelectrons in Hydrocarbon Films." *Journal of Physical Chemistry* **1989,** 93, (4), 1670-1673.

10. Powell, C. J. and Jablonski, A. "Comparisons of Calculated and Measured Effective Attenuation Lengths for Silicon Dioxide over a Wide Electron Energy Range." *Surface Science* **2001,** 488, (1-2), L547-L552.

11. Powell, C. J. and Jablonski, A. "Electron Effective Attenuation Lengths for Applications in Auger-Electron Spectroscopy and X-Ray Photoelectron Spectroscopy." *Surface and Interface Analysis* **2002,** 33, (3), 211-229.

12. Jablonski, A. and Powell, C. J. "Comparisons of Practical Attenuation Lengths Obtained from Different Algorithms for Application in XPS." *Surface Science* **2002,** 520, (1-2), 78-96.

13. Cumpson, P. J. "Angle-Resolved XPS and AES: Depth-Resolution Limits and a General Comparison of Properties of Depth-Profile Reconstruction Methods." *Journal of Electron Spectroscopy and Related Phenomena* **1995,** 73, (1), 25-52.

14. Hollinger, G. and Himpsel, F. "Probing the Transition Layer at the SiO2 Si Interface Using Core Level Photoemission." *Applied Physics Letters* **1984,** 44, (1), 93-95.

15. Teschner, D.; Pestryakov, A.; Kleimenov, E.; Hävecker, M.; Bluhm, H.; Sauer, H.; Knop-Gericke, A. and Schlögl, R. "High-pressure X-Ray Photoelectron Spectroscopy of Palladium Model Hydrogenation Catalysts.: Part 1: Effect of Gas Ambient and Temperature." *Journal of Catalysis* **2005,** 230, (1), 186-194.

16. Bluhm, H.; Andersson, K.; Araki, T.; Benzerara, K.; Brown, G. E.; Dynes, J. J.; Ghosal, S.; Gilles, M. K.; Hansen, H. C.; Hemminger, J. C.; Hitchcock, A. P.; Ketteler, G.; Kilcoyne, A. L. D.; Kneedler, E.; Lawrence, J. R.; Leppard, G. G.; Majzlan, J.; Mun, B. S.; Myneni, S. C. B.; Nilsson, A.; Ogasawara, H.; Ogletree, D. F.; Pecher, K.; Salmeron, M.; Shuh, D. K.; Tonner, B.; Tyliszczak, T.; Warwick, T. and Yoon, T. H. "Soft X-Ray Microscopy and Spectroscopy at the Molecular Environmental Science Beamline at the Advanced Light Source." *Journal of Electron Spectroscopy and Related Phenomena* **2006,** 150, (2-3), 86-104.

17. Ketteler, G.; Yamamoto, S.; Bluhm, H.; Andersson, K.; Starr, D. E.; Ogletree, D. F.; Ogasawara, H.; Nilsson, A. and Salmeron, M. "The Nature of Water Nucleation Sites on TiO2(110) Surfaces Revealed by Ambient Pressure X-Ray Photoelectron Spectroscopy." *The Journal of Physical Chemistry C* **2007,** 111, (23), 8278-8282.

18. Zhang, C.; Grass, M. E.; McDaniel, A. H.; DeCaluwe, S. C.; El Gabaly, F.; Liu, Z.; McCarty, K. F.; Farrow, R. L.; Linne, M. A. and Hussain, Z. "Measuring Fundamental Properties in Operating Solid Oxide Electrochemical Cells by Using in situ X-Ray Photoelectron Spectroscopy." *Nature Materials* **2010,** 9, 944–949.

19. Pelissier, B.; Beaurain, A.; Barnes, J. P.; Gassilloud, R.; Martin, F. and Joubert, O. "Parallel Angle Resolved XPS Investigations on 12 in. Wafers for the Study of W

and WSix Oxidation in Air." *Microelectronic Engineering* **2008,** 85, (9), 1882-1887.

20. Lau, W. M.; He, J. W. and Norton, P. R. "X-Ray Photoemission Studies of the Interfacial Reactions of Pt and Au on Anodic Oxide of Hg0.8Cd0.2Te." *Applied Physics Letters* **1989,** 54, (8), 772-774.

21. Cazaux, J. "Mechanisms of Charging in Electron Spectroscopy." *Journal of Electron Spectroscopy and Related Phenomena* **1999,** 105, (2-3), 155-185.

22. Lau, W. M. "A Surface Charging Technique in Photoemission Spectroscopic Studies of Dielectric-Semiconductor Structures." *Journal of Applied Physics* **1990,** 67, (3), 1504-1509.

23. Larson, P. E. and Kelly, M. A. "Surface Charge Neutralization of Insulating Samples in X-Ray Photoemission Spectroscopy." *Journal of Vacuum Science & Technology A* **1998,** 16, (6), 3483-3489.

24. Cazaux, J. "About the Charge Compensation of Insulating Samples in XPS." *Journal of Electron Spectroscopy and Related Phenomena* **2000,** 113, (1), 15-33.

25. Iwata, S. and Ishizaka, A. "Electron Spectroscopic Analysis of the SiO2/Si System and Correlation with Metal-Oxide-Semiconductor Device Characteristics." *Journal of Applied Physics* **1996,** 79, (9), 6653-6713.

26. Doron-Mer, M.; Hatzor, A.; Vaskevich, A. and Van Der, B. M. "Controlled Surface Charging as a Depth-Profiling Probe for Mesoscopic Layers." *Nature* **2000,** 406, (6794), 382-385.

27. Havercroft, N. J. and Sherwood, P. M. A. "Use of Differential Surface Charging to Separate Chemical Differences in X-Ray Photoelectron Spectroscopy." *Surface and Interface Analysis* **2000,** 29, (3), 232-240.

28. Suzer, S. "Differential Charging in X-Ray Photoelectron Spectroscopy: A Nuisance or a Useful Tool?" *Analytical Chemistry* **2003,** 75, (24), 7026-7029.

29. Suzer, S. "XPS Studies with External Voltage Bias for Probing Nanoparticle-Substrate Interaction." *Abstracts of Papers of the American Chemical Society* **2003,** 225, U509-U509.

30. Ertas, G. and Suzer, S. "XPS Analysis with External Bias: A Simple Method for Probing Differential Charging." *Surface and Interface Analysis* **2004,** 36, (7), 619-623.

31. Ertas, G.; Demirok, U. K.; Atalar, A. and Suzer, S. "X-Ray Photoelectron Spectroscopy for Resistance-Capacitance Measurements of Surface Structures." *Applied Physics Letters* **2005,** 86, (18), 183110.

32. Ertas, G.; Demirok, U. K. and Suzer, S. "Enhanced Peak Separation in XPS with External Biasing." *Applied Surface Science* **2005,** 249, (1-4), 12-15.

33. Cohen, H.; Maoz, R. and Sagiv, J. "Transient Charge Accumulation in a Capacitive Self-Assembled Monolayer." *Nano Letters* **2006,** 6, (11), 2462-2466.

34. Dane, A.; Demirok, U. K.; Aydinli, A. and Suzer, S. "X-Ray Photoelectron Spectroscopic Analysis of Si Nanoclusters in SiO2 Matrix." *Journal of Physical Chemistry B* **2006,** 110, (3), 1137-1140.

35. Suzer, S. and Dana, A. "X-Ray Photoemission for Probing Charging/Discharging Dynamics." *Journal of Physical Chemistry B* **2006,** 110, (39), 19112-19115.

36. Mukherjee, S. and Mukherjee, M. "Controlled Surface Neutralization: a Quantitative Approach to Study Surface Charging in Photoemission." *Journal of Electron Spectroscopy and Related Phenomena* **2007,** 154, (3), 90-95.

37. Suzer, S.; Dana, A. and Ertas, G. "Differentiation of Domains in Composite Surface Structures by Charge-Contrast X-Ray Photoelectron Spectroscopy." *Analytical Chemistry* **2007,** 79, (1), 183-186.

38. Sezen, H.; Ertas, G.; Dana, A. and Suzer, S. "Charging/Discharging of Thin PS/PMMA Films as Probed by Dynamic X-Ray Photoelectron Spectroscopy." *Macromolecules* **2007,** 40, (12), 4109-4112.

39. Sezen, H.; Ertas, G. and Suzer, S. "Methods for Probing Charging Properties of Polymeric Materials Using XPS." *Journal of Electron Spectroscopy and Related Phenomena* **2010,** 178-179, 373-379.

40. Sezen, H. and Suzer, S. "Dynamical XPS Measurements for Probing Photoinduced Voltage Changes." *Surface Science* **2010,** 604, (21-22), L59-L62.

41. Sezen, H. and Suzer, S. "Charging/Discharging Dynamics of CdS and CdSe Films under Photoillumination Using Dynamic X-Ray Photoelectron Spectroscopy." *Journal of Vacuum Science & Technology A* **2010,** 28, (4), 639-642.

42. Suzer, S.; Sezen, H.; Ertas, G. and Dana, A. "XPS Measurements for Probing Dynamics of Charging." *Journal of Electron Spectroscopy and Related Phenomena* **2010,** 176, (1-3), 52-57.

43. Johnson, P. A. and Levicky, R. "X-Ray Photoelectron Spectroscopy and Differential Capacitance Study of Thiol-Functional Polysiloxane Films on Gold Supports." *Langmuir* **2004,** 20, (22), 9621-9627.

44. Yang, D. Q.; Meunier, M. and Sacher, E. "The Estimation of the Average Dimensions of Deposited Clusters from XPS Emission Intensity Ratios." *Applied Surface Science* **2001,** 173, (1-2), 134-139.

45. Tunc, I.; Suzer, S.; Correa-Duarte, M. A. and Liz-Marzan, L. M. "XPS Characterization of Au (Core)/SiO2 (Shell) Nanoparticles." *Journal of Physical Chemistry B* **2005,** 109, (16), 7597-7600.

46. Tougaard, S. and Ignatiev, A. "Concentration Depth Profiles by XPS; a New Approach." *Surface Science* **1983,** 129, (2-3), 355-365.

47. Borchert, H.; Haubold, S.; Haase, M.; Weller, H.; McGinley, C.; Riedler, M. and Moller, T. "Investigation of ZnS Passivated InP Nanocrystals by XPS." *Nano Letters* **2002,** 2, (2), 151-154.

48. Suzer, S.; Abelev, E. and Bernasek, S. L. "Impedance-Type Measurements Using XPS." *Applied Surface Science* **2009,** 256, (5), 1296-1298.

49. Sezen, H.; Ozbay, E.; Aktas, O. and Suzer, S. "Transient Surface Photovoltage in n-and p-GaN as Probed by X-Ray Photoelectron Spectroscopy." *Applied Physics Letters* **2011,** 98, 111901.

50. Sezen, H. and Suzer, S. "Enhancement of Dopant Dependent X-Ray Photoelectron Spectroscopy Peak Shifts of Si by Surface Photovoltage." *Journal of Chemical Physics* **2011,** 135, (14).

51. Sezen, H. and Suzer, S. "Probing Dynamics of Surface Structures Using X-Ray Photoelectron Spectroscopy." *Journal of Spectroscopy and Dynamics* **2012,** 2, 3.

52. Conger, C. P. and Suzer, S. "Response of Polyelectrolyte Layers to the SiO2 Substrate Charging as Probed by XPS." *Langmuir* **2009,** 25, (3), 1757-1760.

53. Amalnerkar, D. P. "Photoconducting and Allied Properties of CdS Thick Films." *Materials Chemistry and Physics* **1999,** 60, (1), 1-21.

54. Greenham, N. C.; Peng, X. G. and Alivisatos, A. P. "Charge Separation and Transport in Conjugated-Polymer/Semiconductor-Nanocrystal Composites Studied by Photoluminescence Quenching and Photoconductivity." *Physical Review B* **1996,** 54, (24), 17628-17637.

55. Plummer, J. D.; Deal, M. D. and Griffin, P. B. **2000.** *Silicon VLSI Technology: Fundamentals, Practice and Modeling*. New Jersey: Prentice Hall Upper Saddle River.

56. Neamen, D. A. **1997.** *Semiconductor Physics and Devices*. (2nd ed.). New York: McGraw-Hill.

57. Himpsel, F. J.; Hollinger, G. and Pollak, R. A. "Determination of the Fermi-Level Pinning Position at Si(111) Surfaces." *Physical Review B* **1983,** 28, (12), 7014-7018.

58. Kronik, L. and Shapira, Y. "Surface Photovoltage Phenomena: Theory, Experiment, and Applications." *Surface Science Reports* **1999,** 37, (1-5), 1-206.

59. Long, J. P. and Bermudez, V. M. "Band Bending and Photoemission-Induced Surface Photovoltages on Clean n-and p-GaN (0001) Surfaces." *Physical Review B* **2002,** 66, (12), 121308.

60. Schroder, D. K. "Surface Voltage and Surface Photovoltage: History, Theory and Applications." *Measurement Science & Technology* **2001,** 12, (3), R16-R31.

61. Foussekis, M.; Ferguson, J. D.; Baski, A. A.; Morkoc, H. and Reshchikov, M. A. "Role of the Surface in the Electrical and Optical Properties of GaN." *Physica B-Condensed Matter* **2009,** 404, (23-24), 4892-4895.

62. Kronik, L. and Shapira, Y. "Surface Photovoltage Spectroscopy of Semiconductor Structures: at the Crossroads of Physics, Chemistry and Electrical Engineering." *Surface and Interface Analysis* **2001,** 31, (10), 954-965.

63. Reshchikov, M. A.; Foussekis, M. and Baski, A. A. "Surface Photovoltage in Undoped n-type GaN." *Journal of Applied Physics* **2010,** 107, (11), 113535.

64. Demuth, J. E.; Thompson, W. J.; Dinardo, N. J. and Imbihl, R. "Photoemission-Based Photovoltage Probe of Semiconductor Surface and Interface Electronic Structure." *Physical Review Letters* **1986,** 56, (13), 1408-1411.

65. Huck, N. R.; Smart, R. S. C. and Thurgate, S. M. "Surface Photovoltage and XPS Studies of Electronic Structure in Defective Nickel Oxide Powders." *Surface Science* **1986,** 169, (1), L245-L252.

66. Halas, N. J. and Bokor, J. "Surface Recombination on the Si(111)2x1 Surface." *Physical Review Letters* **1989,** 62, (14), 1679-1682.

67. Long, J. P.; Sadeghi, H. R.; Rife, J. C. and Kabler, M. N. "Surface Space-Charge Dynamics and Surface Recombination on Silicon (111) Surfaces Measured with Combined Laser and Synchrotron Radiation." *Physical Review Letters* **1990,** 64, (10), 1158-1161.

68. Schellenberger, A.; Schlaf, R.; Pettenkofer, C. and Jaegermann, W. "Synchrotron-Induced Surface-Photovoltage Saturation at Intercalated Na/WSe2 Interfaces." *Physical Review B* **1992,** 45, (7), 3538-3545.

69. Marsi, M.; Nahon, L.; Couprie, M. E.; Garzella, D.; Hara, T.; Bakker, R.; Billardon, M.; Delboulbe, A.; Indlekofer, G. and Taleb-Ibrahimi, A. "Surface Photovoltage in Semiconductors under Pulsed Optical Excitation, and its Relevance to Synchrotron Radiation Spectroscopy." *Journal of Electron Spectroscopy and Related Phenomena* **1998,** 94, (1-2), 149-157.

70. Widdra, W.; Brocker, D.; Giessel, T.; Hertel, I. V.; Kruger, W.; Liero, A.; Noack, F.; Petrov, V.; Pop, D.; Schmidt, P. M.; Weber, R.; Will, I. and Winter, B. "Time-Resolved Core Level Photoemission: Surface Photovoltage Dynamics of the SiO2/Si(100) Interface." *Surface Science* **2003,** 543, (1-3), 87-94.

71. Marsi, M.; Couprie, M. E.; Nahon, L.; Garzella, D.; Bakker, R.; Delboulbe, A.; Nutarelli, D.; Roux, R.; Visentin, B.; Grupp, C.; Indlekofer, G.; Panaccione, G.; TalebIbrahimi, A. and Billardon, M. "Two Color Experiments Combining Free Electron Laser and Synchrotron Radiation." *Nuclear Instruments & Methods in Physics Research Section a-Accelerators Spectrometers Detectors and Associated Equipment* **1997,** 393, (1-3), 548-551.

72. Marsi, M.; Couprie, M. E.; Nahon, L.; Garzella, D.; Hara, T.; Bakker, R.; Billardon, M.; Delboulbe, A.; Indlekofer, G. and TalebIbrahimi, A. "Surface States and Space Charge Layer Dynamics on Si(111)2x1: a Free Electron Laser-Synchrotron Radiation Study." *Applied Physics Letters* **1997,** 70, (7), 895-897.

73. Marsi, M.; Belkhou, R.; Grupp, C.; Panaccione, G.; Taleb-Ibrahimi, A.; Nahon, L.; Garzella, D.; Nutarelli, D.; Renault, E.; Roux, R.; Couprie, M. E. and Billardon, M. "Transient Charge Carrier Distribution at UV-Photoexcited SiO2/Si Interfaces." *Physical Review B* **2000,** 61, (8), R5070-R5073.

74. Brocker, D.; Giessel, T. and Widdra, W. "Charge Carrier Dynamics at the SiO2/Si(100) Surface: a Time-Resolved Photoemission Study with Combined Laser and Synchrotron Radiation." *Chemical Physics* **2004,** 299, (2-3), 247-251.

75. Tokudomi, S.; Azuma, J.; Takahashi, K. and Kamada, M. "Ultrafast Decay of Surface Photo-Voltage Effect on n-type GaAs (100) Surface." *Journal of the Physical Society of Japan* **2007,** 76, (10), 104710.

76. Tokudomi, S.; Azuma, J.; Takahashi, K. and Kamada, M. "Ultrafast Time Dependence of Surface Photo-Voltage Effect on p-Type GaAs (100) Surface." *Journal of the Physical Society of Japan* **2008,** 77, (1), 014711.

77. Carraher, C. E. and Seymour, R. B. **2003.** *Polymer Chemistry: Testing and Spectrometric Characterization of Polymers*. (6th ed.). Marcel Dekker New York.

78. Demirok, U. K.; Ertas, G. and Suzer, S. "Time-Resolved XPS Analysis of the SiO2/Si System in the Millisecond Range." *Journal of Physical Chemistry B* **2004,** 108, (17), 5179-5181.

79. Sezen, H. and Suzer, S. unpublished data.

80. Birer, O.; Sayan, S.; Suzer, S. and Aydinli, A. "XPS Investigation of Thin SiOx and SiOxNy Overlayers." *Journal of Molecular Structure* **1999,** 481, 611-614.

81. Owens, T. M.; Nicholson, K. T.; Banaszak Holl, M. M. and Suzer, S. "Formation of Alkylsilane-Based Monolayers on Gold." *Journal of the American Chemical Society* **2002,** 124, (24), 6800-6801.

82. Owens, T. M.; Suzer, S. and Holl, M. M. B. "Variable Energy X-Ray Photoemission Studies of Alkylsilane Based Monolayers on Gold." *Journal of Physical Chemistry B* **2003,** 107, (14), 3177-3182.

83. Yilmaz, E.; Ertas, G.; Bengu, E. and Suzer, S. "Photopatterning of PMMA Films with Gold Nanoparticles: Diffusion of AuCl4- Ions." *Journal of Physical Chemistry C* **2010,** 114, (43), 18401-18406.

84. Yilmaz, E. and Suzer, S. "Au Nanoparticles in PMMA Matrix: in situ Synthesis and the Effect of Au Nanoparticles on PMMA Conductivity." *Applied Surface Science* **2010,** 256, (22), 6630-6633.

85. Sayan, S.; Garfunkel, E. and Suzer, S. "Soft X-Ray Photoemission Studies of the HfO2/SiO2/Si System." *Applied Physics Letters* **2002,** 80, (12), 2135-2137.

86. Suzer, S.; Sayan, S.; Holl, M. M. B.; Garfunkel, E.; Hussain, Z. and Hamdan, N. M. "Soft X-Ray Photoemission Studies of Hf Oxidation." *Journal of Vacuum Science & Technology A* **2003,** 21, (1), 106-109.

87. Sayan, S.; Emge, T.; Garfunkel, E.; Zhao, X. Y.; Wielunski, L.; Bartynski, R. A.; Vanderbilt, D.; Suehle, J. S.; Suzer, S. and Banaszak-Holl, M. "Band Alignment Issues Related to HfO2/SiO2/p-Si Gate Stacks." *Journal of Applied Physics* **2004,** 96, (12), 7485-7491.

88. Suzer, S.; Sezen, H. and Dana, A. "Two-Dimensional X-Ray Photoelectron Spectroscopy for Composite Surface Analysis." *Analytical Chemistry* **2008,** 80, (10), 3931-3936.

89. Ulgut, B. and Suzer, S. "XPS Studies of SiO2/Si System under External Bias." *Journal of Physical Chemistry B* **2003,** 107, (13), 2939-2943.

90. Karadas, F.; Ertas, G. and Suzer, S. "Differential Charging in SiO2/Si System as Determined by XPS." *Journal of Physical Chemistry B* **2004,** 108, (4), 1515-1518.

91. Karadas, F.; Ertas, G.; Ozkaraoglu, E. and Suzer, S. "X-Ray-Induced Production of Gold Nanoparticles on a SiO2/Si System and in a Poly(methyl methacrylate) Matrix." *Langmuir* **2005,** 21, (1), 437-442.

92. Tunc, I.; Demirok, U. K.; Suzer, S.; Correa-Duatre, M. A. and Liz-Marzan, L. M. "Charging/Discharging of Au (Core)/Silica (Shell) Nanoparticles as Revealed by XPS." *Journal of Physical Chemistry B* **2005,** 109, (50), 24182-24184.

93. Oktem, B.; Kalaycioglu, H. and Ilday, F. O. In *Femtosecond Laser-Induced TiO2 Nanostructures on Titanium*, Lasers and Electro-Optics (CLEO) and Quantum Electronics and Laser Science Conference (QELS), San Jose, **2010**.

94. Oktem, B.; Kalaycioglu, H. and Ilday, F. Ö. "Microjoule Pulse Energies at 1 MHz Repetition Rate from an All-Fiber Nonlinear Chirped-Pulse Amplifier." *Optics Letters* **2010,** 35, (7), 959.

95. Ozgoren, K.; Oktem, B.; Ilday, F. Ö.; Pasin, E. and Eken, K. In *Micromachining with Square-Shaped 1 ns-Long Pulses from an all-Fiber Yb-Doped Laser-Amplifier System*, Optical Society of America, Munich, **2011**.

96. Tak, Y.; Hong, S. J.; Lee, J. S. and Yong, K. "Fabrication of ZnO/CdS Core/Shell Nanowire Arrays for Efficient Solar Energy Conversion." *Journal of Materials Chemistry* **2009,** 19, (33), 5945-5951.

97. McCluskey, M. D.; Van de Walle, C. G.; Master, C. P.; Romano, L. T. and Johnson, N. M. "Large Band Gap Bowing of InxGa1-xN Alloys." *Applied Physics Letters* **1998,** 72, (21), 2725-2726.

98. Monemar, B. "Fundamental Energy Gap of GaN From Photoluminescence Excitation Spectra." *Physical Review B* **1974,** 10, (2), 676-681.

99. Kwok, R. W. M. *XPSPEAK95 v2.0. Available for download at http://phy.cuhk.edu.hk/~surface/XPSPEAK/*.

100. Tasci, T. O.; Atalar, E.; Demirok, U. K. and Suzer, S. "Electrical Circuit Modeling of Surface Structures for X-Ray Photoelectron Spectroscopic Measurements." *Surface Science* **2008,** 602, (1), 365-368.

101. Mead, C. A. and Spitzer, W. G. "Fermi Level Position at Semiconductor Surfaces." *Physical Review Letters* **1963,** 10, (11), 471-472.

102. Waldrop, J. R. and Grant, R. W. "Semiconductor Heterojunction Interfaces: Nontransitivity of Energy-Band Discontiuities." *Physical Review Letters* **1979,** 43, (22), 1686-1689.

103. Kraut, E. A.; Grant, R. W.; Waldrop, J. R. and Kowalczyk, S. P. "Precise Determination of the Valence and Edge in X-Ray Photoemission Spectra: Application to Measurement of Semiconductor Interface Potentials." *Physical Review Letters* **1980,** 44, (24), 1620-1623.

104. Katnani, A. D. and Margaritondo, G. "Microscopic Study of Semiconductor Heterojunctions: Photoemission Measurement of the Valance-Band Discontinuity and of the Potential Barriers." *Physical Review B* **1983,** 28, (4), 1944-1956.

105. Duc, T. M.; Hsu, C. and Faurie, J. P. "Linearity (Commutativity and Transitivity) of Valence-Band Discontinuity in Heterojunctions with Te-based II-VI Semiconductors: CdTe, HgTe, and ZnTe." *Physical Review Letters* **1987,** 58, (11), 1127-1130.

106. Martin, G.; Botchkarev, A.; Rockett, A. and Morkoc, H. "Valence Band Discontinuities of Wurtzite GaN, AlN, and InN Heterojunctions Measured by X-Ray Photoemission Spectroscopy." *Applied Physics Letters* **1996,** 68, 2541.

107. Klein, A.; Löher, T.; Tomm, Y.; Pettenkofer, C. and Jaegermann, W. "Band Lineup Between CdS and Ultra High Vacuum-Cleaved CuInS Single Crystals." *Applied Physics Letters* **1997,** 70, 1299-1301.

108. Bauknecht, A.; Blieske, U.; Kampschulte, T.; Albert, J.; Sehnert, H.; Lux-Steiner, M. C.; Klein, A. and Jaegermann, W. "Band Offsets at the ZnSe/CuGaSe2 (001) Heterointerface." *Applied Physics Letters* **1999,** 74, (8), 1099-1101.

109. Phaneuf, R. J.; Kan, H. C.; Marsi, M.; Gregoratti, L.; Gunther, S. and Kiskinova, M. "Imaging the Variation in Band Bending across a Silicon pn Junction Surface Using Spectromicroscopy." *Journal of Applied Physics* **2000,** 88, (2), 863-868.

110. Ballarotto, V. W.; Siegrist, K.; Phaneuf, R. J.; Williams, E. D. and Mogren, S. "PEEM Imaging of Dopant Contrast in Si(001)." *Surface Science* **2000,** 461, (1-3), L570-L574.

111. Lang, O.; Klein, A.; Pettenkofer, C.; Jaegermann, W. and Chevy, A. "Band Lineup of Lattice Mismatched InSe/GaSe Quantum Well Structures Prepared by van der Waals Epitaxy: Absence of Interfacial Dipoles." *Journal of Applied Physics* **2009,** 80, (7), 3817-3821.

112. Barrett, N.; Zagonel, L. F.; Renault, O. and Bailly, A. "Spatially Resolved, Energy-Filtered Imaging of Core Level and Valence Band Photoemission of highly p and n Doped Silicon Patterns." *Journal of Physics-Condensed Matter* **2009,** 21, (31), 314015.

113. Hirose, K.; Nohira, H.; Azuma, K. and Hattori, T. "Photoelectron Spectroscopy Studies of SiO2/Si Interfaces." *Progress in Surface Science* **2007,** 82, (1), 3-54.

114. Hirose, K. "XPS Time-Dependent Measurement of SiO2/Si and HfAlOx/Si Interfaces." *Journal of Electron Spectroscopy and Related Phenomena* **2010,** 176, (1-3), 46-51.

115. Gatos, H. C. and Lagowski, J. "Surface Photovoltage Spectroscopy--A New Approach to the Study of High-Gap Semiconductor Surfaces." *Journal of Vacuum Science and Technology* **1973,** 10, (1), 130-135.

116. Liqiang, J.; Xiaojun, S.; Jing, S.; Weimin, C.; Zili, X.; Yaoguo, D. and Honggang, F. "Review of Surface Photovoltage Spectra of Nano-Sized Semiconductor and its Applications in Heterogeneous Photocatalysis." *Solar Energy Materials and Solar Cells* **2003,** 79, (2), 133-151.

117. Munakata, C.; Nishimatsu, S.; Honma, N. and Yagi, K. "AC Surface Photovoltages in Strongly-Inverted Oxidized p-type Silicon-Wafers." *Japanese Journal of Applied Physics Part 1-Regular Papers Short Notes & Review Papers* **1984,** 23, (11), 1451-1461.

118. Kobayashi, H.; Kubota, T.; Kawa, H.; Nakato, Y. and Nishiyama, M. "Oxide Thickness Dependence of Energy Shifts in the Si 2p Levels for the SiO2/Si Structure, and its Elimination by a Palladium Overlayer." *Applied Physics Letters* **1998,** 73, (7), 933-935.

119. Šarapatka, T. J. "XPS Study of Lead on SiOx/Si: Temperature and Light Effects." *Surface Science* **1992,** 275, (3), 443-449.

120. Robertson, J. "High Dielectric Constant Oxides." *The European Physical Journal Applied Physics* **2004,** 28, (3), 265-291.

121. Munakata, C. and Nishimatsu, S. "Analysis of a AC Surface Photovoltages In A Depleted Oxidized p-type Silicon-Wafer." *Japanese Journal of Applied Physics Part 1-Regular Papers Short Notes & Review Papers* **1986,** 25, (6), 807-812.

122. Foti, G.; Rimini, E.; Vitali, G. and Bertolotti, M. "Amorphous-Polycrystal Transition Induced by Laser Pulse in Self-Ion Implanted Silicon." *Applied Physics A: Materials Science & Processing* **1977,** 14, (2), 189-191.

123. Gat, A.; Gibbons, J.; Magee, T.; Peng, J.; Williams, P.; Deline, V. and Evans, C. "Use of a Scanning CW Kr Laser to Obtain Diffusion Free Annealing of B Implanted Silicon." *Applied Physics Letters* **1978,** 33, (5), 389-391.

124. Boyd, I. W. and Wilson, J. I. B. "Laser Processing of Silicon." *Nature* **1983,** 303, (5917), 481-486.

125. Sezen, H.; Oktem, B.; Ilday, F. O. and Suzer, S. unpublished data.

126. Gaur, A.; Sharma, D. K.; Ahlawat, D. S. and Singh, N. "Optical Nonlinearities in Direct and Indirect Band Gap Crystals on the Z-Scan Technique with Nanosecond Laser." *Solid State Communications* **2007,** 141, (8), 445-448.

127. Zunger, A. "Practical Doping Principles." *Applied Physics Letters* **2003,** 83, 57.

128. Jie, J. S.; Zhang, W. J.; Jiang, Y.; Meng, X. M.; Li, Y. Q. and Lee, S. T. "Photoconductive Characteristics of Single-Crystal CdS Nanoribbons." *Nano Letters* **2006,** 6, (9), 1887-1892.

129. Chernow, F.; Eldridge, G.; Ruse, G. and Wahlin, L. "High Conductivity p-type CdS." *Applied Physics Letters* **1968,** 12, (10), 339-341.

130. Sebastian, P. J. "p-type CdS Thin Films Formed by in-situ Cu Doping in the Chemical Bath." *Applied Physics Letters* **1993,** 62, (23), 2956-2958.

131. Aqili, A. K. S.; Shafique, M.; Ali, Z.; Maqsood, A. and Kazmi, A. "Properties of Silver-Doped CdS Thin Films Prepared by Closed Space Sublimation (CSS) Techniques." *Journal of Materials Science Letters* **2003,** 22, (2), 127-129.

132. Lagowski, J.; Balestra, C. L. and Gatos, H. C. "Photovoltage Inversion Effect and its Application to Semiconductor Surface Studies: CdS." *Surface Science* **1971,** 27, (3), 547-558.

133. Schellenberg, J. J. and Kao, K. C. "On the Relationship Between Photoconductivity and Light Intensity in Solids." *Journal of Physics D: Applied Physics* **1988,** 21, (12), 1764.

134. Giesen, M.; Phaneuf, R. J.; Williams, E. D.; Einstein, T. L. and Ibach, H. "Characterization of p-n Junctions and Surface-States on Silicon Devices by Photoemission Electron Microscopy." *Applied Physics a-Materials Science & Processing* **1997,** 64, (5), 423-430.

135. El Gabaly, F.; Grass, M.; McDaniel, A. H.; Farrow, R. L.; Linne, M. A.; Hussain, Z.; Bluhm, H.; Liu, Z. and McCarty, K. F. "Measuring Individual Overpotentials in an Operating Solid-Oxide Electrochemical Cell." *Phys. Chem. Chem. Phys.* **2010,** 12, (38), 12138-12145.

136. Bagnall, D. M.; Ullrich, B.; Qiu, X. G.; Segawa, Y. and Sakai, H. "Microcavity Lasing of Optically Excited Cadmium Sulfide Thin Films at Room Temperature." *Opt. Lett.* **1999,** 24, (18), 1278-1280.

137. Pantel, R. "Auger Voltage Contrast Depth Profiling of Shallow p-n Junctions." *Applied Physics Letters* **1983,** 43, (7), 650-652.

138. Patterson, J. M. and Smith, M. C. "A Non Contact Voltage Measurement Technique Using Auger Spectroscopy." *Reliability Phys. Symp., 1983. 21st Annual* **1983,** 150-152.

139. Comizzoli, R. B. and Opila, R. L. "Electrical-Conduction Mechanism in Semiinsulating Polycrystalline Silicon Films." *Journal of Applied Physics* **1987,** 61, (1), 261-270.

140. Opila, R. L.; Marchut, L. and Hollenhorst, J. N. "Measurement of the Surface Electrical Potential in a Planar Avalanche." *Journal of the Electrochemical Society* **1990,** 137, (2), 703-705.

141. Opila, R. L. "Electron Spectroscopies for Simultaneous Chemical and Electrical Analysis." *Applied Surface Science* **2009,** 256, (5), 1313-1315.

142. Hill, J. E. and Chamberlin, R. R., Method for Making Conductive Film and Film Making Equipment. In United States Patent Office: 1964.

143. Rose, D. H.; Hasoon, F. S.; Dhere, R. G.; Albin, D. S.; Ribelin, R. M.; Li, X. S.; Mahathongdy, Y.; Gessert, T. A. and Sheldon, P. "Fabrication Procedures and Process Sensitivities for CdS/CdTe Solar Cells." *Prog in Photovolt. Res. and Appl.* **1999,** 7, (5), 331-340.

144. Barbet, S.; Aubry, R.; di Forte-Poisson, M. A.; Jacquet, J. C.; Deresmes, D.; Melin, T. and Théron, D. "Surface Potential of n- and p-type GaN Measured by Kelvin Force Microscopy." *Applied Physics Letters* **2008,** 93, (21), 212107.

145. Bermudez, V. M. "Study of Oxygen Chemisorption on the GaN (0001) (1x1) Surface." *Journal of Applied Physics* **2009,** 80, (2), 1190-1200.

146. Foussekis, M.; Baski, A. A. and Reshchikov, M. A. "Photoadsorption and Photodesorption for GaN." *Applied Physics Letters* **2009,** 94, 162116.

147. Tracy, K. M.; Mecouch, W. J.; Davis, R. F. and Nemanich, R. J. "Preparation and Characterization of Atomically Clean, Stoichiometric Surfaces of n- and p-type GaN(0001)." *Journal of Applied Physics* **2003,** 94, (5), 3163-3172.

148. Van de Walle, C. G. and Segev, D. "Microscopic Origins of Surface States on Nitride Surfaces." *Journal of Applied Physics* **2007,** 101, 081704.